EFFECT OF THIOSULATE ON PASSIVITY AND CORROSION PROPERTIES OF STAINLESS STEELS

A Thesis
Presented to
The Academic Faculty

by

Yushu Wang

In Partial Fulfillment
of the Requirements for the Degree
Doctor of Philosophy in the
School of Materials Science and Engineering

Georgia Institute of Technology
August, 2015

EFFECT OF THIOSULATE ON PASSIVITY AND CORROSION PROPERTIES OF STAINLESS STEELS

Approved by:

Dr. Preet M. Singh, Advisor
School of Materials Science and Engineering
Georgia Institute of Technology

Dr. Lawrence A. Bottomley
School of Chemistry and Biochemistry
Georgia Institute of Technology

Dr. Arun M. Gokhale
School of Materials Science and Engineering
Georgia Institute of Technology

Dr. Yulin Deng
School of Chemical and Biomolecular Engineering
Georgia Institute of Technology

Dr. Faisal Alamgir
School of Materials Science and Engineering
Georgia Institute of Technology

Date Approved: July 13, 2015

[To the two other doctors in my family, Dr. Li Wang and Dr. Xiqing Wang]

ACKNOWLEDGEMENTS

First of all, I would like to thank my advisor, Dr. Preet M. Singh, for the guidance and support during the course of my research. He has been like a patient father to me. He cultivated my self-confidence, and gave me chances to correct my own mistakes. I was amazed by how he can always keep a warm heart and his devotion to educate. For me, there is much to learn from him, both on how to do research and be a human being.

I would like to extend my appreciation to my committee members. Thanks to Dr. Arun M. Gokhale, for his lectures on alloys and microstructures. They prepared me well for the career ahead of me. Thanks to Dr. Faisal for his guidance on XPS and surface analysis for my research. The discussions we had were quite helpful and insightful. Thanks to Dr. Lawrence A. Bottomley for his wonderful lectures on electrochemistry. I really enjoyed his way of teaching, which provoked critical thinking and made it fun to learn. Thanks to Dr. Yulin Deng for his guidance and critical evaluation in my proposal defense, which prompted me to dig deeper into my area of research.

Many thanks to my lab mates and group alumni: Jamshad Mahmood, Liang He, Gaoxiang Wu, Zhiyuan Liang, Sanjay John, and Omar Elsayed for helping with my experiments; Dr. Lindsey Goodman, Dr. KkochNim Oh, Dr. Kevin Chasse, for helpful discussions on my research; Dr. Di Yang, Dr. Xiaoyuan Lou, Dr. Dong Yang, Dr. Stefanie Asher, Prof. Zhengfei Hu, for insightful discussions on career development; Joseph Meyer, Alexandra Firebaugh, Dr. Ananya Bhattacharya, Stephani Gulbrandsen,

Sam Raji, Simon Puydebois, Charlotte Renard, Aydin Baykal, Kevin Chan, for being supportive of me.

I also want to thank my friends who helped me with my research: Koushik Ramachandran, Mengdi Luo, Tianxi Gao, Jingyi Zhang, Siyuan Zhang, Kesong Hu, Bin Hu, Yang Yang, Yuan Li, Sui An, Zhihang Liu, Xin Chen, Yisong Su, and Xuehong Yu. Special thanks to my girlfriend, Lu Yang, for the constant pestering on keeping up with my thesis writing schedule.

Finally, I would like to say that I cannot finish my degree without the love, support, and a little push from my parents, Li Wang and Xiqing Wang.

This work was supported by the PSE fellowship from Renewable Bioproducts Institute, Georgia Institute of Technology.

TABLE OF CONTENTS

LIST OF TABLES

LIST OF FIGURES

SUMMARY

Stainless steels are widely used in the chemical process and other industries due to their mechanical properties and superior corrosion resistance. Corrosion resistance of stainless steels is attributed to the formation of a passive oxide film on their surfaces. On the other hand, corrosion issues in stainless steels almost exclusively result from the breakdown of this passive film. For instance, pitting is due to the local passivity breakdown on the open surface. SCC is due to the passivity breakdown at the crack tip. Understanding how the environmental parameters influence the passivation behavior of stainless steels is crucial for mechanistic study of different types of corrosion as well as mitigation of these corrosion problems.

Thiosulfate ions are present in many environments for variety of industrial applications, such as the pulp and paper industry, the nuclear industry, as well as the oil and gas industry. It is known to affect localized corrosion such as pitting corrosion and stress corrosion cracking (SCC) in stainless steels, especially in the presence of chlorides. In the case of pitting in chloride and thiosulfate containing environments, while the existing phenomenological studies have given general information about the role of thiosulfate and the chemical composition of stainless steels on localized corrosion, a clear picture of how thiosulfates participate in the different stages of pitting (pit initiation, pit growth) was not very clear. Moreover, there was limited amount of information reported on pitting corrosion in chloride and thiosulfate containing environments for duplex stainless steels (DSS). Furthermore, the interaction between

individual alloying elements and thiosulfate ions needs to be studied, which will provide better understanding of pitting corrosion in presence of thiosulfate and the influence of thiosulfate on repassivation kinetics.

The present study was aimed to understand the effect of thiosulfate addition on pit initiation as well as pit growth. Different aspects of interaction between thiosulfate and passive film was probed with electrochemical methods such as cyclic potentiodynamic polarization measurement and potentiostatic polarization. Cyclic potentiodynamic polarization tests showed that the presence of thiosulfate hinders the repassivation of the pits. Increase in temperature and decrease in pH of the simulated papermachine white water environment promotes pitting corrosion. Pit morphology for austenitic stainless steel is hemispherical while preferential dissolution was found in duplex stainless steels. A statistical analysis of the metastable pitting events monitored by chronoamperometry revealed that thiosulfate promotes pit initiation and stabilizes the growth of metastable pits. The metastable to stable pit transition as well as pit grow in duplex stainless steel 2101 was found to be closely related to its microstructure. Due to the fact that pit initiation and pit growth on 2101 preferably occurs on the ferritic phase. Its microstructure and the pit initiation site determines the formation of stable pits and the pitting kinetics. Mechanical scratch tests, designed to study the repassivation kinetics and interactions between a bare metal and thiosulfate, revealed the effect of potential and microstructure on the growth of pitting in presence of thiosulfate. Interaction of alloying elements such as chromium, nickel, and molybdenum with thiosulfates were evaluated with thermodynamic analysis and XPS (X-ray

Photoelectron Spectroscopy) combined with scratch tests. XPS and EDS (Electron Dispersive Spectroscopy) showed presence of reduced sulfur species within the pits, which provided information regarding the overall corrosion process by combining thermodynamic analysis. Reduced sulfur species was also found to form in the repassivation process of the stainless steels even if no localized corrosion occurs. Based on these results, understanding a mechanism of pitting in the presence of thiosulfate was proposed.

1. INTRODUCTION

1.1. Motivation Statement

Passivation behavior of stainless steels relies on the thin (often a few nanometers thick) oxide film (passive film) formed on their surface [1]. Almost all types of corrosion in stainless steels are related to the breakdown of this protective oxide film. For instance, pitting and crevice corrosion initiates due to the localized breakdown of passive films [3]; erosion-corrosion occurs due to thinning or removal of passive films [4]; stress corrosion cracking mechanisms are related to the passive film breakdown at the crack tip as well as passivation kinetics [5].

Sulfur species are ubiquitous, and the effect of sulfur species on passivity of stainless steels determines the performance of these materials in many applications. For instance, sulfate ions are readily available in concrete pore solutions [6] and are found to cause stress corrosion cracking in some cases [7]. Sulfide may be present in some environments, they may also exist in the form of inclusions in many grades of stainless steel (e.g. MnS). The chemical dissolution of these inclusions may lead to pitting [8]. Sulfide corrosion cracking is also a big concern for pipeline steel [9] as well as stainless steels [10] in sour gas service due to the presence of H_2S in these environments.

Thiosulfate is present in many industrial environments, such as pulp and paper industry, nuclear industry, oil industry, etc. In the case of pulp and paper industry, it is a byproduct of bleaching chemicals in the paper making process. Thiosulfate is known to aggravate pitting corrosion in brass and stainless steels [11]. Since most corrosion

issues arise due to the interaction between metals and environment, how thiosulfate influence the chemical and physical characteristics of the passive films becomes an extremely important issue. Present study was focused on studying the phenomenological as well as mechanistic aspects of this interaction and the results have provided us with insights for mitigating corrosion issues in all above-mentioned applications.

1.2. Research Objective and Technical Approaches

From the published literature, a few gaps still remained in the understanding of thiosulfate-related localized corrosion of stainless steels. In order to address these knowledge gaps, specific technical objectives for the present study were:

(1) To study pitting corrosion behavior of duplex stainless steels in thiosulfate-containing environments, and to compare with pitting corrosion of austenitic stainless steels. To study the effects of water chemistry, pH, and temperature.

(2) To investigate the role of thiosulfate in the pit initiation process and metastable pitting stage. Specifically, the effect of thiosulfate on pit initiation frequency and metastable pit growth were explored.

(3) To address the effect of microstructure on pitting corrosion. Since duplex stainless steels used in this study is wrought, it is important to understand how the anisotropy may affect thiosulfate-related corrosion.

(4) To explore the interaction between thiosulfate and individual alloying element.

To understand how thiosulfate ions participate in different stages of pitting on various alloys.

(5) To understand the effect of thiosulfate on repassivation kinetics of austenitic stainless steels. Two existing models were used to help understand the role of thiosulfate in the repassivation process of 304L.

In order to meet these objectives, various electrochemical and characterization tools were used. Cyclic potentiodynamic polarization measurements were used to determine the pitting and repassivation potentials of the stainless steels. Potentiostatic polarization measurements were used to collect metastable pitting signals in order to statistically analyze these pitting events. Potentiostatic scratch tests were used to study the role of potential and microstructure in the growth stage of pitting, and repassivation kinetics of stainless steels. Optical microscope and Scanning Electron Microscope (SEM) were used to observe the morphology of the pits. Electron Dispersive Spectroscopy (EDS) and X-ray Photoelectron Spectroscopy (XPS) were used to provide information regarding participation of thiosulfate in the pitting process as well as the interaction between thiosulfate and individual alloying elements.

1.3. Organization of Upcoming Chapters

In the following chapters, a general review of localized corrosion in stainless steel as well as existing knowledge on thiosulfate-related pitting are provided in Chapter 2. The experimental procedures are summarized in Chapter 3. A phenomenological study

on pitting in simulated papermachine white water of duplex stainless steels compared with austenitic stainless steels are presented in Chapter 4. The role of thiosulfate in pit initiation and metastable pit growth is studied in Chapter 5. Effect of microstructure on pitting potentials, pit initiation, and pit growth is discussed in Chapter 6. The interaction between individual alloying element and thiosulfate are explored in Chapter 7. The role of thiosulfate on repassivation kinetics of 304L is given in Chapter 8. A big picture and some recommendations for future research are suggested in Chapter 9.

2. BACKGROUND INFORMATION

2.1. Steels and stainless steels

Stainless steels are iron based alloys that contain at least 10.5% chromium, which is able to form an oxide film on the surface of the stainless steel and result in a passive behavior for an otherwise reactive metal. Chromium is probably the most important element in stainless steels and is mainly added for corrosion resistance by forming a passive film. Nickel is added to stabilize austenitic phase and results in better weldability and workability. It is also a relatively noble element and improves general corrosion resistance. Molybdenum is added to martensitic stainless steels to improve high temperature strength; it also improves alloy's resistance to both general corrosion and localized corrosion. Nitrogen is added to steels for high strength, wear resistance as well as corrosion resistance. Copper is an austenite stabilizer and it increases general corrosion resistance and reduce work hardening rate. Carbon is an austenite stabilizer and improves strength of the stainless steel. However, carbon tends to bind with chromium and form chromium carbide precipitates under intermediate temperature (typically 400 – 850 ℃), which may result in a depletion of chromium in the grain boundary regions and increases the tendency for intergranular corrosion. When it is not feasible to keep carbon content low, titanium and niobium are added to enable preferential formation of carbides so that depletion of chromium by sensitization is no longer a concern. Sulfur and phosphorus are usually regarded as contaminants, but are sometimes added to improve the machinability of the steel. Manganese is added to

remove contaminants such as sulfur, phosphorous, and oxygen. It also increases solubility of nitrogen for the purpose of replacing nickel. Silicon is added to steel as a deoxidizing agent, and results in hardening.

There are mainly four types of stainless steel, ferritic, martensitic, and duplex stainless steel. The phase of the stainless steel is determined by its composition, as indicated in the Schaeffler Diagram shown in Figure 2-1.

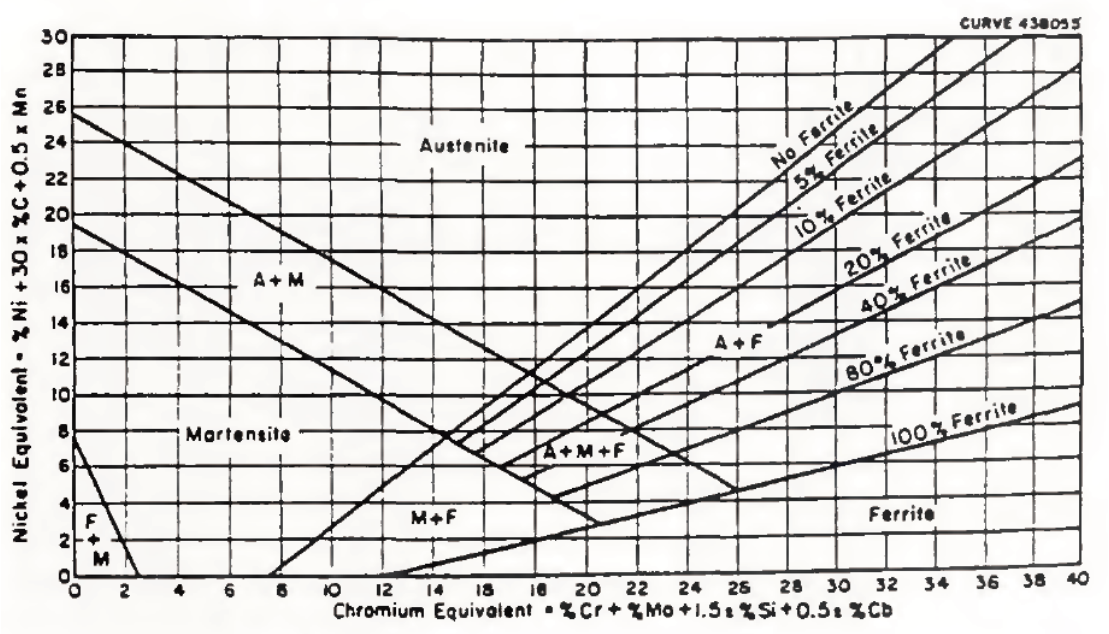

Figure 2-1. Schaeffler Diagram [1]

(a) Ferritic stainless steels. Ferritic stainless steels have the body-centered cubic crystal (BCC) structure. They have relatively good formability and ductility. They possess better corrosion resistance than martensitic stainless steels. These nickel-free stainless steels are not heat treatable, and may suffer from loss of mechanical properties in welded area due to grain growth.

(b) Martensitic stainless steels. Martensitic stainless steels undergo a martensitic transformation when quenched from higher temperature. This transformation results in a body-centered tetragonal crystal structure. Martensitic stainless steels may be tempered to gain a variety of mechanical properties, and their hardenability can be adjusted by changing alloy composition.

(c) Austenitic stainless steels. Austenitic stainless steels possess a face-centered cubic crystal (FCC) structure. Nickel is usually added in this type of stainless steel to stabilize the austenite phase. Leaner grades have been developed with nitrogen and manganese addition. Austenitic stainless steels have excellent formability and ductility. Although heat treatment is not feasible for hardening, work hardening properties makes them very good candidates for applications. They do not undergo ductile to brittle transition at lower temperatures, and are widely used in cryogenic applications. They have good weldability.

(d) Duplex stainless steels. Duplex stainless steels possess both ferrite phase (BCC) and austenite phase (FCC). Since duplex stainless steels consist of two phases, a good combination of strength and ductility is obtained. Duplex stainless steels are a relatively new group of stainless steels are gradually replacing traditionally used stainless steels in many applications.

2.2. The Nature of Passive films

With the addition of elements, such as Cr, Ni, Mo, Mn, N, etc., varieties of stainless steels were developed for different applications. Passive films formed on stainless steels

result in the passivation of the otherwise reactive metals. Passive behavior of alloys has been of interest to researchers for centuries. The phenomenon of "passivity" was first defined by James Keir in 1790's [1]. The well-known demonstration of passivity of iron in nitric acid by Faraday was one of the successful later explorations (cited in [11]). With new surface characterization and electrochemical techniques emerging, the passive films have been studied from many different angles. Chemical composition of passive films can be determined by different surface analysis methods. Passive films on austenitic stainless steels were found to be enriched in oxides of Chromium [13] by X-ray Photoelectron Spectroscopy (XPS). The passive film on iron-chromium alloys was reported to be amorphous in a study in a borate buffer solution [14]. Long range ordering of passive film after aging under polarization [15][16][17] was found using scanning tunneling microscope (STM), the passive films grow in crystalline islands with an orientation close to Cr (110) on iron-chromium alloys**.**

2.3. Pitting and localized breakdown of passive films

Corrosion is the degradation and gradual destruction of metals. Most corrosion processes are electrochemical processes. Based on appearances, corrosion is divided into eight categories:

(1) General corrosion is by uniform thinning of materials. The metal becomes thinner throughout the whole surface, which eventually leads to failure. General corrosion can be found everywhere, but it is probably the least dangerous form of corrosion because the corrosion rate can be easily measured and the remaining life of the

component can be predicted.

(2) Pitting and crevice corrosion. These types of corrosion are due to the localized passivity breakdown. They result in localized deep penetration into the material while most of the other material is intact. They are very dangerous forms of corrosion for the integrity of structural materials. Pitting and crevice corrosion are auto-catalytic in nature, and usually involve corrosion by differential aeration cell.

(3) Galvanic corrosion occurs when two metals of different corrosion potential are in contact. The nobler metal polarizes the more active metal anodically and cause the corrosion rate of the active metal to increase. This form of attack can usually be avoided by proper design and installation. On the other hand, galvanic may occur inside a metal where second phase particles having different corrosion potential from the matrix, which causes localized galvanic corrosion. This could eventually lead to pitting.

(4) Erosion corrosion is a type of corrosion assisted by physical erosion. The damage of passive film and subsequent corrosion as well as mechanical erosion of the material work together in this type of attack. Flow assisted corrosion, slurry abrasion, and cavitation all fall into this category.

(5) Dealloying is the selective leaching of alloying elements in an alloy. This type of corrosion will lead to a foam-like porous material structure and substantial degradation of mechanical properties. A common example of this type of corrosion is the dezincification of brass.

(6) Intergranular corrosion is the preferential attack on the grain boundary areas of a

material. Grain boundary usually possess different properties than the matrix and in some cases are less corrosion resistant. A typical example would be intergranular corrosion of sensitized 304 stainless steel, due to the formation of chromium carbides which causes depletion of chromium in area near grain boundary.

(7) Microbial corrosion is caused or accelerated by microbes. Sulfide and thiosulfate species produced by some sulfur reducing bacteria may lead to pitting and stress corrosion cracking. Sometimes the biofilms may cause crevice corrosion.

(8) Environmentally assisted cracking includes stress corrosion cracking, corrosion fatigue, hydrogen embrittlement, as well as liquid metal embrittlement. They are all failures caused by stress and aggressive environment working together.

Pitting corrosion is a dangerous form of corrosion. It is very hard to predict and not easily seen with the naked eye. Pitting occurs when the passive film is locally broken down and anodic dissolution beneath the passive film results in the formation of a pit by an autocatalytic reaction mechanism. Detailed information regarding pitting is given later in this section. Crevice corrosion is a form of attack that tends to occur when there is a tight crevice exposed to specific corrosive environments. In most cases, crevice initiation essentially is due to the formation of a differential aeration cell where deep-inside the crevice oxygen is depleted and that part acts as an anode and actively corrodes, and the propagation mechanism is quite similar to that of pitting.

2.3.1. Initiation of Pitting Corrosion

Pitting corrosion initiates by the localized breakdown of passive film. Propagation of this localized form of corrosion generates pits in stainless steels, and could be detrimental in many applications. Pits formed in pressure vessels, transportation and storage infrastructure could lead to leaks, which can disrupt production, and potentially result in environmental hazards.

Pitting corrosion can be divided into two main stages, the pit initiation and the pit propagation. Several mechanisms have been proposed for the pit initiation, and it is commonly accepted that real life situations could be the result of one or several mechanisms [3]. For instance, local film disruption due to microstructural inhomogeneities at the surface, like inclusions or second phase, may lead to the local pit initiation through a chemical dissolution of inclusions or galvanic corrosion. According to the penetration mechanism, aggressive species such as chloride anions could migrate to the metal/oxide interface and promote anodic dissolution [18]. Adsorption mechanism shines light on how chloride and other aggressive species could be competitively chemisorbed on the metal surface causing passive film breakdown [19]. Film breaking mechanism suggests that mechanical stresses exist in passive film due to electrostriction, surface tension, or external stresses [20], and breakdown of passive film could occur due to these mechanical stresses. Point defect model was later developed by McDonald and co-workers [21] that explains many of the phenomena which precedent theories could not account for. This theory, similar to Wagner's high temperature oxidation theory [22], is based on defect reaction at interfaces and

transportation of ionic defects through the passive film. A brief explanation of pit initiation is given in this theory. Excessive vacancy formation results in a condensate of vacancies beneath the passive film which separates the film from the metal surface. The passive film on top of the hollow area is thus easily ruptured by surface tension, exposing the bare metal underneath, as shown in Figure 2-2.

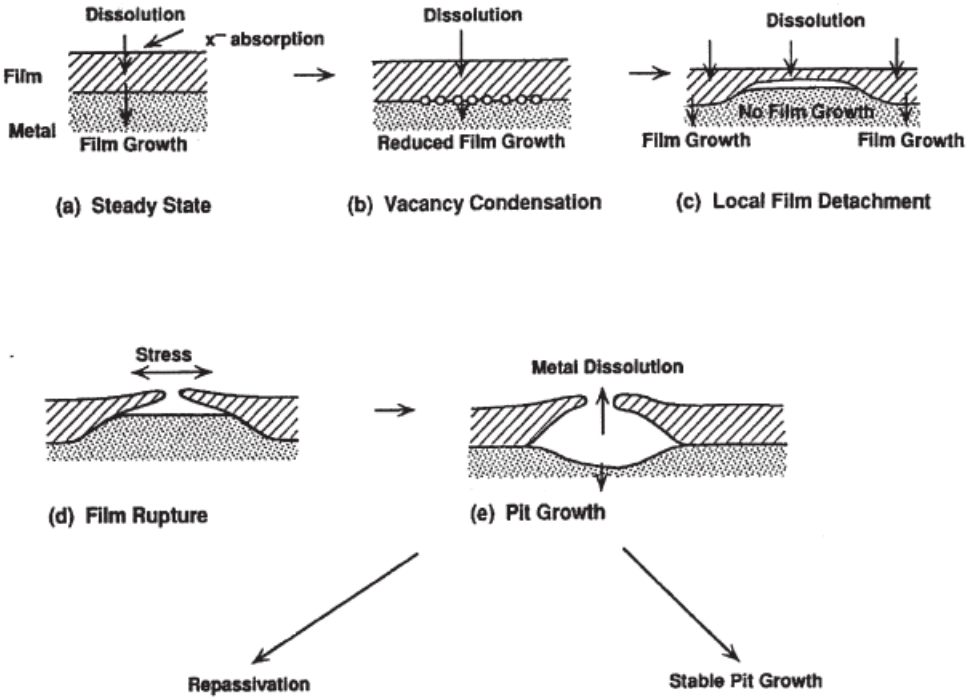

Figure 2-2. A schematic for pit initiation process given by point defect model [1]

2.3.2. Metastable Pitting

A schematic of pit growth is given in Figure 2-3.

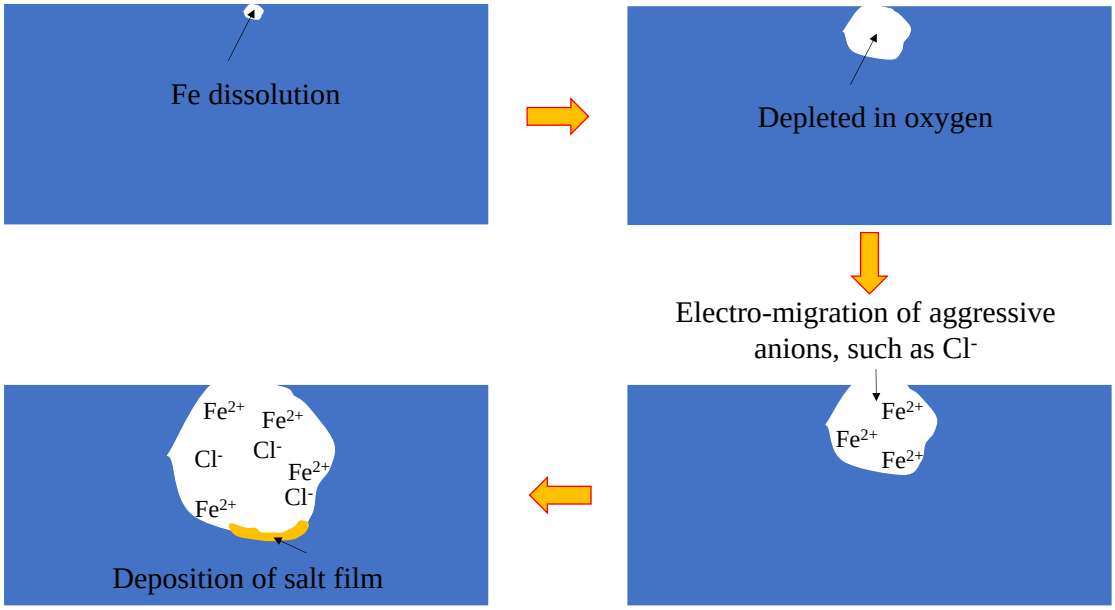

Figure 2-3. A schematic of pit growth

Once the bare metal surface is exposed due to the localized breakdown of passive film, local dissolution by anodic activity occurs. The environment inside the pit quickly becomes depleted in oxygen and other species that can be reduced to provide cathodic reaction. The cathodic reaction is subsequently "moved" to passive areas. Electrons would transfer in the alloy from pitted area to the passive areas. Only anodic reaction occurs within the pit. Electrons are transferred through the bulk metal to the alloy surface covered with passive films where the cathodic reaction occurs. As pits grow, the pit solution becomes rich in metal cations. As a result, anionic species such as chloride ions electro-migrates into the pit. Anionic species that correspond to strong acid are particularly aggressive, because the hydrolysis of corresponding ferrous salt results in an acidic pit environment, accelerating iron dissolution even more [23]. In many cases, pit growth is in the form of lacy pit growth [24]. In lacy pit growth, undercutting of metal beneath the passive film was observed, leaving porous oxide film

as a diffusion barrier, which is referred to as the pit cover.

In some cases the pits propagate for a small amount of time and then repassivate. These pits are referred to as metastable pits. A metastable pit has to grow to a certain size before it can stably grow. It was found that the metastable pits may repassivate due to rupture of passive film cover, unless a critical concentration of salts is reached in the pit to maintain the aggressiveness of the local chemistry. Metastable pits may have a life span of a few milliseconds to more than 10 seconds. They may exist even at potentials [25] and temperatures [26] where no stable pits can be observed.

The difference between the two outcomes (stable pit growth and repassivation) of a metastable pit may depend on the pit chemistry, size, and geometry of the metastable pit when the passive film that covers the pit-opening breaks. Metastable pitting has been studied extensively in chloride containing environments for stainless steels. Frankel et al. studied the kinetics of metastable pitting [25]. It was found that metastable pits may occur at -210mV vs. SCE at room temperature in near neutral to acidic chloride containing solutions. It was also found that the current density of the metastable pits remain constant during the metastable pit growth, and repassivation is due to rupture of the pit cover, which may allow the bulk solution to mix with the local pit solution. It was also shown that when a metastable pit grows large enough before the rupture of the pit cover, pit growth is stabilized. Current was found to increase proportionally to the t^2 in most potential range, where t is time. A sharp increase in current was also found before repassivation. It was argued that the process involved was neither diffusion controlled (since the current density of the metastable pit growth was found to be

potential dependent) nor ohmic controlled (since the growth of the metastable pits had a constant current density), but mixed in nature with charge transfer playing a role.

Pistorius and Burstein studied the metastable pitting of 304 wire in an acidic solution (pH=0.7) containing 1M Cl^-. Based on the assumption that surface concentration must be greater than 3M to sustain pit growth and that current of pit growth equals to the diffusion rate at the pit opening [27], they came to the conclusion that the criterion for metastable to stable transition is $i * a > 0.3 Am^{-1}$, where i is the current density of pit growth and a is the depth of the pit. Current was found to quickly increase in several segments of time, which corresponds to damages to the pit cover and enhanced diffusion (or drop in resistance according to Frankel et al. [25]). Metastable pit was found to be diffusion controlled, in contrast to the study by Frankel et al., while the effect of increase in potential is to activate more sites as metastable pits.

Moayed and Newman studied metastable pitting of 904L near its critical pitting temperature [26] in 1M NaCl at 45, 49, and 54 ℃. The current was found to increase proportional to t^n (time to the power of n) before repassivation. The value of the exponent n increased from 0.5 to 1.5 with increase in the temperature. Scully et al. studied the spatial distribution of initiation of pits. They discovered that the abrupt increase of current at pitting potential, which is usually attributed to the growth of pits, could also be due to the onset of metastable pit clustering [27]. The pitting potential also depends on the relationship between the lateral diffusion length and nearest neighbor distance of pit initiation sites. Addition of other anions also affect the metastable pitting behavior, Zuo et al. explored the addition of several anions in

solution containing NaCl [28]. Anions such as PO_4^{3-}, CrO_4^{2-}, SO_4^{2-}, and NO_3^- were found to inhibit metastable pitting of 316L.

2.3.3. Stable Pit Growth

As ion concentrations increase above the solubility limit, salt films start to deposit at the bottom of the pits. Chloride is known as the leading cause for pitting in stainless alloys for several reasons. First of all, hydrochloric acid is a strong acid, so the hydrolysis of ferrous chloride results in a highly acidic pit environment. Secondly, the solubility of ferrous chloride is very high, 5.4M at 20 ℃ [25]. Although sulfuric acid is a strong acid, the solubility of ferrous sulfate is only 1.94M at 25 ℃ [31], the salt film begins to form before the acidity and the local environment becomes aggressive enough to sustain the self-catalytic growth of the pits. In fact, sulfate is commonly considered to be an inhibitor to chloride pitting under room temperature, in most industrial applications. Finally, the diffusivity and charge density of the chloride is high. Pitting is a dynamic process, and without enough aggressive anions migrating into the pit, the repassivation of the pit could occur.

One other form of localized corrosion is crevice corrosion. For the crevice corrosion to occur, passivation breakdown and later stages of corrosion are very similar to pitting, except that an occluded site already exists due to the geometry of the crevice. Crevice corrosion is thus more detrimental than pitting, and has an easier initiation. Since tendency for the crevice corrosion varies with the geometry of the crevice, testing crevice corrosion is either by studying pitting or with a reproducible crevice- generating

device [32][33].

In a cyclic potentiodynamic polarization scan, critical potential for crevice corrosion is reached at lower potentials than pitting potential, thus it is very important to avoid crevice corrosion when testing for the pitting tendency. A number of techniques were used to eliminate crevice corrosion, including pre-passivation, insulation paint, silicone seal, and exposing part of the specimen below waterline (only works for deaerated cells). By far the relatively successful ways to eliminate crevice corrosion are flushed port cell (also known as Avesta cell [34]), applying punched electroplating tape, and using some special grades of epoxy or wax.

2.4. Material and Environmental Factors Affecting Pitting Corrosion

Pitting corrosion susceptibility in an alloy/environment system depends on the environmental as well as alloy variables. The effect of material and environmental factors on pitting corrosion is discussed in the following section.

2.4.1. Effect of Electrochemical Potential and Temperature

In modern chemical processing industry, structural materials are subjected to wide ranges of electrochemical potentials due to the chemical species they are exposed to. Electrochemical potential is crucial to the pitting such that most stainless steels have a critical potential only above which the pits grow stably. Since pitting involves active dissolution of metals, it is unlikely that pitting would occur below the reduction potential of the metal/metal ion. However, it is important to point out that pitting could

occur below the free corrosion potential or open circuit potential.

Cyclic potentiodynamic polarization is a commonly accepted approach to characterize the pitting tendency of a material. A hysteresis in the cyclic polarization curve suggests localized corrosion, as shown in Figure 1. Two parameters in this experiment, pitting potential E_p and repassivation potential E_r, are used to indicate two very important tendency in the pitting process. E_p is the potential at which the current sharply increases during the forwards scan. E_r is the potential at which the reverse scan current falls below the passivation current density in the forward scan at the same potential. E_p is considered to indicate the material's tendency to pit in a certain environment, and E_r the tendency to repassivate once it starts. The higher the E_p and E_r values, the more resistant the material is to pitting. $E_p - E_r$ is also related to the pitting resistance. Potential is also influenced by the dissolved gaseous species in the solution. The free corrosion potential shifts considerably due to de-aeration, since the mixed potential is changed by suppressing cathodic reaction involving dissolve oxygen. The pitting potential, on the other hand, was found to be the same [35].

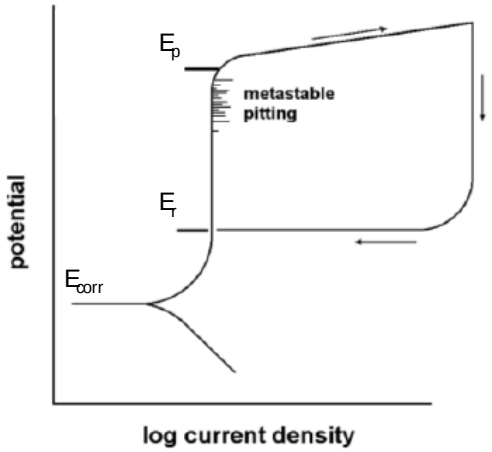

Figure 1. Typical cyclic polarization curve that shows pitting

Temperature is another very important factor controlling pitting process. A critical pitting temperature, below which pitting does not occur for a specific environment, is found for many alloys. The use of critical pitting temperature as a criterion for pitting resistance was first introduced in the 70s [36], pitting potential was found to drastically change in a certain range of temperature, and eventually become higher than the transpassive potential at a low enough temperature. Critical pitting temperature was later adopted to characterize the change in pitting tendency due to composition [37], environment [38][39][40], microstructure [41], as well as surface roughness [42].

2.4.2. Effect of Alloying Element and Microstructure on Pitting Corrosion

Alloy composition plays a vital role in pitting corrosion. Chromium is mainly responsible for the passive film formation in stainless steels. In steel industry, addition of at least 12% chromium is required for the steel to be graded “stainless”. It was found that an increase in the chromium content increases the pitting potential of Fe-Cr alloy [43]. Even though chromium is the main element in the passive film of a stainless steel, addition of other elements can alter the pitting behavior dramatically as well. It is important to note that the same element behaves very differently in different electrolyte, and may exhibit beneficial effect in one environment while being harmful in another. For instance, nickel is a more noble metal than iron and chromium [44], and promotes pitting resistance of Fe-Cr alloy in chloride media [43].However, nickel is shown to be very sensitive to reduced sulfur species related pitting [45]. Mo enrichment was not found in passive films [13][46][47], yet shown to drastically improve an alloy’s

resistance to pitting in chloride containing solutions[46][48]. It was suggested that molybdate adsorbs on the metal surface [47] and helps mitigating the pitting corrosion by forming a complex in the active area [49][50], number of both pit nucleation and metastable pits was reduced by the addition of molybdenum [51]. Nitrogen is often added to strengthen the steel, a beneficial effect on pitting resistance was also found [52]. Pitting resistance equivalent (PRE) is a concept developed in the 80s and widely used among researchers [53][54][55], which suggests that these beneficial alloying elements are contributing independently to pitting resistance of the material. A general equation is given as: PRE = %Cr + a ×(%Mo) + b ×(%N). Constants a and b may take different value depending on different references. On the other hand, PRE is used more as a guideline rather than a standard due to the fact that pitting is a highly localized process that depends on the local electrochemical conditions [56] and microstructure. Furthermore, synergistic effects of different elements on improving pitting resistance were found. For instance, nitrogen promotes the retention of chromium in the passive film and pitting resistance [53][57].

Pitting is sensitive to surface inhomogeneities, such as inclusions and second phase particles. Microstructure is thus very important for pit initiation. The pitting resistance in chloride media and corrosion resistance in sulfuric acid of a high alloyed austenitic stainless steel both decreases after heat treatment, due to segregation of alloying elements [58]. Dissolution of inclusions in steels may lead to exposure of bare metal surface and provide heterogeneous sites required for pit initiation. Second phase particles such as sigma-phase particles in stainless steels are also known to affect pitting

tendency [59]. Grain boundaries are sometimes preferentially attacked due to its higher energy, while in the case of sensitized 304 steel, could be preferentially attacked because of chromium carbide formation and resulting chromium deficiency near grain boundary regions. Preferential dissolution of different phases in duplex stainless steels was reported [60], where the preferential corrosion happens in the austenitic phase in sulfuric and phosphoric acid, and the ferritic phase is preferentially attacked in hydrochloric acid and oxidizing chloride solutions, for the high-N duplex stainless steel austenite. Surface roughness influences pitting tendency as well. As pit initiation site becomes more occluded due to the higher surface roughness, so the pitting tendency increases. Increase in the surface roughness usually increases the pitting tendency, as was confirmed with studies on pit initiation [61], metastable pit transient [62], and critical pitting temperature [42].

2.5. Pitting corrosion and solution chemistry

2.5.1. Effect of Halide and Sulfur Species

Halide ions, especially chlorides are the most common cause for pitting corrosion. Chloride is ubiquitous as a process chemical or as a contaminant. A linear decrease of pitting potential with increase in log of chloride ion concentration was found for 304 stainless steel in aqueous environment [63]. A number of researchers also found that the number of pit initiation incidents increases with an increase in the chloride concentration. Presence of nitrate ions was found to inhibit chloride pitting [64].

However, nitrate ions could cause pitting and stress corrosion cracking on carbon steels in alkaline environment for nuclear applications. Nitrites, on the other hand, tend to act as inhibitor for nitrate corrosion**.**

Sulfate is also considered to be an inhibitor for chloride pitting. Sulfates were reported to inhibit pit initiation on SS304 in chloride solutions [65]. Pistorius and Burstein [66] reported that the addition of sulfates in chloride solutions decreased pit initiation sites as well as current density of pit growth, while under high potential no decrease in number of pit initiation sites were found. The addition of sulfate species does not always favor corrosion control. Moayed and Newman [39] discovered that addition of sulfates lowers the critical pitting temperature of SS904L and resulted in smaller pores in lacy pit cover. This result was confirmed with electrochemical impedance spectroscopy. They also reported that increase in either the chloride or the sulfate concentration decreases the stability of the formed passive film, reflected by the increased exchange current and critical current [67]. Deng et al. also discovered that below a concentration of 0.42%, addition of sulfate lowers the critical pitting temperature of SS 316. Ernst and Newman [68] used steel foils in their experiments and observed alteration in pit morphology with addition of sulfates, and concluded that the inhibition effect of sulfates contributed to the stabilization of pit growth by retaining pit covers (allow pits to stably grow under less current density).

Sulfide in the solution, in many cases, comes from the sulfide inclusions in stainless steels. Chemical dissolution of sulfide inclusions were monitored using AFM [69]. In this case, the molybdenum in the material binds to the adsorbed sulfur and

dissolves [70], which improves pitting resistance of the material. In sour environments of oil industry, hydrogen sulfide may react to form hydrogen atoms and cause hydrogen embrittlement in stainless steels. On the other hand, pitting forms at higher temperatures, due to the passive film breakdown and ductility recovery, the range for embrittlement shrinks.

Thiosulfate ions have been reported to activate pitting corrosion. In one study, thiosulfate together with sulfate, caused pitting in 304L [71]. In this case, sulfate, which normally would not pit the stainless steels, provides the acidity of the pit environment in the presence of thiosulfate. Sensitized 304 were found to be especially susceptible to thiosulfate pitting, while 316 showed much higher resistance [71].

2.5.2. Effect of Thiosulfate Ions on Localized Corrosion

Thiosulfate is present in many industrial process streams. Small amount of thiosulfate is introduced into paper making process, in paper-machine white water, by the use of hydrosulfite as brightening agent. In oil industry, thiosulfate may be generated due to the oxidation of sulfides. In nuclear industry, thiosulfates may also be introduced into the system from microbial activities [11][73][74].

Pitting in the presence of thiosulfate is shown to be most aggressive in papermachine white water when the molar ratio of chloride and sulfate ions is in between 10 and 30 [71][75][76]. Thiosulfate serves as an activator for the pit initiation as it can be reduced to sulfur or sulfide, which adsorbs on bare metal surface and impede repassivation [77][78]. It was argued that too much of thiosulfate, which consumes

proton in the process of being electro-reduced, may neutralize the pit. On the other hand, too little thiosulfate ions may not be enough to impede passivation and activate pitting [71]. On the other hand, small amount of chloride enhance thiosulfate adsorption, while large amount of chloride is competitive to thiosulfate adsorption [79]. Increase in temperature decreases the pitting potential and increases the most aggressive [chloride] : [thiosulfate] ratio [76]. Increase in the nickel content of the alloy lowers the pitting potential, and in most cases increases their susceptibility to thiosulfate pitting [45]. Addition of molybdenum in stainless steels was shown to increase their resistance to pitting corrosion in chloride and thiosulfate containing environment by inducing desorption of the adsorbed sulfur species [76][80]. Potentiodynamic testing of thiosulfate pitting was generally not preferred as the pit initiation process is slow, yet some useful information was still generated with the slow-scan-rate potentiodynamic testing [78][81]. Crevice corrosion of 304, 316L, and 904L was studied in 1M NaCl with and without the addition of 0.01M $Na_2S_2O_3$ [82]. Addition of thiosulfate increased penetration rate by tenfold, and the mechanism of this increase was proposed to be the formation of H_2S. It was also stated that crevice corrosion has to be able to occur without thiosulfate in order to observe this increase in corrosion rate.

Thiosulfate related pitting also occurs in nickel based alloys. It was demonstrated that while thiosulfate by itself does not cause pitting in alloy 690, the addition of 0.01M thiosulfate to 1wt% chloride solution greatly enhances pit growth [83]. Formation of nickel sulfides were found on the surface of the steel, which may be the corrosion product of pitting corrosion, since the interaction between thiosulfate and passive films

are limited. Inconel 600 was found to have lower resistance to thiosulfate-related pitting with increased chloride concentration, increased temperature, lowered pH to 3, and deoxynation [84].

2.6. Stress corrosion cracking

Another very common type of corrosion related failure found on structural materials, which is probably even more detrimental than pitting, is stress corrosion cracking (SCC). Stress corrosion cracking is a premature fracture phenomenon that involves interactions of stress, material, and environment. For stainless steel, as passive film is the reason for corrosion resistance, therefore, how passive film performs under stress and in a given environment becomes utterly important. Commonly accepted SCC mechanisms are anodic dissolution mechanism [85], film induced cleavage mechanism [86], atomic surface mobility mechanism [87], and adsorption induced embrittlement mechanism [88]. Among these mechanisms, the anodic dissolution mechanism and the film induced cleavage mechanism are closely related to passive film breakdown and repassivation. Anodic dissolution model suggests that a brittle path for stress corrosion crack is formed by repetition of repassivation and breakdown of passive film at the crack tip, and subsequent anodic dissolution. Film cleavage model, on the other hand, suggests crack propagation by fast passive film formation and the rupture of the film due to straining. In both cases, the repassivation kinetics as well as the local chemistry at the crack tip are determining factors, similar to pitting. Corrosion fatigue was also reported to be a problem in paper machine white water [89][90]. Heat treatment and

chloride addition was found to affect passivation behavior and stress corrosion cracking behavior while thiosulfate was not found to promote pitting in the specific white water range reported in the study for the heat-treated duplex stainless steel [90]. On the other hand, chloride concentration and heat treatment was found to have small influence over corrosion fatigue properties, it was argued that this may be due to the fact that exposure times for the crack tip to aggressive environment was not long enough under high cycling frequency [89].

Chloride, sulfate, thiosulfate may all lead to stress corrosion cracking of stainless steels. Increase in chloride concentration was found to lead to higher SCC tendency [91]. Stress corrosion cracking of sensitized 304 stainless steel under 250^{o}C was found to have a critical potential for intergranular stress corrosion cracking (IGSCC) that is not dependent on anion species in the environment (for either chloride or sulfate), which depends on degree of sensitization [92]. SCC was observed at 100^{o}C in chloride solutions, while in sulfate solution SCC did not occur up to 0.4V_H. SCC was found in solution containing dilute sulfate and thiosulfates only when repassivation in simulated crack tip solution is slow, addition of sufficient sulfate in this environment eventually inhibit SCC [93]. Similar to pitting, initiation, temporary propagation, and repassivation of microcracks come before the initiation of a propagating crack in dilute thiosulfate solutions [94]. Once a microcrack repassivates, it does not re-initiate [95]. It was suggested that thiosulfate penetration along grain boundaries occur even without loading, and that tensile loading accelerates this process [96].

It is believed by many researchers that the repassivation rate plays an important role

in determining stress corrosion cracking susceptibility [95][98][99][100][101]. Scully discussed the relationship between strain rate and repassivation rate of an alloy [102]. It was argued that crack arrest results from a small strain rate to repassivation rate ratio. This ratio may also determine crack morphology and crack velocity.

2.7. Gaps in Understanding the Role of Thiosulfate in Localized Corrosion

Duplex stainless steels are being used in thiosulfate containing environments. However, there is currently no phenomenological studies nor mechanistic understanding concerning the effect of thiosulfate on pitting corrosion of duplex stainless steels.

Metastable pitting of austenitic stainless steels and duplex stainless steels was not studied before. The role of thiosulfate on pit initiation and metastable to stable pit transition was not understood, which plays a vital role in pitting corrosion in environments containing thiosulfates.

The interactions between thiosulfate and individual alloying elements was not investigated. The study of these interactions helps further the understanding of the effect of thiosulfate in pitting corrosion.

Effect of thiosulfate on repassivation kinetics of stainless steels has not been studied nor published in open literature. Since thiosulfate has a strong interaction with bare alloy/metal surface, and that the addition of thiosulfate to chloride containing environment causes stress corrosion cracking of stainless steels, it should influence the repassivation kinetics of stainless steels.

3. EXPERIMENTAL PROCESURES

3.1. Materials and sample design

Materials used in the research were machined from wrought stainless 304L and 316L plates with the thickness of 3mm and wrought duplex stainless steels 2101 and 2205 plates with the thickness of 1cm. The chemical composition of the materials is given in Table 3.1.

Table 3.1. Chemical composition of steels used in this study

	304L	316L	2101	2205
UNS number	304L	316L	2101	2205
Fe (%)	Bal.	Bal.	Bal.	Bal.
C (%)	0.01	0.02	0.024	0.021
Mn (%)	1.91	0.97	5.07	1.53
P (%)	0.031	0.024	0.017	0.028
S (%)	0.013	<0.005	0.001	<0.005
Si (%)	0.44	0.59	0.69	0.48
Cr (%)	18.0	17.6	21.36	22.6
Ni (%)	8.1	11.4	1.49	5.78
Co (%)	–	–	0.03	–
Mo (%)	0.35	2.2	0.3	3.07
Cu (%)	0.35	0.29	–	0.36
N (%)	–	–	0.23	–
Al (%)	0.008	0.011	0.008	0.008
V (%)	0.07	0.07	–	0.06

The steels used in this study were selected as these are some of the most common grades used in the chemical process industry. The duplex stainless steels have relatively higher chromium and lower nickel content compared to the austenitic stainless steels selected for this study. Alloys 2205 and 316L have much molybdenum content than 2101 and 304L. Microstructures of the stainless steels are shown in Figure 3-1.

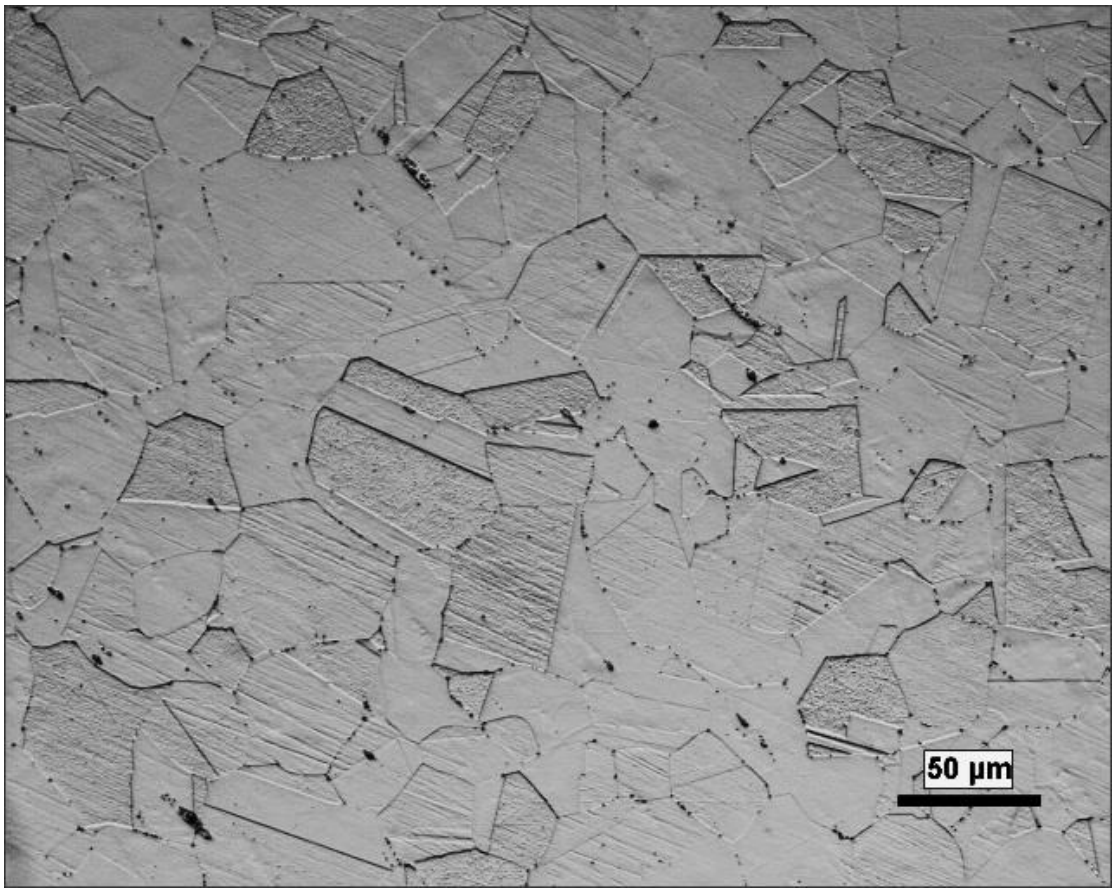

(a)

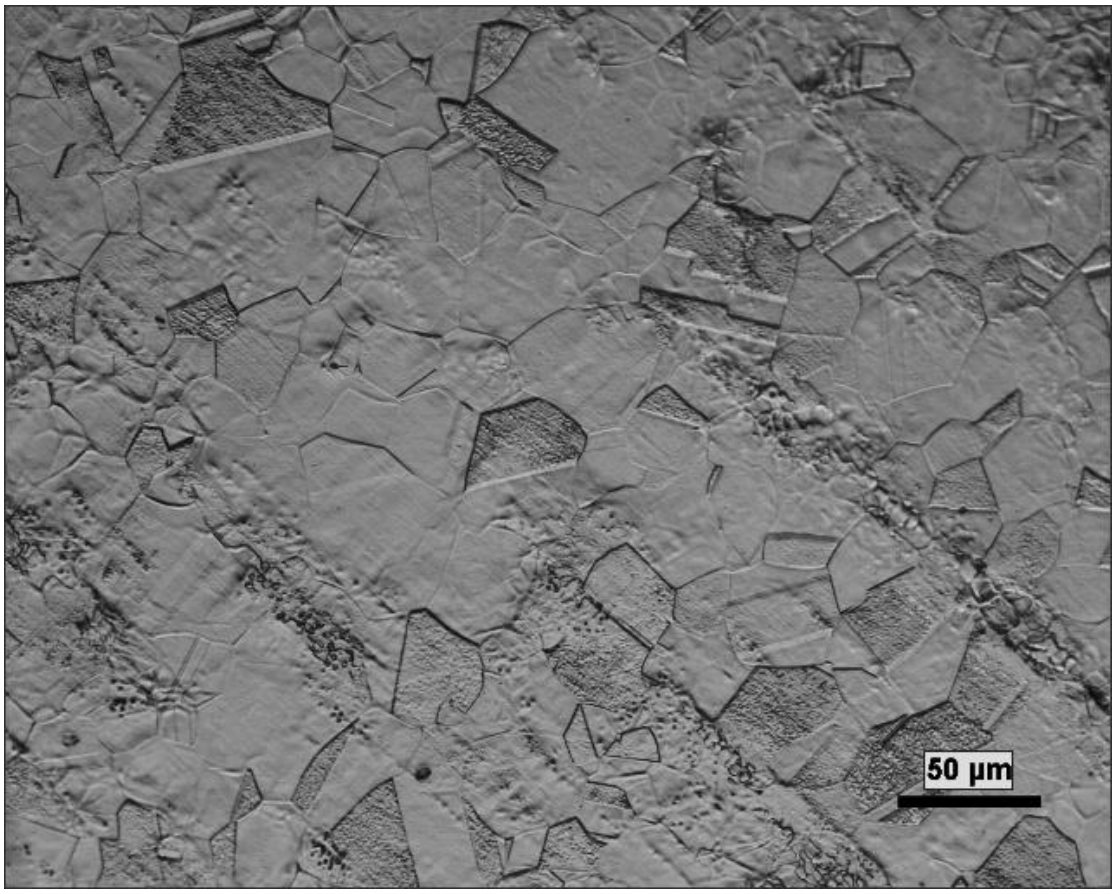
50 µm

(b)

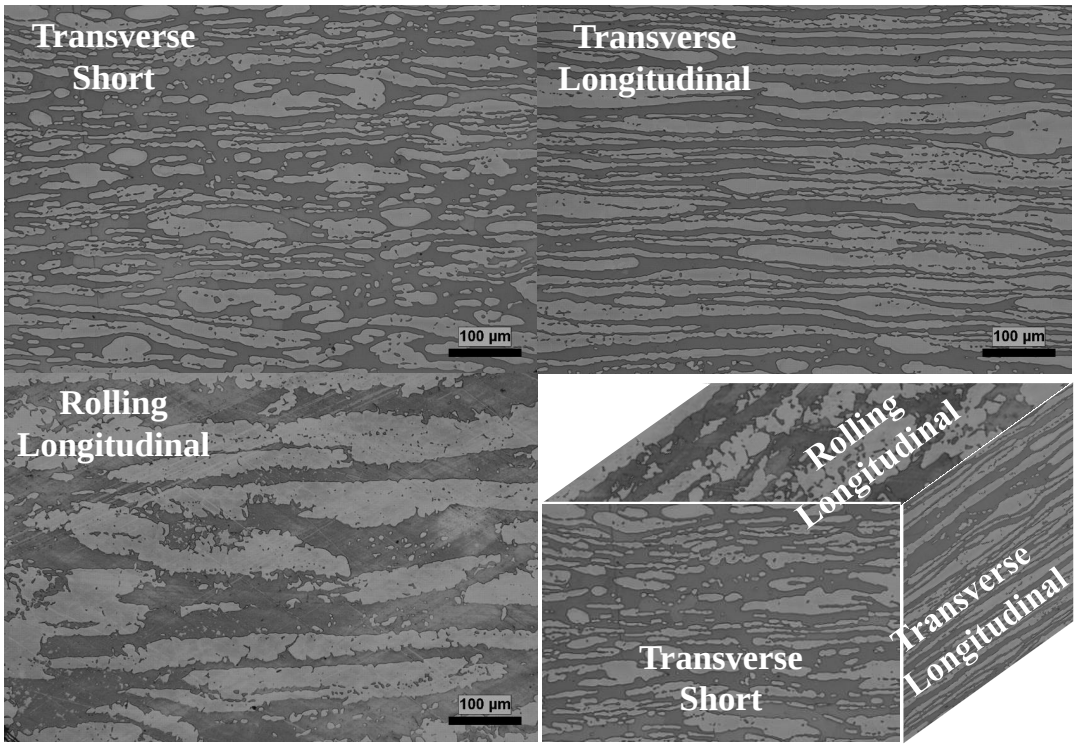
Transverse
Short
100 µm
Transverse
Longitudinal
100 µm
Rolling
Longitudinal
100 µm
Rolling
Longitudinal
Transverse
Short
Transverse
Longitudinal

(c)

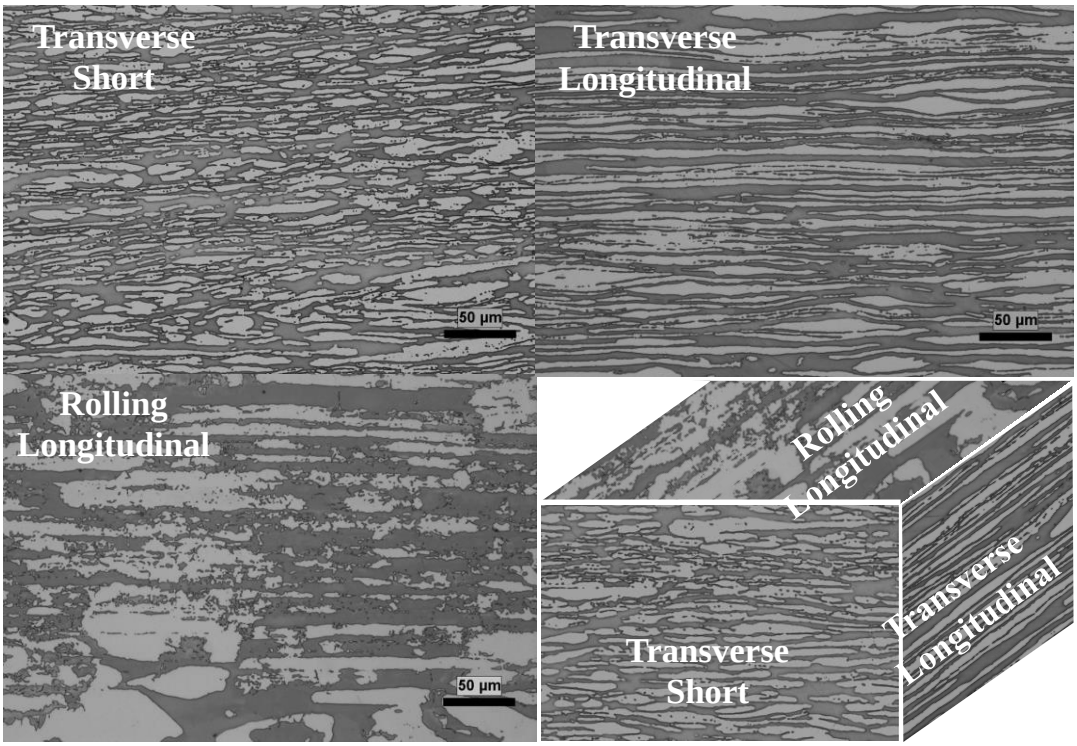

(d)

Figure 3-1 Microstructures of the stainless steels used in the study

(a) 304L (b) 316L (c) 2101 (d) 2205

3.2. Sample Preparation for Metallography and Electrochemical Tests

Alloy samples for metallography and electrochemical tests were sectioned in specific orientation and were mounted in cold-set epoxy molds. Grinding of epoxy mounted specimens were carried out on an ECOMET 6 variable speed grinder-polisher. Surfaces of all electrochemical test specimens were ground from 120 grit sandpaper to 2000 grit sandpaper, unless stated otherwise. The specimens were rinsed with deionized water and then ethanol, and blew dry with air. For metallography, specimens were ultrasonically cleaned in ethanol and further polished in a VIBROMET 2 vibratory polisher with 0.05 micron alumina powder to a mirror finish. Austenitic stainless steels

were etched in 10% oxalic acid solution at 10V whereas duplex stainless Steels were etched in 40% NaOH solution at 2.5V. The darker phase observed under the optical microscope after etch in the duplex stainless steels is the ferritic phase while the lighter phase is austenite.

3.3. Cyclic Potentiodynamic Polarization Tests

One of the most common types of accelerated electrochemical test for evaluation of localized corrosion or pitting resistance of alloys is the cyclic potentiodynamic polarization test. In this test, the electrochemical potential of the alloy sample in a given environment is swept within a range of potentials and the resulting changes in the current are recorded. The potential is essentially the driving force for localized corrosion, while the current indicates the kinetics of the corrosion reactions involved. Pitting potential corresponds to the potential value at which the current increases abruptly upon anodic potential scan. The higher the pitting potential, the higher the driving force required for the pits to initiate on the alloy, and therefore the more resistance to pitting corrosion the material has in the given environment. A typical polarization curve for cyclic potentiodynamic polarization measurement is shown in Figure 3-2.

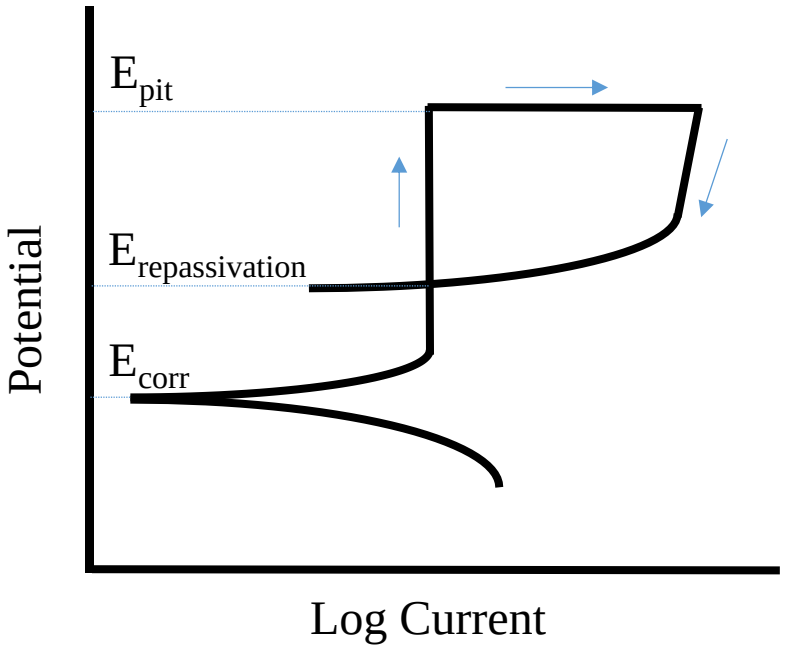

Figure 3-2. A schematic of typical cyclic potentiodynamic polarization curves for specimens with localized corrosion

In cyclic potentiodynamic polarization, the potential sweep is reversed when potential reaches a certain value, or current, if localized corrosion occurs on the test specimen. In the case of pitting corrosion, the potential of the point at which the current abruptly increases is called pitting potential. The current increase in due to clustering of metastable pits or growth of a stable pit. Since an aggressive environment is established locally, the potential required for repassivation of the pits are usually more negative than the pitting potential, depending on how large the established pit is. The repassivation potential is defined as the potential of the point at which the hysteresis loop closes. The higher the repassivation potential is, the higher the tendency for a pit to repassivation, which means higher pitting resistance. A standard three electrode

system with a working electrode, counter electrode, and a reference electrode was used for cyclic potentiodynamic polarization tests. The image and schematic of the experimental set-up is shown in Figure 3-3.

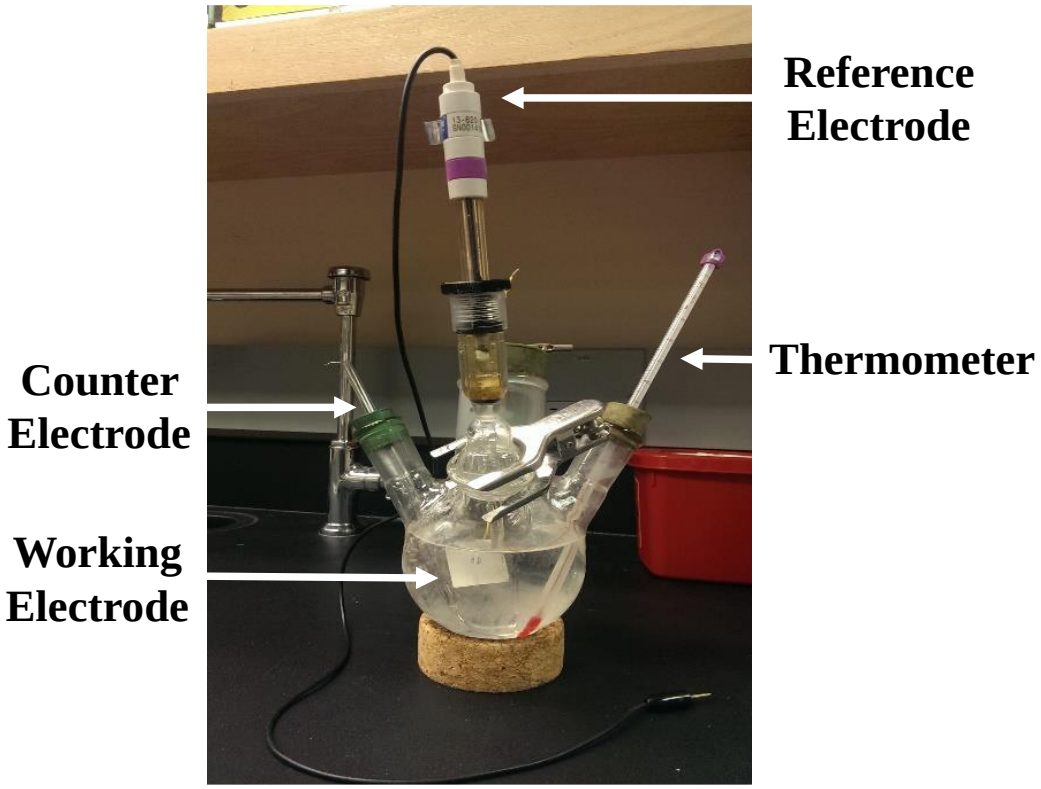

Figure 3-3. The three electrode system set-up

The stainless steel samples were cut using either an abrasive high-speed saw or a diamond low-speed saw into small specimens with the size of approximately 1cm×1cm×3mm. For electrochemical tests that require electrical connection, stainless steel wires were spot weld onto the back of the specimens. The welded specimens were encapsulated in epoxy resin to ensure electrical insulation, leaving only the 1cm×1cm surface of the alloy exposed. The mounted and polished sample was then masked with

the electroplating tape with a 0.1256cm^2 punch hole, to avoid the occurrence of crevice corrosion in the crevice formed between the sample and the epoxy, as shown in Figure 3-4.

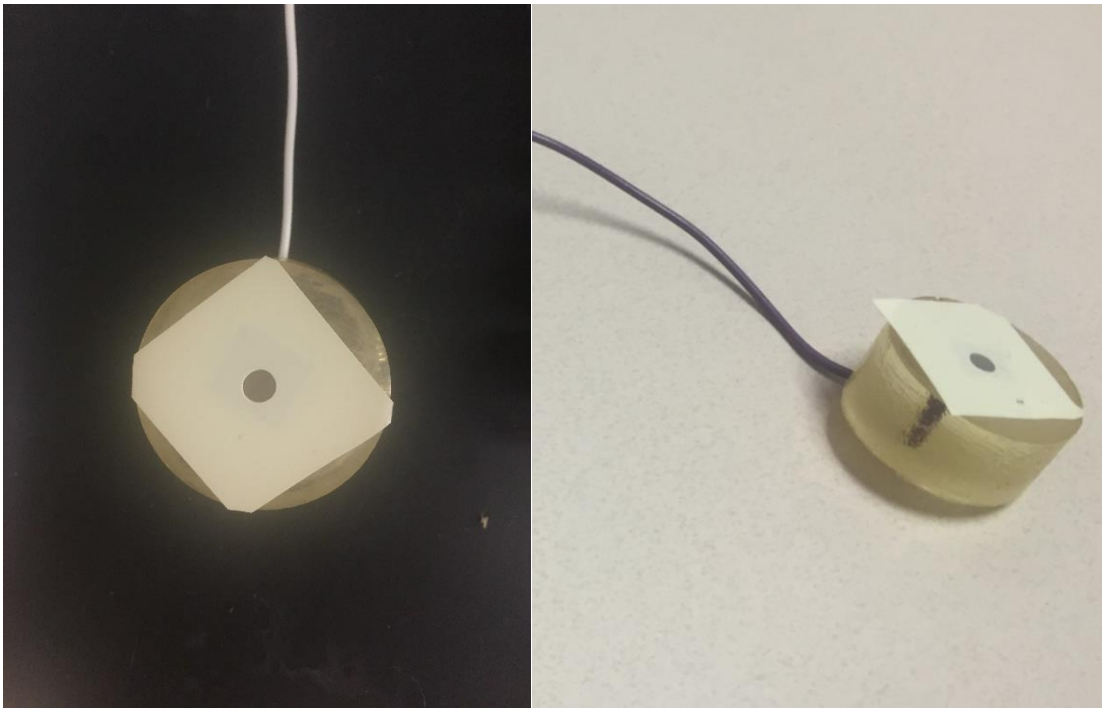

Figure 3-4. Samples with electrical connection

For all cyclic potentiodynamic polarization tests, solutions were made with deionized water and analytical grade NaCl, Na_2SO_4, and $Na_2S_2O_3$. In chloride containing environment, required pH was obtained by addition of hydrochloric acid (NaCl is added after excluding the concentration of Cl^- from the target concentration) or NaOH. If the required testing temperature was not ambient, the solution was left in a water bath for at least 30min until the target temperature was reached before the experiment. The potential scan was typically from -0.6V vs. SCE to 1.2V vs. SCE, or

when the current reached 25μA, and back to -0.6V vs. SCE. Forward scan rate was 0.1mV/s, so that pitting at lower potentials that required formation of reduced sulfur species could be measured without error. Backward scan rate was 1.5mV/s to avoid excessive growth of pits.

3.4. Potentiostatic Polarization Tests

3.4.1. Tests to Study Metastable Pitting

To study the effect of potential on corrosion behavior of materials, potentiostatic polarization tests (chronoamperometry) were carried out. In these tests, applied potential is set to 0V vs. SCE, the current change with time were recorded. These tests are used in this study to monitor the metastable pitting behavior of the stainless steels. The sampling rate was set to 50Hz.

The potentiostatic polarization tests to study metastable pitting were carried out in a standard electrode system in a round bottom flask. Specimen design was same with potentiodynamic polarization measurements.

3.4.2. Potentiostatic Scratch Tests

Thiosulfate is known to be much more interactive with bare metal surface than passive surfaces of the stainless steels. Therefore, scratch tests were designed where mechanical scratches were made to disrupt the passivity of the stainless steel so that the interaction between thiosulfate and the bare metal surfaces can be observed. Meanwhile, the specimens were under potentiostatic polarization. The current transient was

recorded after the scratch. Information regarding the repassivation kinetics as well as the pit growth kinetics is contained within the current transient data.

For all scratch tests, specimens were made in a similar fashion to the polarization tests described earlier. A side hole was drilled and tapped in the epoxy, so that a bolt could be attached into the hole to fasten the specimen for a stable scratch test. For pit growth kinetics, the 3mm×1cm side was exposed, so that a scratch could be made in milliseconds across the thickness of the metal specimen, leaving a scratch with the length of 3mm. For repassivation kinetics, since a longer scratch time duration may interfere with the short repassivation time span and have a negative effect on the data analysis, the specimen is ground to a thickness of 200μm.

The potentiostatic scratch test set-up is shown in Figure 3-5.

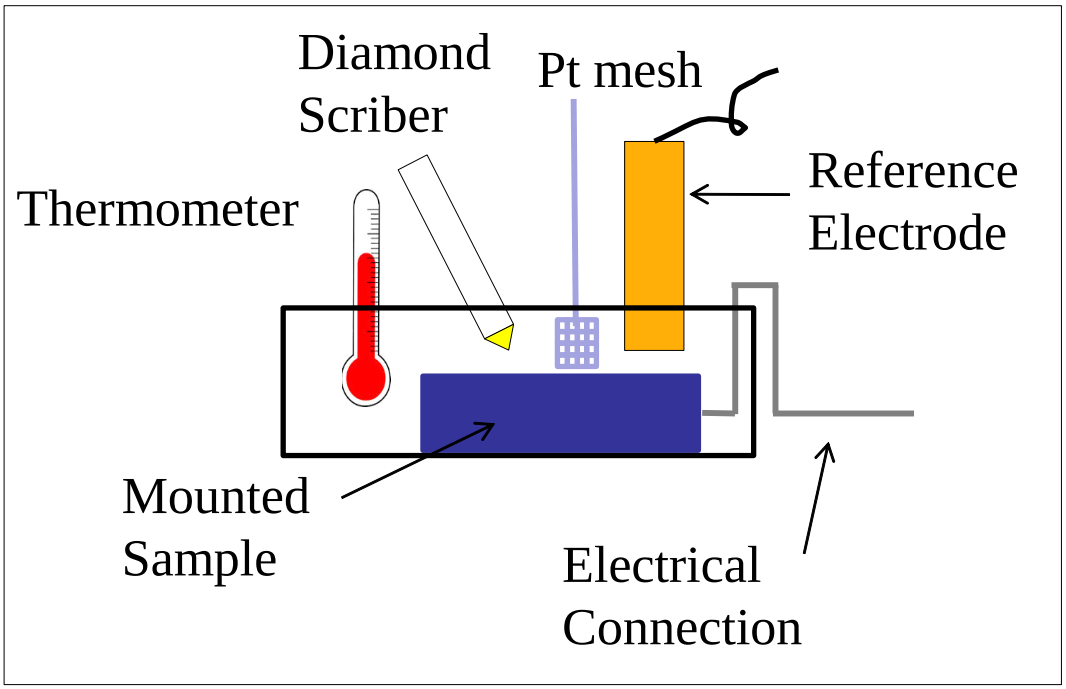

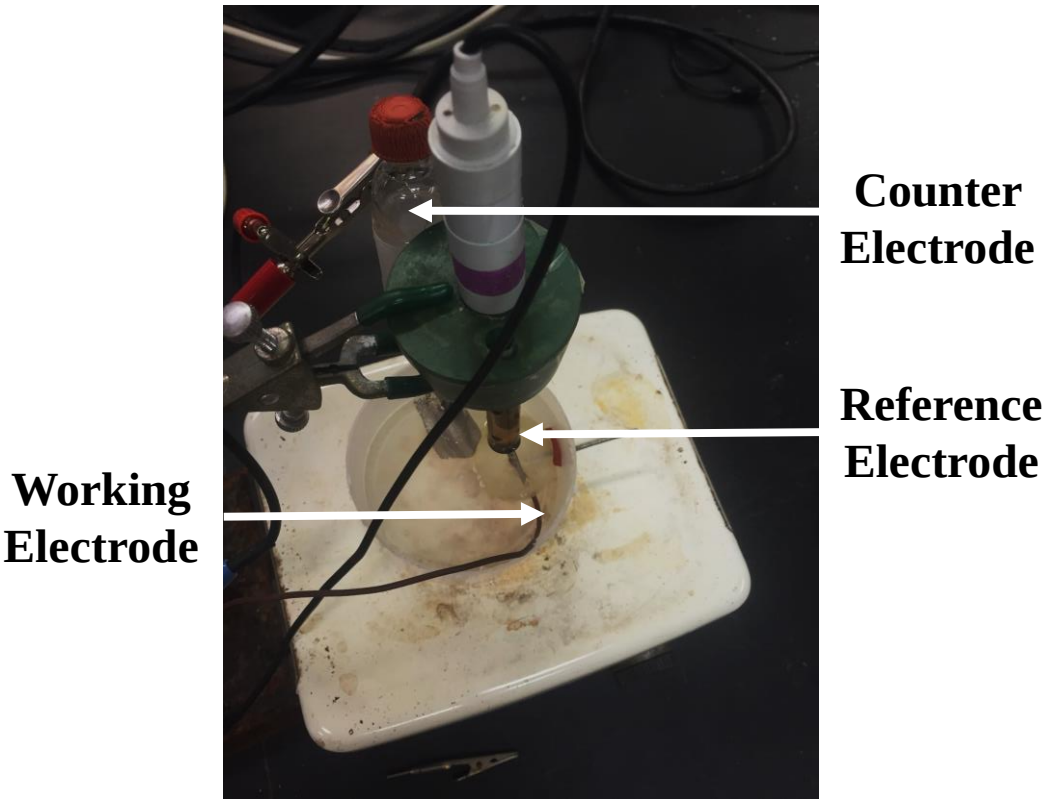

Figure 3-5. Schematic and photo of the scratch test set-up

3.5. Chemical and Physical Characterization Methods Used

Microstructures and surface corrosion attack was observed and characterized using both optical and scanning electron microscopes (SEM). Optical images were taken using a Nikon Optishot-2 optical microscope after the polarization tests to observe the extent and morphology of corrosion pits. A Zeiss Ultra60 FE-SEM with an Energy Dispersive Spectroscopy (EDS) system was used to characterize the morphology of the pits and perform chemical analysis on the corrosion products.

Detailed chemical analysis of the corrosion products was carried out with a Thermo K-Alpha XPS system. The specimen was polarized while the surface of sample was scraped (scratched) using a ceramic rod, so that the bottom of the (~50 to 100 micron)

wide scratch would be approximately flat. Polarization was continued for another 10 min after the scraping to allow either the passive film to grow or for the corrosion pit to grow to large size for further chemical characterization. The metal specimen was removed from the epoxy resin and left in a vacuum chamber for 1 hour. A brief ion etching was carried out before XPS analysis to remove the possible contamination on the surface of the specimen. Details of the XPS analysis and other characterization methods is discussed in details in Chapter 8.

4. PHENOMENOLOGICAL STUDY OF PITTING IN PAPER MACHINE WHITE WATER

Pitting in papermachine white water environment was first discovered in the 1980s when bisulfite was added as a bleaching agent [11]. Papermachine white water refers to the aqueous environment in the wet-end of paper machine where the stock-making water is removed through a series of forming and press sections to turn a wet web of fibers into dry paper, as shown in Figure 4.1.

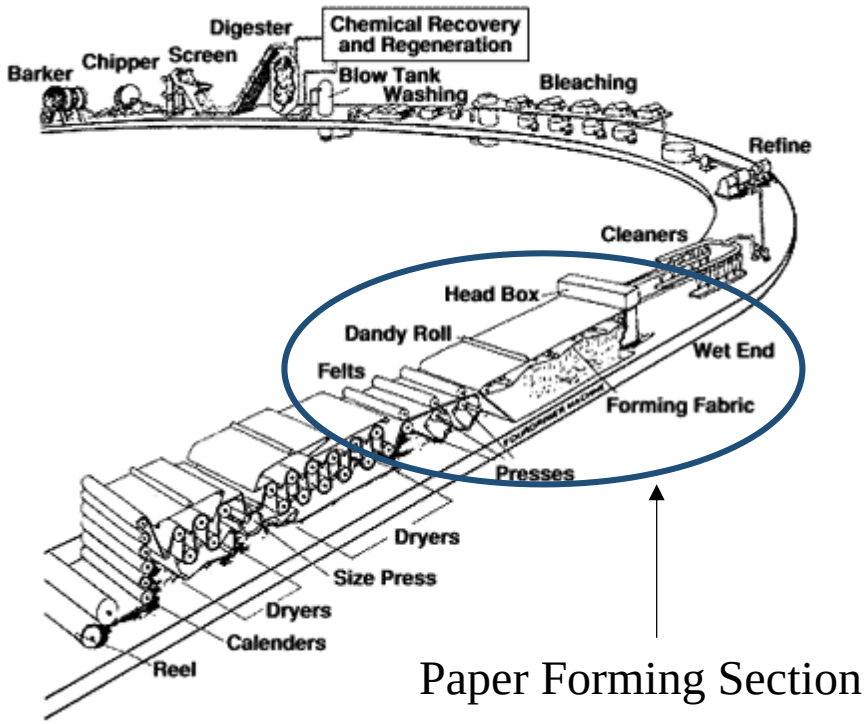

Figure 4.1. Schematic of the paper production process

The main reason for pitting of stainless steel equipment was discovered to be the presence of thiosulfate in the white water, which is a by-product of bisulfite. A typical range of white water chemistry in different mills or different parts of a mill is given in Table 4-1.

Table 4-1. Typical white water composition range of interest

White Water Environmental Parameter	Typical Range in Paper Mills
Temperature	40 – 60 ℃
Cl^-	10 – 500 ppm
SO_4^{2-}	200 – 1000 ppm
$S_2O_3^{2-}$	0 – 30 ppm

In this chapter, the effect of temperature, pH, and concentrations of chloride, sulfate, and thiosulfate on pitting corrosion was investigated for austenitic stainless steels 304L and 316L, and duplex stainless steels 2101 and 2205. The phenomenological study for these materials is a good starting point for the investigation of the role of thiosulfate on pitting corrosion in these stainless steels, and the interaction between thiosulfate and individual alloying elements of the stainless steels.

4.1. Effect of Thiosulfate Concentration

Effect of chloride and sulfate concentrations on pitting has been studied by other groups in the past few decades [46][103]. In this study, we focused on the effect of thiosulfate (in typical papermachine white water range) on pitting corrosion of stainless

steels. .

To observe the effect of sulfate ions on pitting corrosion, two different baseline solution compositions were used, baseline solution-1 with only chlorides and the baseline solution-2 contained both chlorides and sulfate ions. Incremental amounts of thiosulfates were added to these solutions. The concentrations were chosen such that they represent a range of white water compositions. The chloride concentration [Cl^-] was fixed to 300ppm ($8.45*10^{-3}$mol/L) in this study. Sulfate concentration [SO_4^{2-}] was 600ppm ($6.25*10^{-3}$mol/L). Experiments were carried out in the two series of environments (with and without sulfate ions) with addition of different concentrations of thiosulfate ions. Thiosulfate concentration were chosen as such that ([Cl^-] + [SO_4^{2-}])/[$S_2O_3^{2-}$] ratios were the same in the two series of environments. Selected duplex as well as austenitic stainless steels were tested in different simulated white water environments with cyclic polarization tests. In the cyclic polarization tests, alloys that are susceptible to the pitting corrosion exhibit a hysteresis in their polarization curve. The experimental results for the localized corrosion susceptibility of tested alloys in different environments are summarized in

Table 4-2 and Table 4-3, four to ten experiments were carried out for each environment/material combination.

Table 4-2. Localized corrosion susceptibility from the cyclic polarization tests in Baseline solution-1 (300 ppm Cl^-) with different concentrations of thiosulfate added

Test Environment	Localized Corrosion			
	Austenitic Stainless Steels		Duplex Stainless Steels	
	304L	316L	2101	2205
Baseline Solution-1	Yes	Yes*	Yes	No
Baseline Solution-1 + 29ppm $S_2O_3^{2-}$	Yes	Yes*	Yes	No
Baseline Solution-1 + 58ppm $S_2O_3^{2-}$	Yes	Yes*	Yes	No
Baseline Solution-1 + 116ppm $S_2O_3^{2-}$	Yes	No	Yes	No

* - Hysteresis not observed on all tested samples.

Table 4-3. Localized corrosion susceptibility from the cyclic polarization tests in Baseline solution-2 (300 ppm Cl^- + 600 ppm SO_4^{2-}) with different concentrations of thiosulfate added

Test Environment	Localized Corrosion			
	Austenitic Stainless Steels		Duplex Stainless Steels	
	304L	316L	2101	2205
Base Solution-2	Yes	No	No	No
Base Solution-2 + 50ppm $S_2O_3^{2-}$	Yes	No	Yes*	No
Base Solution-2 + 100ppm $S_2O_3^{2-}$	Yes*	No	No	No
Base Solution-2 +	Yes*	No	No	No

200ppm $S_2O_3^{2}$				

* - Hysteresis not observed on all tested samples.

Comparing results in

Table 4-2 and Table 4-3, it is clear that the pitting tendency is generally lower for the tested stainless steel specimens in the presence of sulfate. A previous study showed that in a solution with sulfate and thiosulfate, pitting can occur on stainless alloys, where sulfate plays a similar role as chloride [71]. In this case, however, it is probably due to the difference in the degree of hydrolysis or solubility between chlorides and sulfates that caused this decrease in pitting tendency. Molybdenum containing alloys 316L and 2205 have higher corrosion resistance than the other grades tested. The effect of thiosulfate in baseline-1 solution for 304L is shown by three cyclic polarization curves in Figure 4-1. Open circuit potential decreases with the addition of thiosulfate, indicating a destabilized passive film. In the presence of thiosulfate, once pitting corrosion occurs, the repassivation potential decreases significantly. The addition of sufficient amount of thiosulfate ions seem to suppress pitting corrosion susceptibility, as shown by the cyclic polarization results for 304L in baseline solution-1 (300ppm Cl^-) by addition of 1000ppm $S_2O_3^{2-}$ions.

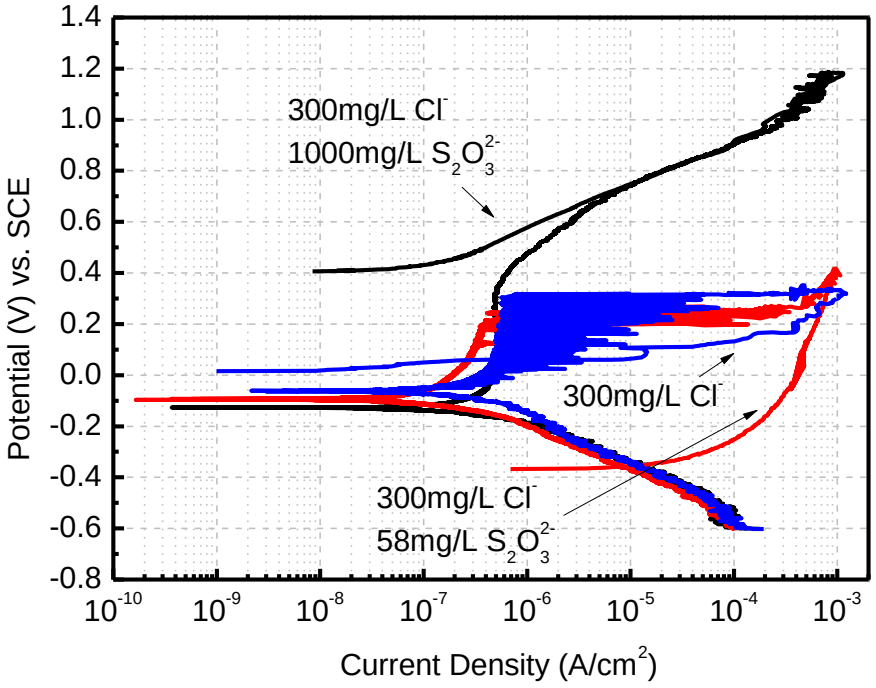

Figure 4-1. The Effect of Thiosulfate in Cyclic Polarization Tests of 304L

All specimens of non-molybdenum containing stainless steel grades, 304L and 2101, showed localized corrosion in the baseline solution-1. Pitting potential, repassivation potential, as well as open circuit potential values for 304L and 2101 in these environments were compared and the results are shown in Table 4-4.

Table 4-4. Pitting/Repassivation/Corrosion Potential of 304L and 2101 Specimens Tested in Baseline Solution-1 with Addition of Thiosulfate Ions

	304L						2101					
	Pitting Potential (mV)		Repassivation Potential (mV)		Corrosion Potential (mV)		Pitting Potential (mV)		Repassivation Potential (mV)		Corrosion Potential (mV)	
	Avg	SD	Avg	SD	Avg	SD	Avg	SD	Avg	SD	Avg	SD
Baseline Solution-1	302	11	106	35	-72	15	441	96	66	35	-101	24
Baseline	349	67	-79	176	-87	4	377	27	-185	144	-109	22

Solution-1 + 29ppm $S_2O_3^{2-}$												
Baseline Solution-1 + 58ppm $S_2O_3^{2-}$	275	116	-303	34	-98	10	453	210	-441	5	-125	20
Baseline Solution-1 + 116ppm $S_2O_3^{2-}$	217	59	-265	79	-99	8	418	329	-437	14	-145	21

With the addition of thiosulfate to the baseline solution-1, corrosion potential gradually decreased for both 304L and 2101. Pitting potential peaked at thiosulfate concentration of 29ppm and then decreased with further increase for 304L. A possible explanation for this is that presence of small amount of thiosulfate causes competition in adsorption of chloride ions, and reduced chloride pitting tendency. Further addition of thiosulfate is inhibiting the repassivation process, which made metastable pits stable at lower potentials, resulting in an earlier stabilization of metastable pits during the anodic polarization scan. Changes in pitting potentials due to the addition of thiosulfate were not definitive for 2101. Repassivation potential decreased with addition of 58ppm of thiosulfate ions but increased with further addition. The increase could be attributed to higher concentration of thiosulfate, reduction of which buffered the pit solution, according to earlier research [72][77]. Note that duplex stainless steel 2101, with higher chromium content, tends to have a higher pitting potential and a lower repassivation potential than 304L. SEM images of pits formed in base solution-1 and base solution-1 with 58ppm $S_2O_3^{2-}$ are shown in Figure 4-2.

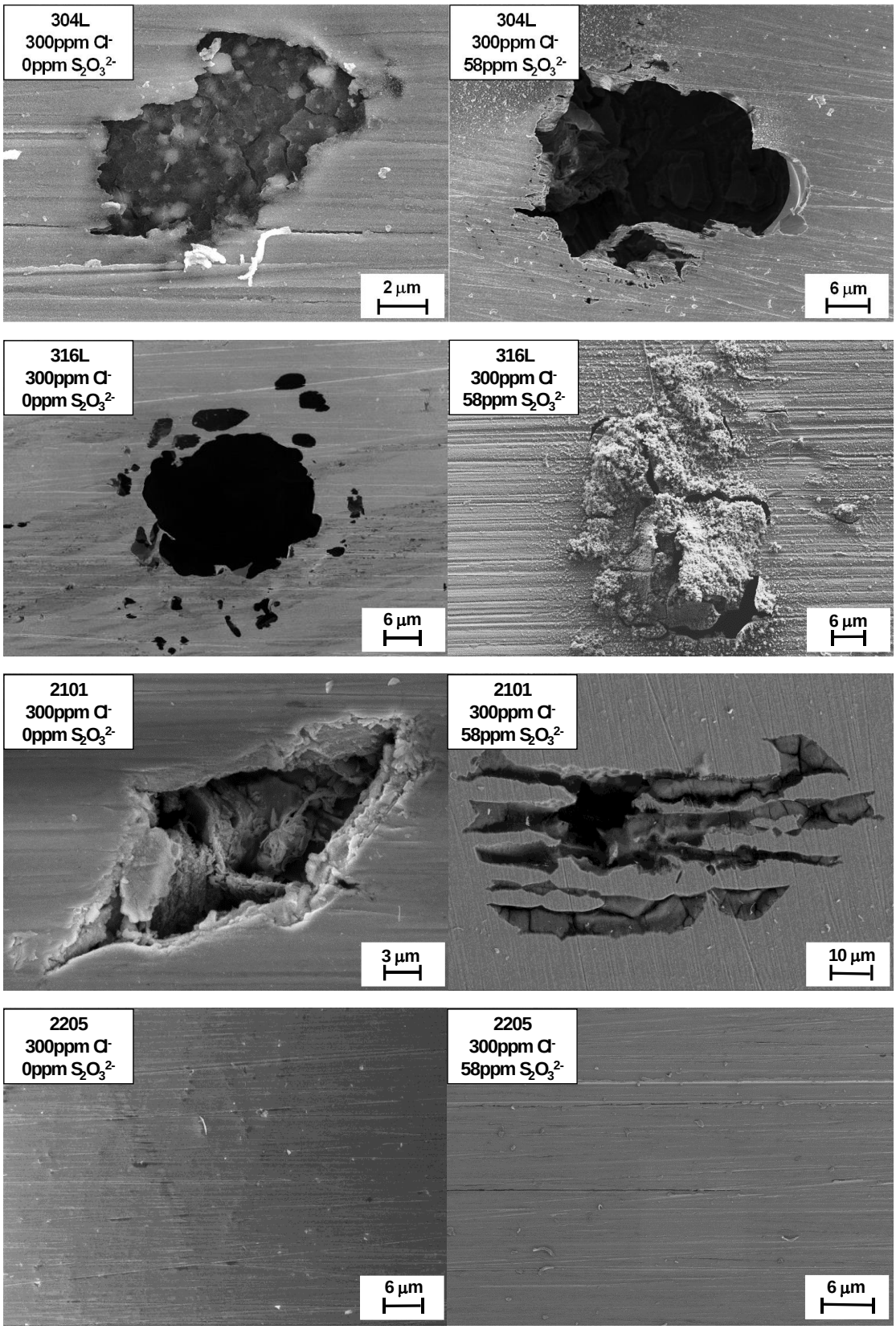

Figure 4-2. SEM image of pits formed on 304L, 316L, 2101 and unattacked surfaces for 2205 after cyclic polarization tests in base solution-1 and base

solution-1 with 58ppm $S_2O_3^{2-}$

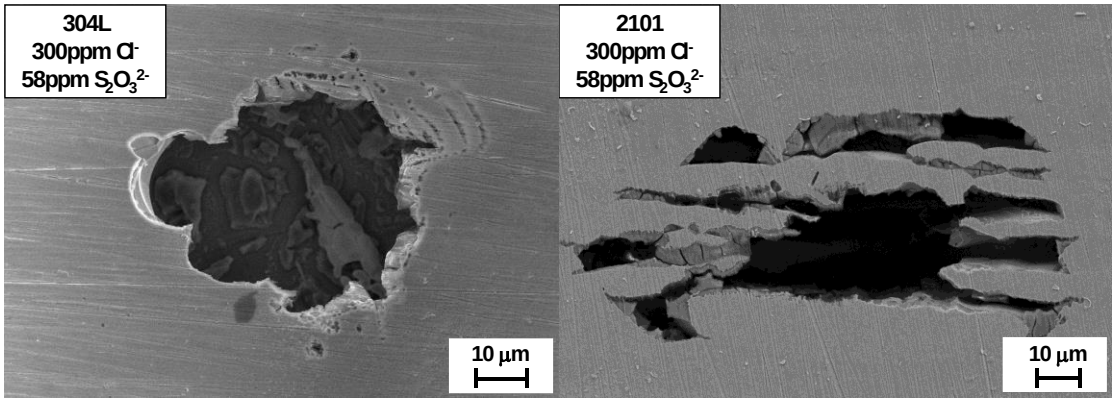

Figure 4-3. SEM image of pits formed on 304L and 2101 in base solution-1 with 58ppm $S_2O_3^{2-}$ after sonication

No pitting corrosion attack was detected for DSS2205 alloy surfaces in either of the tested environments. Pits formed during the polarization tests in thiosulfate containing environments are larger than those in chloride-only environment, due to longer growth time caused by the lower repassivation potentials. Corrosion products built-up can be observed for pits formed in thiosulfate containing environments, as shown in Figure 4-3.

The morphology of the pits for the austenitic stainless steels is quite different from the duplex stainless steels, as shown in Figure 4-3. For austenitic stainless steels, lacy pits formed on all specimens. The morphology of the pit formed on 304L is similar to what has been earlier reported [78], as can be observed in Figure 4-3. The pit formed on 2101, on the other hand, has a preferential orientation which aligns with the rolling

direction. It was found in an earlier study that the ferritic phase undergoes preferential dissolution in duplex stainless steels in near-neutral environment with 0.6M NaCl and 0.03M $Na_2S_2O_3$ [104]. Similar phenomenon was also observed in this study in dilute solutions containing chloride and thiosulfate ions, as is shown in Figure 4-3.

EDS analysis on pits formed in 300ppm Cl^- + 58ppm $S_2O_3^{2-}$ solution for 304L and 2101 is shown in Figure 4-4 and Figure 4-5, respectively.

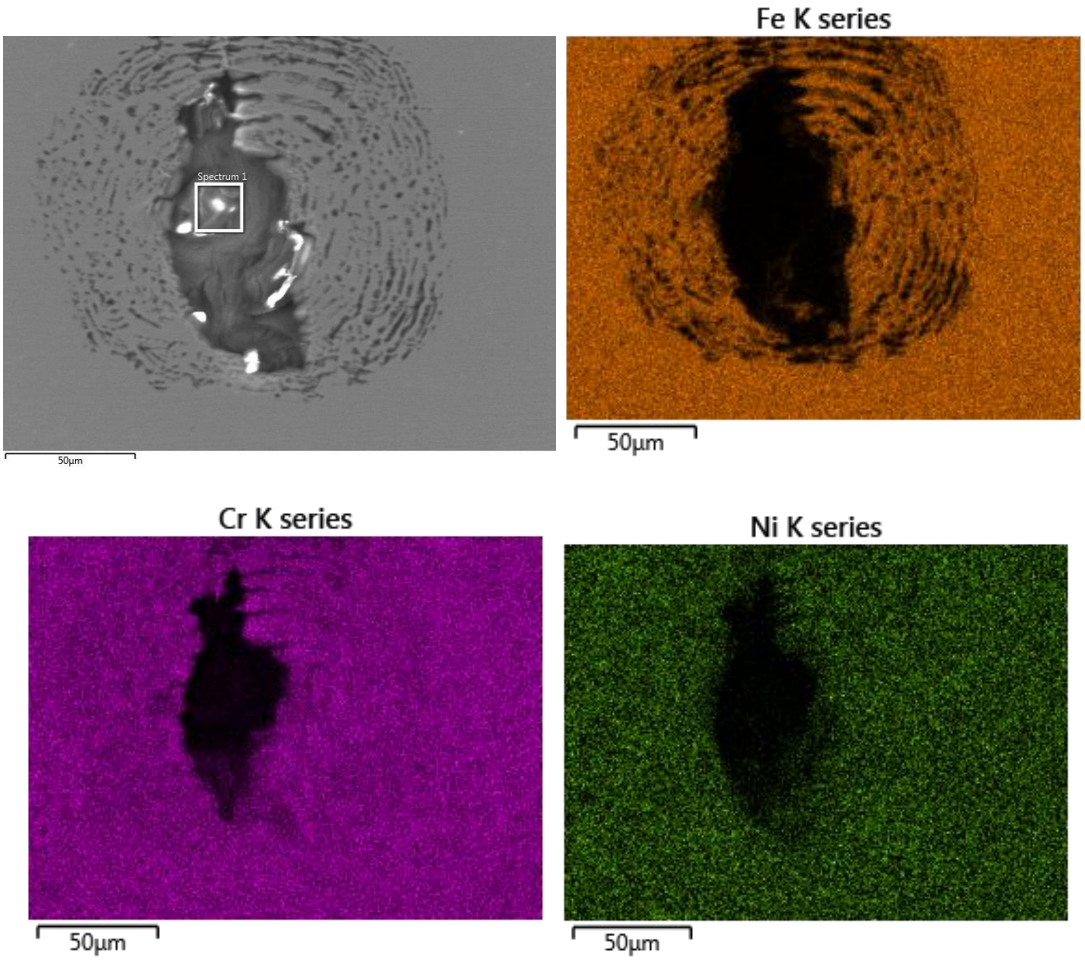

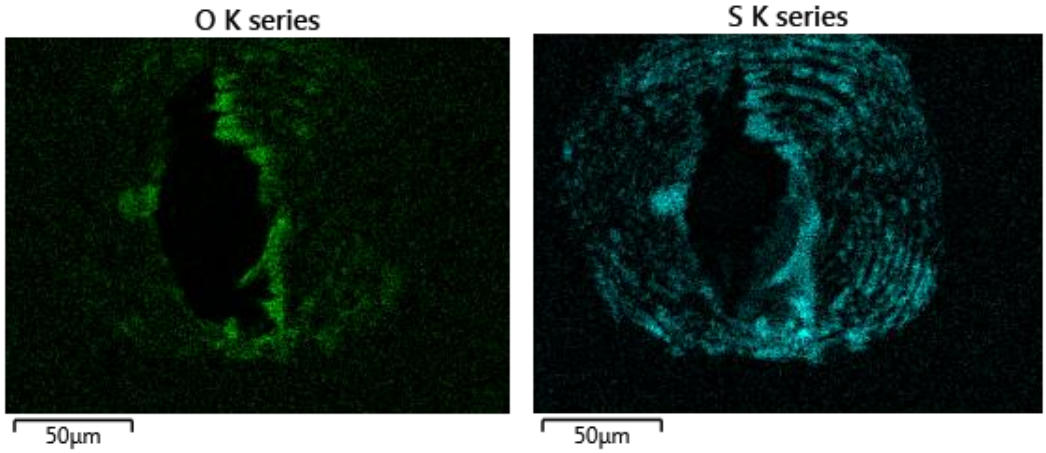

Figure 4-4. EDS of pits formed on 304L in 300ppm Cl^- + 58ppm $S_2O_3^{2-}$ solution

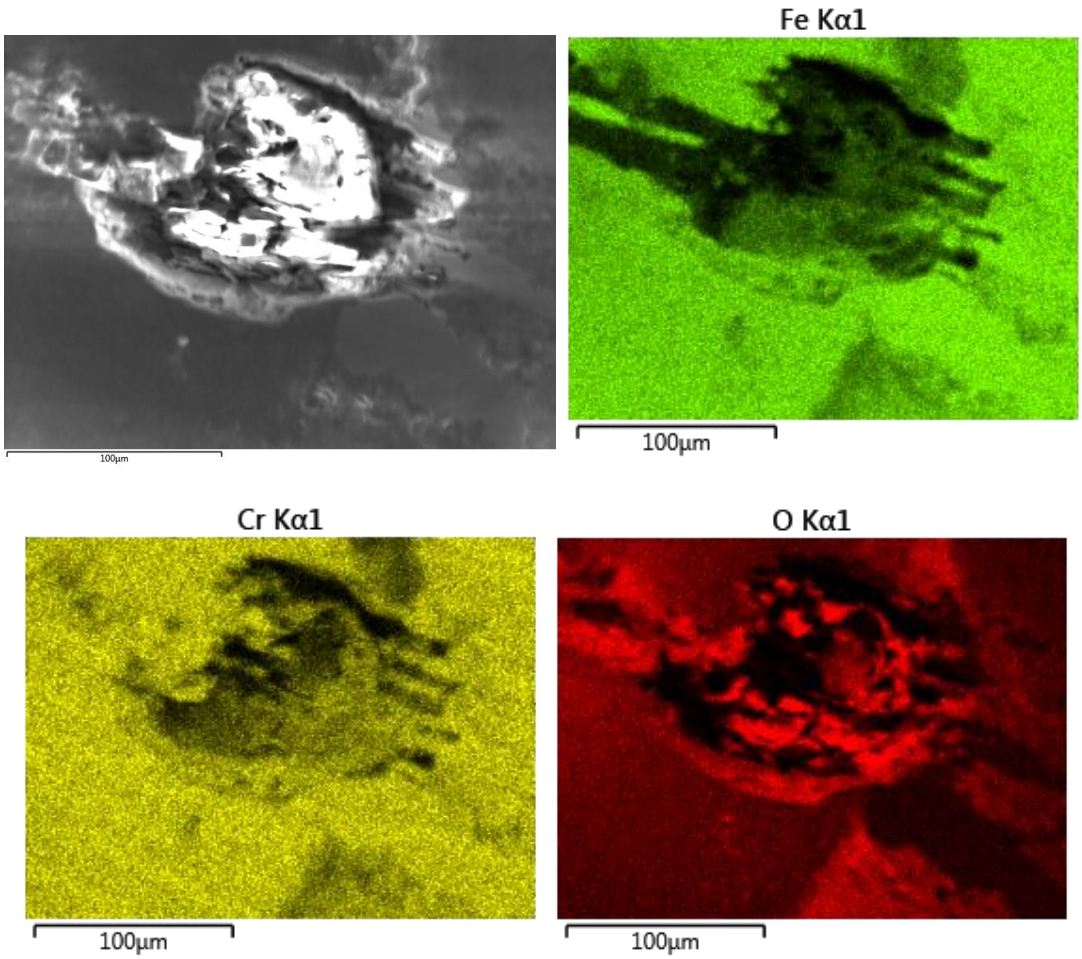

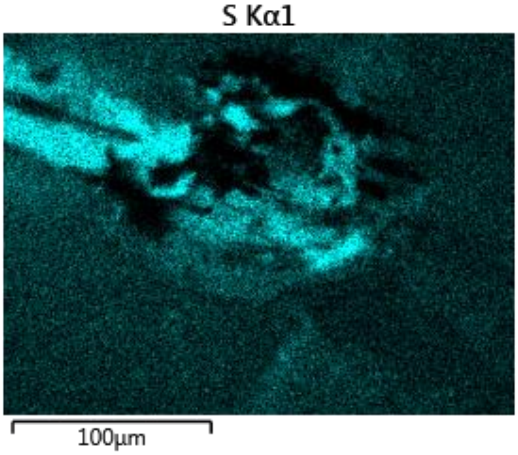

Figure 4-5. EDS of pits formed on 2101 in 300ppm Cl^- + 58ppm $S_2O_3^{2-}$ solution

A clear enrichment of sulfur element on the oxide pit cover was observed for both 2101 and 304L. However, it is hard to tell whether it is due to the adsorption of corrosion product on the porous oxide film or formation of sulfur species on the film during pitting process.

4.2. Effect of pH on Pitting Corrosion

Chemical process variations in paper making process produce differences in the paper-machine white water, which also includes pH. Pitting tendency may vary a lot due to differences in pH values of the environment, which has impact on the pitting process as well as the behavior of individual alloying element. Typical white water has a pH value in the range of 5 to 8. In this study, we varied the pH from 3 to 10, to investigate how pH affects the pitting behavior or the two more susceptible alloys, 304L and 2101. The testing environment for this study contained 300ppm Cl^- and 58ppm $S_2O_3^{2-}$. The pH adjustments were made with hydrochloric acid and the amount of NaCl was changed to keep the same Cl^- concentration in each test condition. The pH of the basic environment were adjusted with NaOH.

All the reported potentials here are pitting potentials except for the 304L at pH of 10, which is the potential for crevice corrosion. It was observed during the course of this research that usually the less aggressive the environment is, higher the tendency for crevice corrosion to show up. This is probably due to the longer diffusion path for the crevice corrosion, which results in a lower tendency to repassivate.

The pitting and the repassivation potential from various experiments in solutions with different pH are given in Figure 4-6. At least 3 experiments were carried out for the same environment/material combination. Error bar for these results are also included. Error bars in this thesis should be treated as the scattering of the experiment results, but not a reflection of where the pitting potentials of these material in these environments should be.

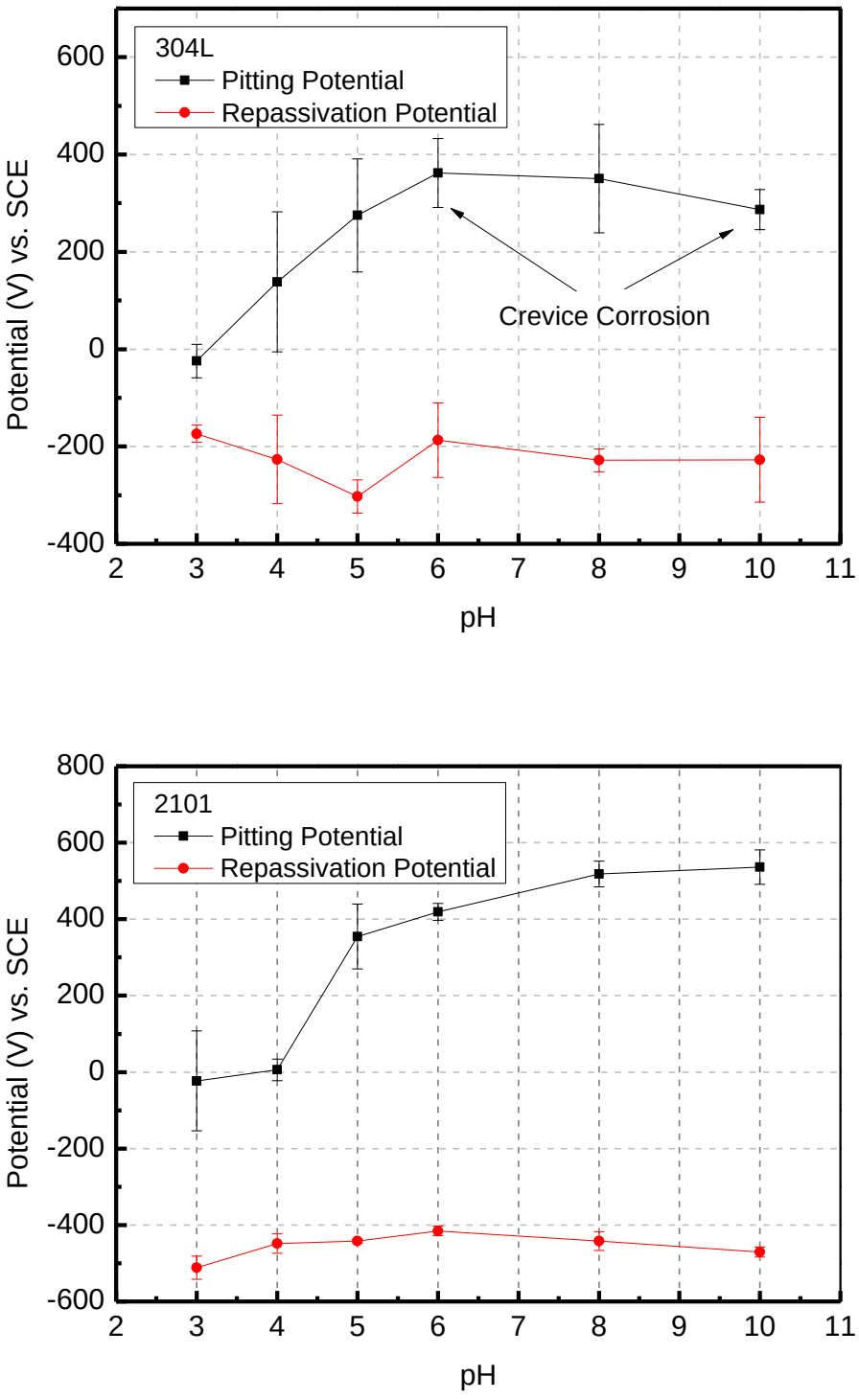

Figure 4-6. Effect of pH on the pitting and repassivation potentials of 304L and 2101

As can be observed from the two graphs in Figure 4-6, the lower the pH value, generally the lower the pitting potential is. This is quite intuitive as the passive film is generally less stable in more acidic environment. It is also easier for lower pH environment to establish a more aggressive pit environment where an auto-catalytic reaction may occur. A significant change in the pitting potential was observed for both 304L and 2101 in pH range of 4 to 6. On the other hand, the repassivation potential for these environments remained relatively the same, which means that once a stable pit forms in the presence of thiosulfate, the pit environment does not vary to a large extent in spite of the pH of the environment they are exposed to. The pit morphology of 304L and 2101 is compared in Figure 4-7.

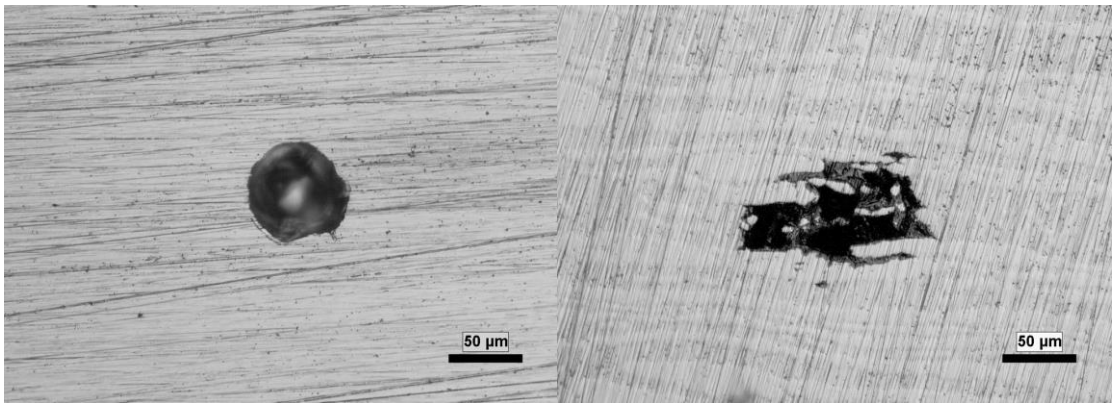

304L pH=3 2101 pH=3

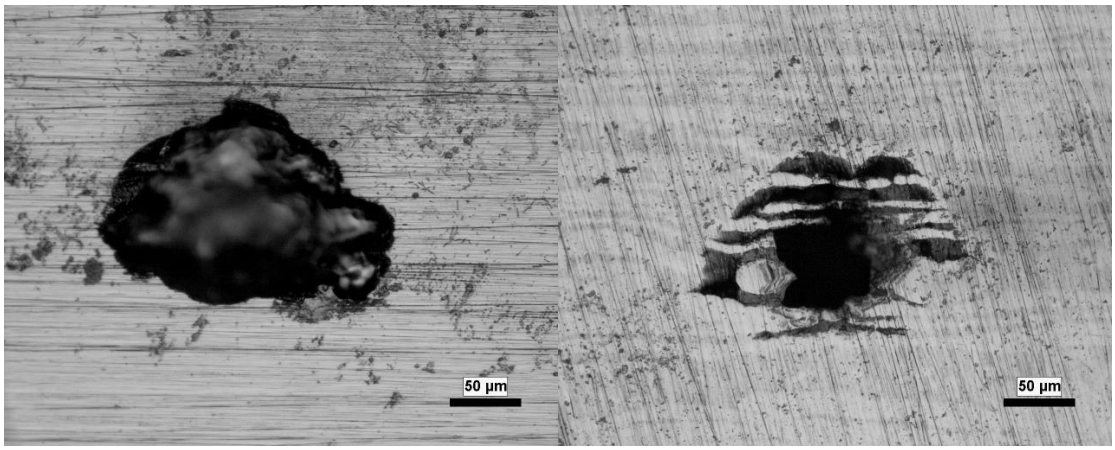

304L pH=8 2101 pH=8

Figure 4-7. Pit morphology of 304L and 2101 in 300ppm Cl^- 58ppm $S_2O_3^{2-}$ solution

Again, a clear distinction in the pit morphology between 304L and 2101 was observed in all pH environment tested. Hemispherical pits were observed on 304L, while preferential dissolution was found on the surface of DSS2101. However, it is interesting that in lower pH environment the preferential dissolution of 2101 seems to be more pronounced than in higher pH environment, as shown in Figure 4-8.

pH=4 pH=6 pH=8 pH=10

Figure 4-8. Change in pit morphology for 2101 as a function of pH

This is probably due to the fact that for specimens tested at higher pH, the pitting potential is much higher than at lower pH. This results in a longer pit growth time and thus larger pit. The formation of the large pit destroyed some of the features formed due

to selective dissolution.

4.3. Effect of Temperature on Pitting Corrosion

Differences in the chemical process stream could also include a difference in the process temperature, which plays an important role in the pitting corrosion of stainless steels. A set of tests were done to evaluate this effect in chloride and thiosulfate containing environment of paper machines. Cyclic potentiodynamic polarization measurements were carried out in a solution containing 300ppm Cl^- and 58ppm $S_2O_3^{2-}$. Testing temperature was 5℃, 25℃, 40℃, 60℃, 75℃. The breakdown and repassivation potential for localized corrosion of 304L and 2101 is given in Figure 4-9.

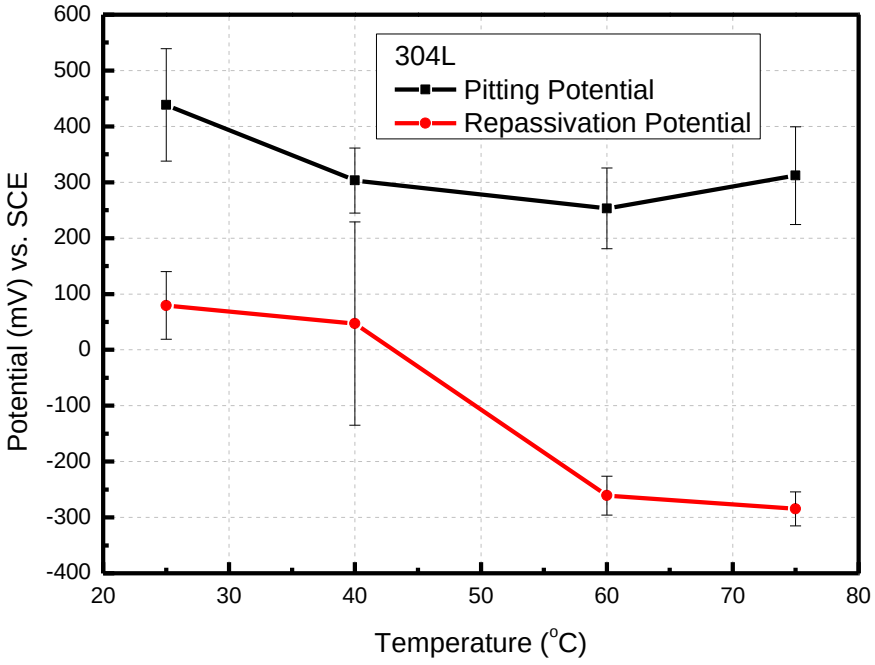

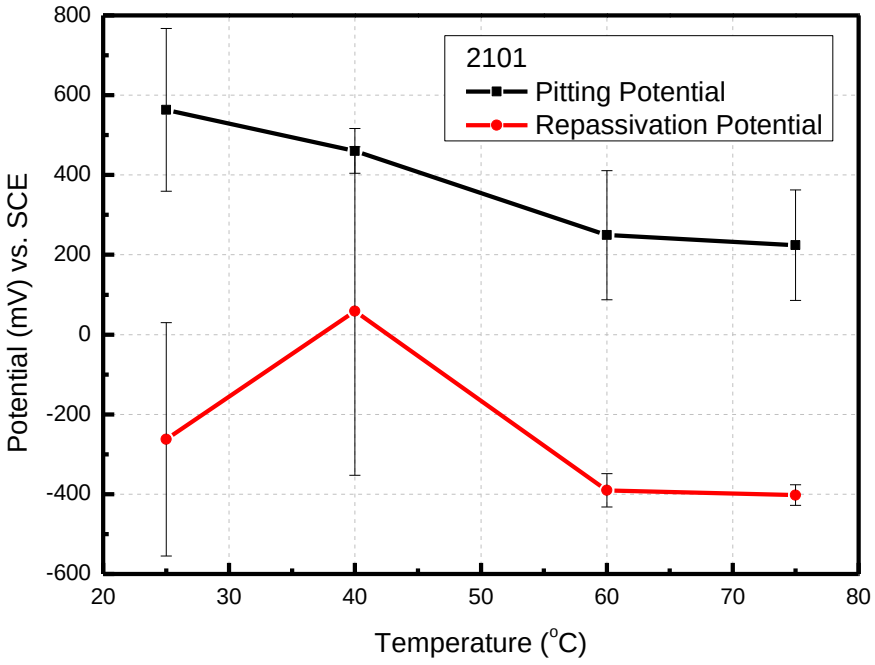

Figure 4-9. Effect of temperature on the pitting and repassivation potentials of 304L and 2101

As can be observed from Figure 4-9, temperature influences the pitting potential as well as the repassivation potential. It is generally a trend that as the temperature increases, both pitting and repassivation potentials of 304L and 2101 decreases. The effect of temperature on repassivation potentials is even greater than on the pitting potentials for these alloys. Temperature determines the solubility of the chloride salts, which hydrolyze to create an aggressive environment. Higher the temperature, higher is the solubility, and more aggressive is the pit environment, thus lower repassivation potentials. Higher temperature also affect the diffusion and transportation of ions involved in pitting mechanism, which may also affect the overall pitting and repassivation process. The effect of temperature on pitting potential may also be attributed to this aspect since the aggressiveness of the metastable pit during metastable to stable transition is crucial in determining pitting potential. A lot of scattering showed up in the repassivation potentials for 2101, especially at lower temperatures. This could be attributed to the aspect of the microstructure, which will be discussed later in Chapter 6.

4.4. Effect of Applied Potential on Pit Growth

It is clear from the results presented earlier in this chapter that the thiosulfate ions does not affect pitting corrosion in these systems when the passive film is intact. However, once the passive film breaks down, thiosulfate tends to sustain pit growth by lowering the repassivation potential. This means that the bare metal surface is much more responsive to the activation of pitting by thiosulfate. To study the interaction

between the bare metal surface and thiosulfate, as well as the effect of potential on pit growth, scratch tests under potentiostatic control were performed.

The potentiostatic scratch tests were conducted to study how thiosulfate ions interact with the bare stainless steel surface. In scratch tests, passive films were mechanically removed with a diamond scriber. The subsequent current transient was monitored using chronoamperometry. Potentiostatic scratch tests were conducted on all four grades of steels to compare their susceptibility to thiosulfate pitting as a function of alloy composition. Typical results from a scratch tests are given in Figure 4-10.

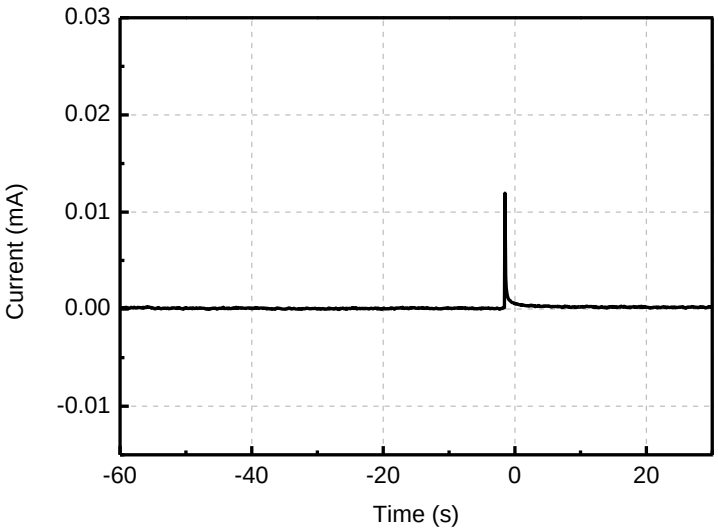

Fully Repassivated

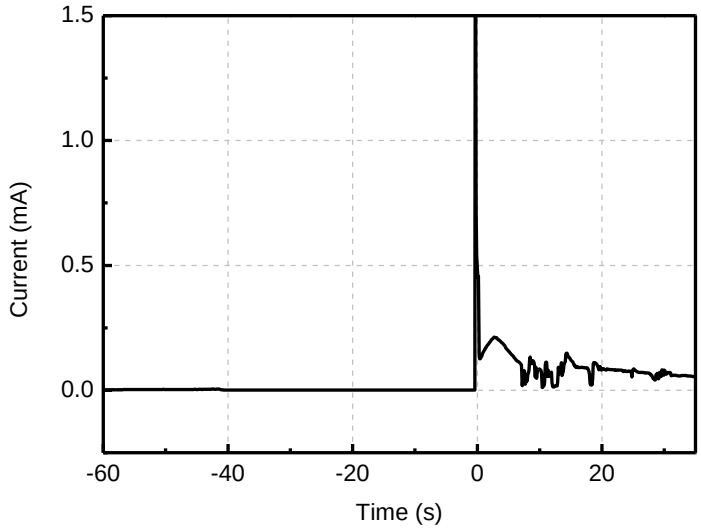

Repassivated, with Local Activity

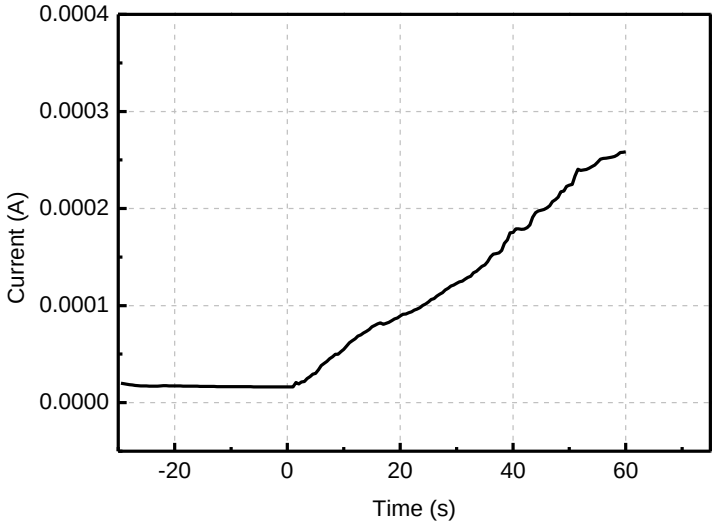

Pitting after Scratch

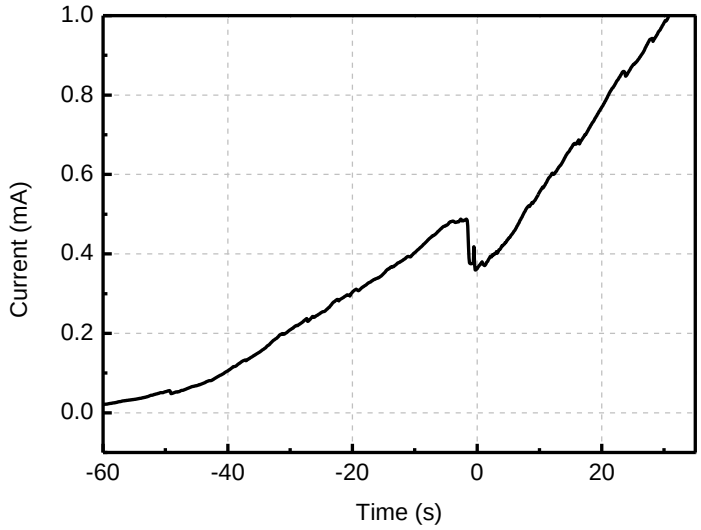

Figure 4-10. Typical results from a scratch test

As a mechanical scratch is made across the sample surface, a current suddenly increases due to the anodic activity and reformation of a passive film in this area. Depending on how the environment interacts with the bare metal surface, the result could be full repassivation of scratched area, repassivation with local activities (due to the formation of a defective film), pit growth after the scratch, or even pit growth without scratch (if the passive film breaks down due to potentiostatic polarization before the scratch is made). Typical current response for the four situations described are shown in Figure 4-10.

Test environment for the repassivation tests or scratch tests was solution-3, which is 6000ppm Cl^-, 12000ppm SO_4^{2-}, and 2000ppm $S_2O_3^{2-}$. It was used to simulate a possible chemical enrichment due to mill shut-down and/or evaporative concentration in paper machine splash zones. A comparison of the corrosion resistance among the

four grades of stainless steels was made in this environment. Current transients after the scratch for 316L and 2205 in the solution-3 under 50 ℃ are given in Figure 4-11 and Figure 4-12. Optical microscope images of scratches after the test are also shown.

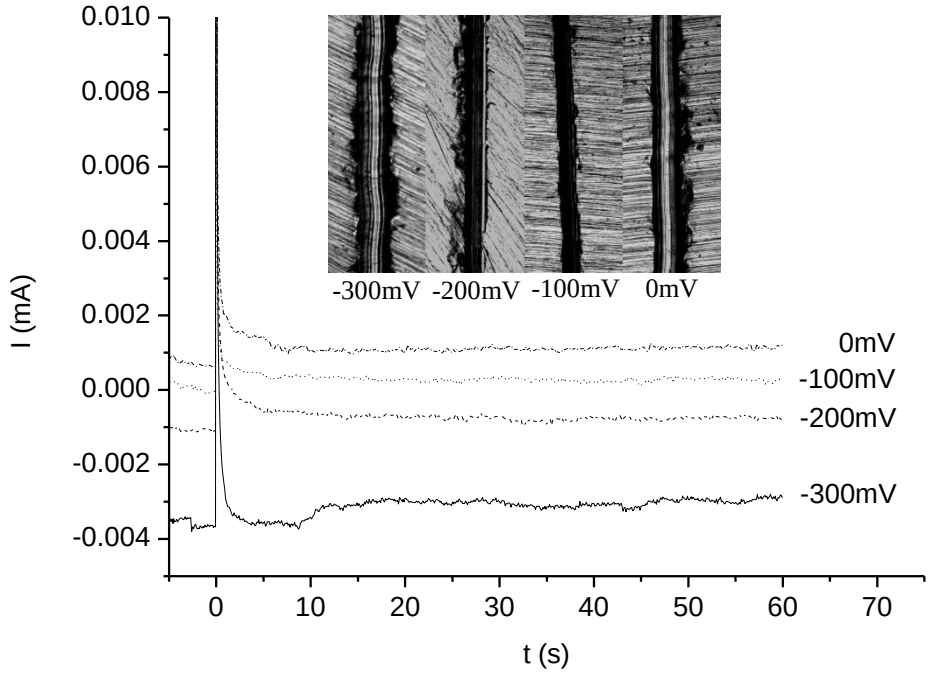

Figure 4-11. Current transients and optical microscope images for 316L in solution-3 at 50 ℃

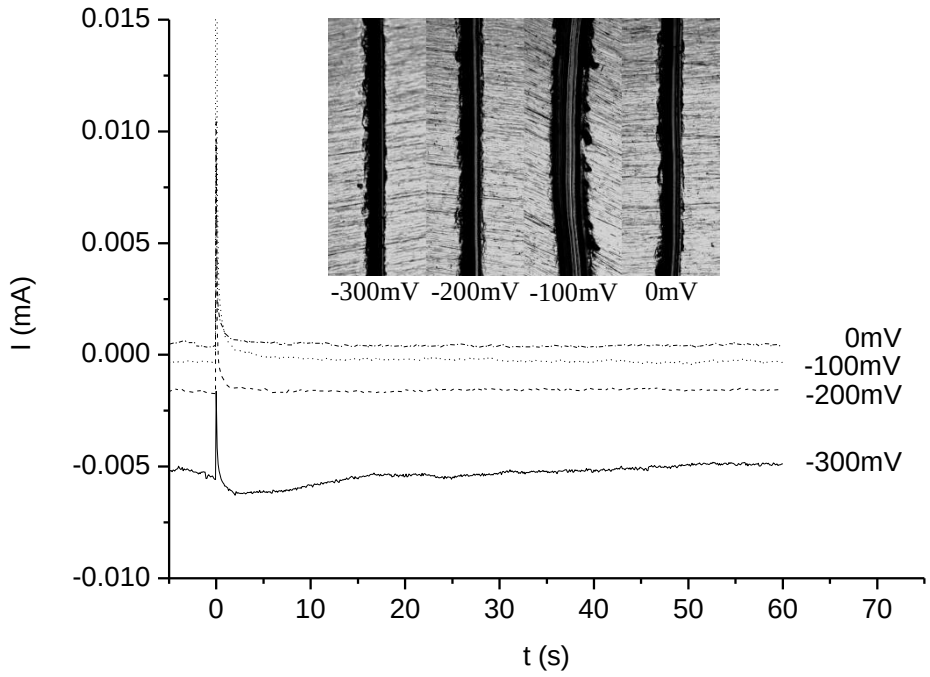

Figure 4-12. Current transients and optical microscope images for 2205 in solution-3 at 50 ℃

For the two molybdenum-containing grades, 316L and 2205, specimens did not show any sign of localized corrosion, even after the passive film was removed by scratching. The current after scratching (from -300mV to 0mV vs. SCE) decreased to the passive current within a few seconds and remained relatively unchanged. The passive current varied with the potential applied. The higher the applied potential, the higher the passive current was. Addition of molybdenum is known to improve the resistance of steels to pitting in chloride environments. It has also been reported to increase the corrosion resistance for chloride pitting in sulfur containing environment, which is also demonstrated by the present set of results showing a superior corrosion

resistance of 316L as well as 2205.

On the other hand, pitting corrosion was observed on most specimens of grades 304L and 2101. For 304L, shown in Figure 4-13, localized corrosion was observed for all specimens except the one polarized at -300mV. As the applied potential increases, from -200mV to 0mV vs. SCE, the current after 60 seconds of scratch also increased for 304L samples. Black corrosion product was observed wherever pits formed. The severity of pitting on the specimens correlated well with the magnitude of the current transient.

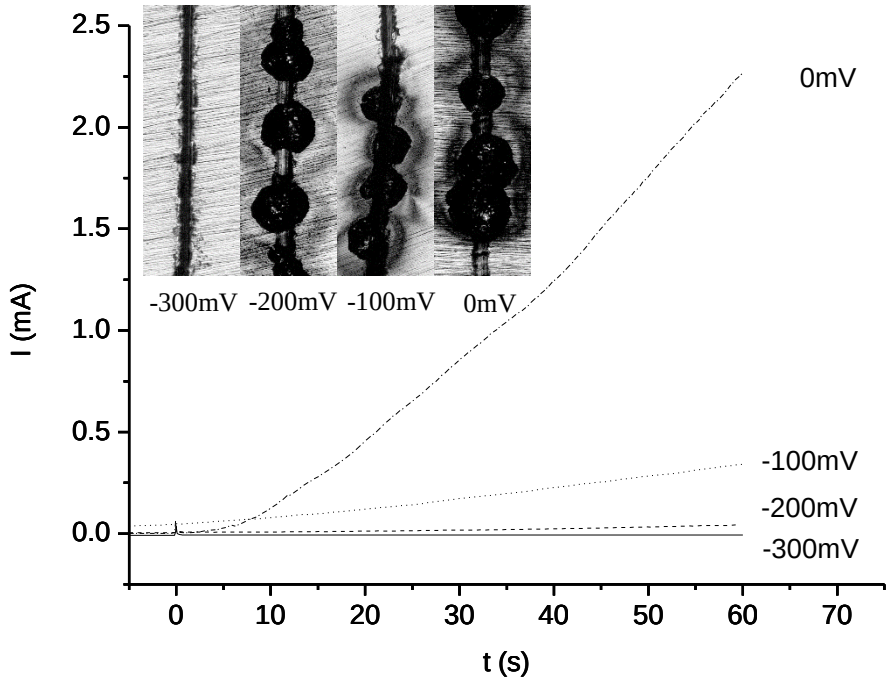

Figure 4-13. Current transients and optical microscope images for 304L in solution-3 at 50 ℃

In the case of 2101, localized corrosion was also found on all specimens polarized at -300mV to 0mV vs. SCE. The current after 60 seconds of the mechanical scratch increases with increased applied potential, as is shown in Figure 4-14. Optical microscope images and current transients are shown in Figure 4-14. The pits found on 304L were of hemispherical shape, while the pits on 2101 were elongated. Again preferential dissolution of ferritic phase was found on 2101 specimens, leading to trench-like pits extending in the direction that is perpendicular to the scratch. This means that not only passivity breakdown occurs preferentially on ferritic phase, but also pit growth.

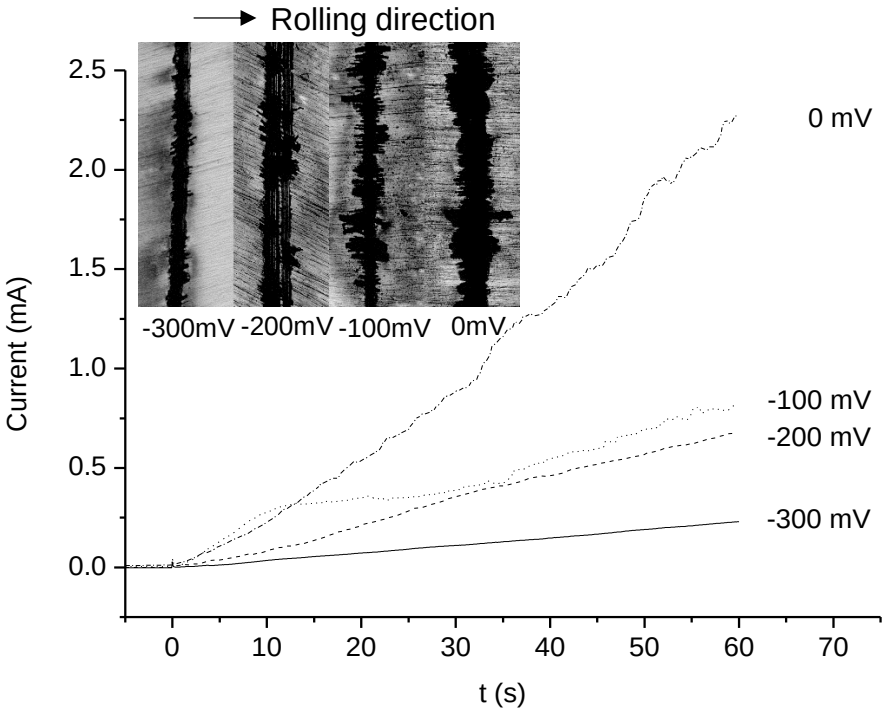

Figure 4-14. Current transients and optical microscope images for 2101 in solution-3 at 50 ℃

Preferential dissolution of a certain phase was found for duplex stainless steels in many earlier studies. Dissolution of ferrite and retention of austenite for 2101 were found in a caustic solution with 4g/L $Ca(OH)_2$ and 1M Cl^- [105]. This preferential dissolution of ferrite is attributed to the higher corrosion resistance of austenitic phase due to the enrichment of N and Ni [105]. Sometimes the phase with higher pitting resistance equivalent number (PREN) is preferentially attacked. Preferential dissolution of the ferritic phase on UNS S32550 was reported in 10% $FeCl_3$ solution, the cause of which was argued to be the difference in the chemical composition of the two steel phases [106]. Preferential dissolution was also found to play a role in the SCC mechanism in duplex stainless steels [107]. In sulfide-containing caustic solutions, crack initiation was mostly in the austenitic phase [108]. Moreover, both increase in sulfidity and addition of chloride in these environments favors selective corrosion of austenite, which serves as precursors to crack initiation [109]. On the other hand, crack initiation also may be associated with precipitates in ferritic phase formed after aging at 475 ℃ [110]. SCC of LDX 2101 in a concentrated solution containing 20% sodium chloride and various concentrations of thiosulfate ions was recently reported [111]. Selective dissolution of ferritic phase was found to accompany the stress corrosion crack growth. In the case of this study, 2101 is much less prone to sigma or chi phase formation than for 2205 [112]. Microscopic observations also did not show any second phase particles for tested 2101 (Figure 4-15). Reasons for a preferential pitting attack of ferritic phase, is most likely to be attributed to difference in chemical compositions between the two phases.

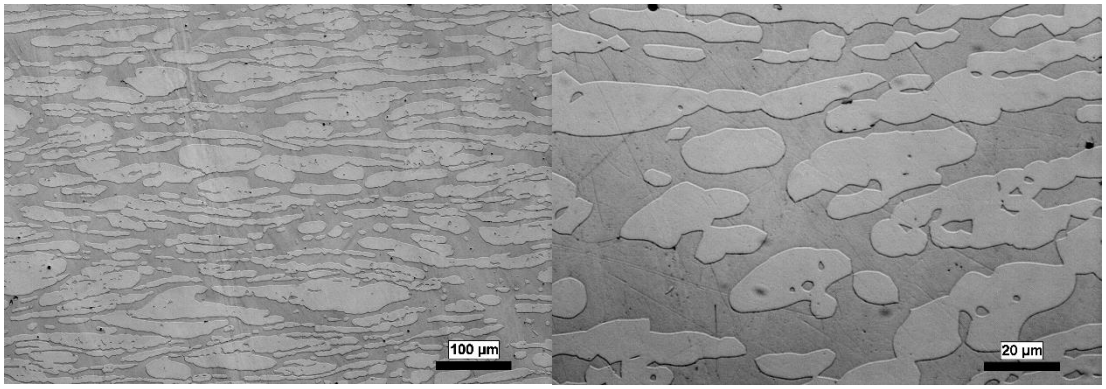

Figure 4-15. Metallography of 2101

4.5. Conclusions

In this chapter, we investigated the pitting and repassivation behavior of austenitic and duplex stainless steels in typical white water environments as well as concentrated white water solutions. Potentiodynamic polarization results show that the addition of sulfate in typical chloride and thiosulfate containing white water environments inhibits pitting corrosion. Pitting potentials did not change significantly with the addition of thiosulfate in dilute solutions. Presence of thiosulfate hinders repassivation process, resulting in lower repassivation potentials. Repassivation potentials for 304L and 2101 were at a minimum when 58ppm of thiosulfate was added to a dilute chloride containing solution (300 ppm NaCl), while addition of higher concentrations of thiosulfates (1000 ppm) inhibit pitting on 304L.

Decrease in pH lowered pitting potentials of both 304L and 2101, yet the repassivation of which remained relatively unchanged. Increase in temperature lowered both pitting and repassivation potentials of 304L and 2101.

Generally, higher chromium content in an alloy is associated with its higher pitting corrosion resistance. Duplex stainless steel 2101, with higher chromium content than 304L, showed higher pitting potential. However, repassivation potential for 2101 was lower than 304L. At the same time, pits in lean duplex grade 2101 form on ferritic phase, which has higher chromium content than the austenitic phase. Molybdenum containing grades 316L and 2205 showed more resistance to pitting corrosion than 304L and 2101.

Study of pitting kinetics using potentiostatic scratch tests in concentrated simulated white water showed that molybdenum containing grades 316L and 2205 were not susceptible to localized corrosion. However, for low molybdenum containing grades 304L and 2101, pitting was observed when the passive film was locally disrupted by a mechanical scratch. Severity of pitting was found to increase with applied potential, from -300mV to 0mV (vs SCE). Duplex stainless steel 2101 was susceptible to localized corrosion under lower potential than 304L. Again, a preferential dissolution of ferritic phase was observed for the pits formed in scratched area on 2101.

In general, stainless alloys that contain more chromium and molybdenum, such as 316L and 2205, have better pitting resistance in presence of thiosulfate in the papermachine white water environments.

5. EFFECT OF THIOSULFATE ON PIT INITIATION AND PIT GROWTH OF STAINLESS STEELS

The initiation and metastable growth stage of pits are very important in pitting corrosion. A decrease in pit initiation tendency usually leads to a decrease in pitting tendency. On the other hand, even if pit may initiate on the surface of stainless steels as metastable pits, if no stable growth of pits is possible (metastable to stable transition), pitting could still be eliminated. The effect of thiosulfate on metastable pitting of austenitic stainless steels as well as duplex stainless steels in chloride containing solutions has not been published before. Moreover, the interaction between thiosulfate ions and stainless steel in metastable pit growth was not clear. It is thus vital to study the effect of thiosulfate on these stages of pitting. In Chapter 5, the study was focused on the effect of thiosulfate on metastable pitting.

In chapter 4, the change in pitting potential was observed with the addition of thiosulfate ions to the chloride solution. However, in a dilute environment, this effect was not prominent for 2101. Four cyclic polarization tests were carried out for 304L and 2101, in more concentrated solutions, 0.6M NaCl and 0.6M NaCl + 0.03M $Na_2S_2O_3$. The polarization curves of the tests are shown in Figure 5-1.

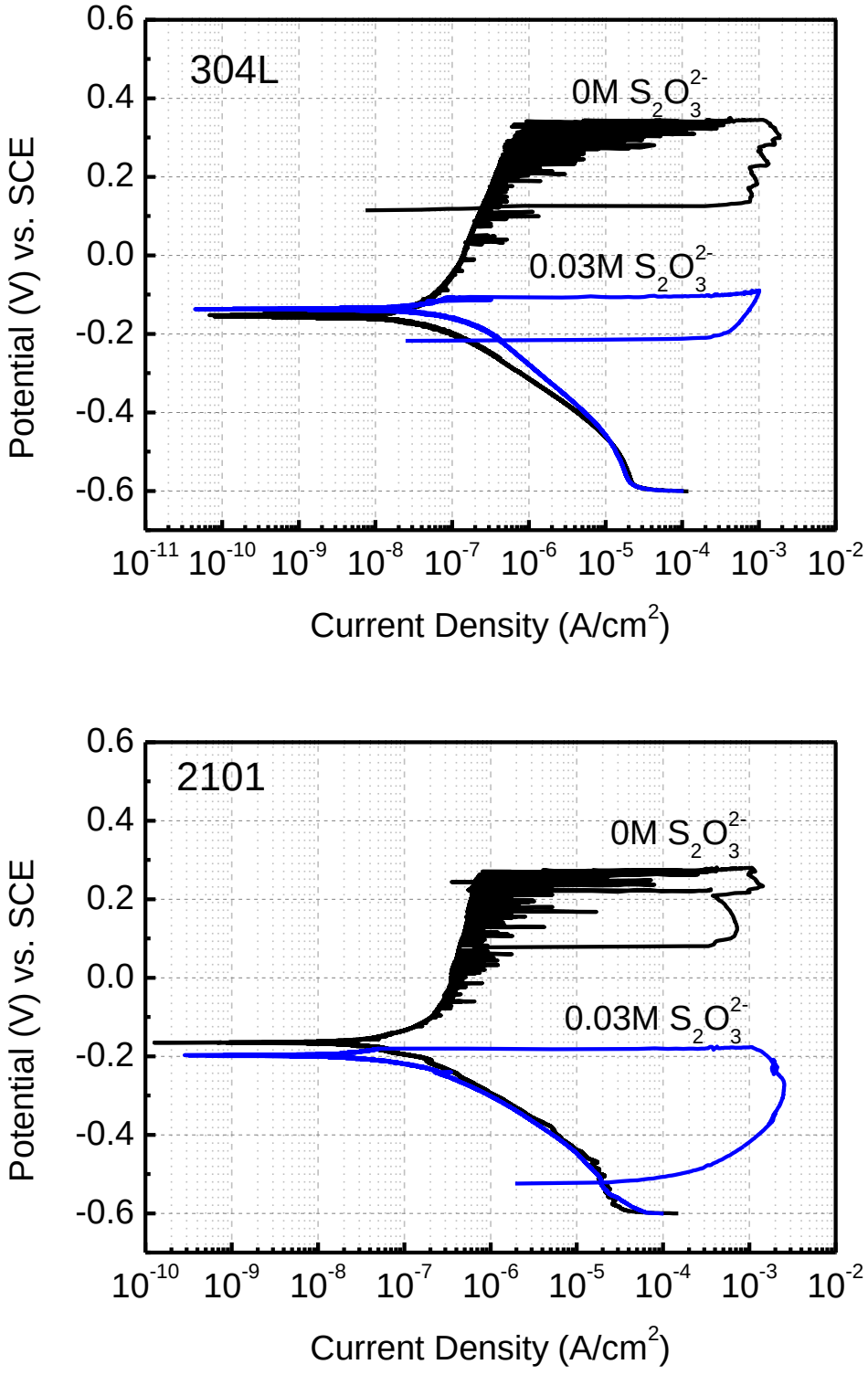

Figure 5-1. Cyclic Polarization Curves of 304L and 2101 in 0.6M NaCl and 0.6M NaCl + 0.03M $Na_2S_2O_3$

The pitting potential for both steels as well as the repassivation potential decreased significantly with the addition of 0.03M thiosulfate. In 0.6M NaCl solution, metastable pits were observed for 304L as well as DSS2101, at applied potential as low as -100mV vs. SCE. Metastable pitting has been shown to occur in chloride only environment at potentials as low as -210mV vs. SCE [25]. The addition of thiosulfate was obviously stabilizing the pit growth and resulted in stable pit formation at much lower potentials. It is thus crucial to understand the effect of thiosulfate on metastable pit growth as well as metastable to stable pit transition.

5.1. Statistical Analysis of the Metastable Pitting Events

The effect of thiosulfate on metastable pitting behavior of 304L and 2101 was studied by potentiostatic polarization. The testing environment is a baseline solution of 0.6M NaCl. To observe the effect of thiosulfate concentrations, addition of 0M, 0.003M, 0.006M, 0.012M, and 0.018M thiosulfate ion was made to the baseline solution. Specimens were polarized at 0V vs. SCE for 1 hour. A section of the typical current transients during potentiostatic polarization is shown in Figure 5-2. Metastable pitting and repassivation events are reflected as current spikes in the graph. Metastable pitting events usually do not overlap, due to the small pit growth time and relatively small exposure area (0.1256 cm^2). Therefore, each current spike was treated as one metastable pitting event.

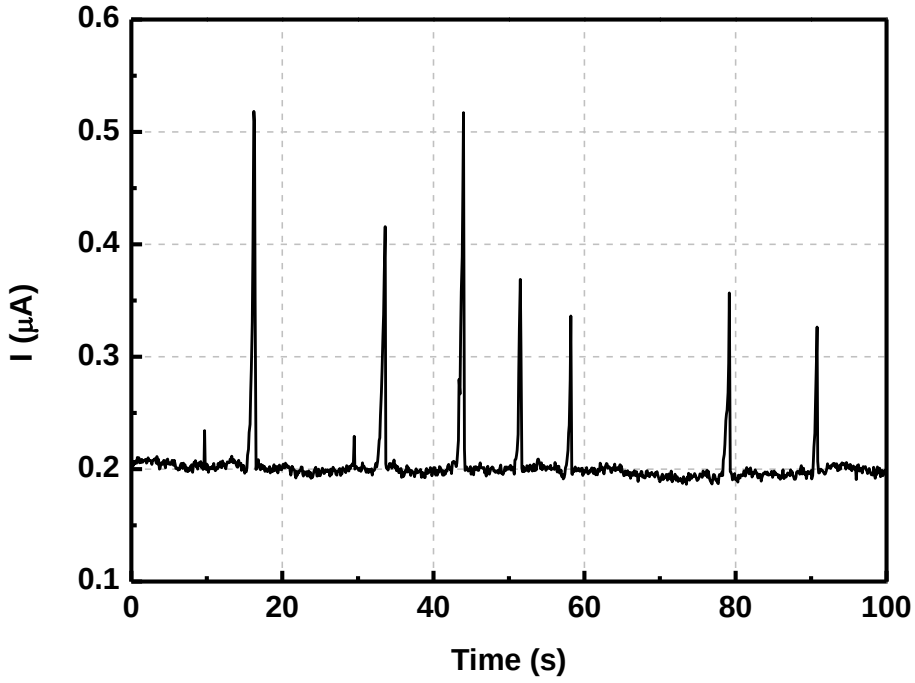

Figure 5-2. Typical current transients under potentiostatic polarization

Experimental results from potentiostatic polarization measurements were analyzed statistically. A Matlab program was written to automatically obtain the peak current, pit growth time, pit occurrence time, as well as pit initiation frequency. Peak current is the highest current in the process of metastable pit growth, which is usually the point at before repassivation. Pit growth time is the time span from the initiation of pit to the occurrence of peak current. Combining peak current and pit growth time, information regarding size of metastable pits and metastable pitting kinetics may be acquired. Pit occurrence time is the time at which the peak current occurs with respect to the start of potentiostatic polarization. A statistical compilation of pit occurrence times for each metastable pitting events provides information on the promotion of metastable pitting at available sites. A typical metastable pit current transient is shown in Figure 5-3.

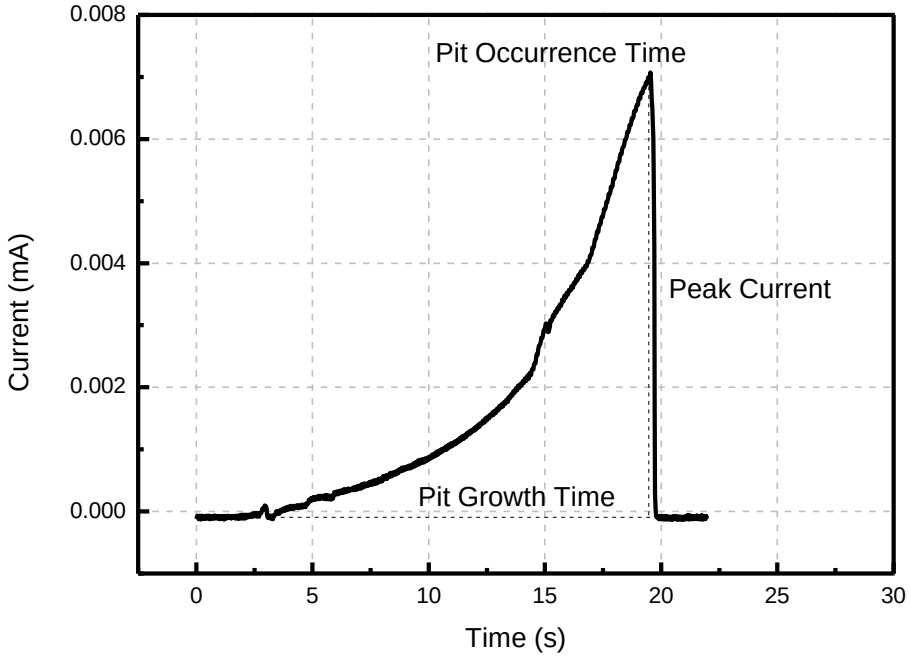

Figure 5-3. A typical metastable pitting current transient

A few attempts in determining peak current, peak growth time, and peak occurrence time have been made before a standard was set. A monotonically decreasing segment of current that is larger than 1.5 times the noise span (difference between largest and lowest current in a segment of background current) is treated as the repassivation transient of a metastable pitting. The current at the highest point of the segment is set as the peak current of the metastable pit. The time at the highest point is set as the pit occurrence time. The starting point of the pit is set as the first point before the peak within 0.3 times the noise span range of the lowest point in the repassivation segment. The pit growth time is defined as the time difference between the starting point and the peak.

5.2.Effect of Thiosulfate on Pit Initiation and Metastable Pitting for 304L

The influence of thiosulfate addition on pit initiation frequency is shown in Figure 5-4. Each data point is from three repetitive experiments. The pit initiation frequency is the number of metastable pitting events in a unit time.

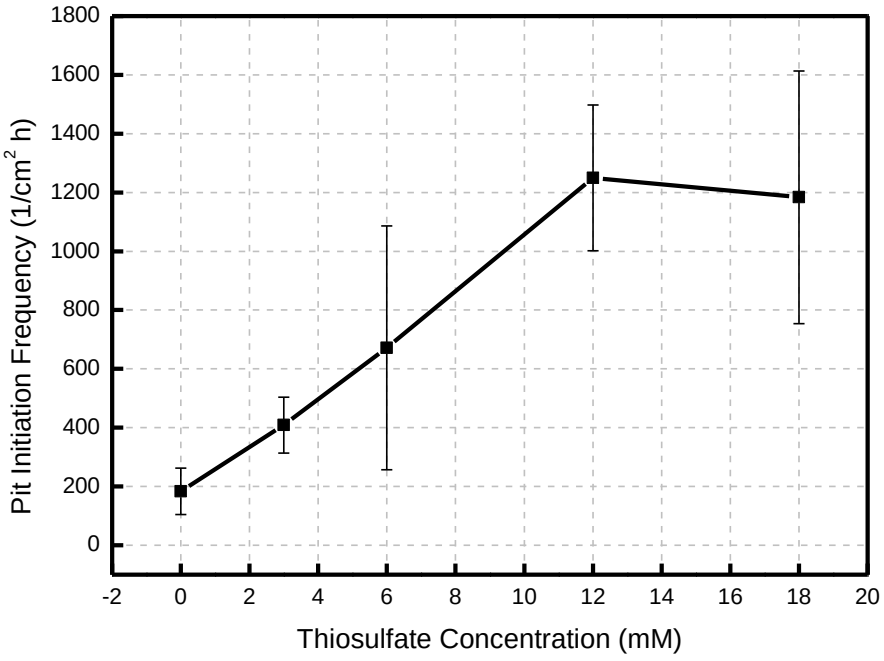

Figure 5-4. Pit initiation frequency for 304L specimens polarized at 0V vs. SCE

The inhibition of repassivation by thiosulfate were reported by several researchers [71][77][78][116]. On the other hand, results from the present study have clearly demonstrated that the addition of thiosulfate in chloride containing solutions could also promote pit initiation, depending on the concentration. As can be observed in the graph,

increase in thiosulfate concentration results in an increase of the pit initiation frequency of the 304L specimens, in contrast to the inhibiting effect of several other anions [28].

Values of peak currents were arranged in an ascending order. Cumulative frequency was calculated from the data such that the cumulative frequency of a peak current is taken as the fraction of peaks with current less than its value. Cumulative frequency has a maximum value of 1. Log I_{peak} vs. cumulative frequency curves were graphed so that the distribution of peak current for the metastable pits could be analyzed. Zuo et al. studied the cumulative frequencies of metastable pit peak currents [28]. Their results indicated that in chloride solutions the cumulative frequencies were proportional to the logarithm of peak current densities. Similar results were found in the present study, as shown in Figure 5-5 for specimens polarized at 0V.

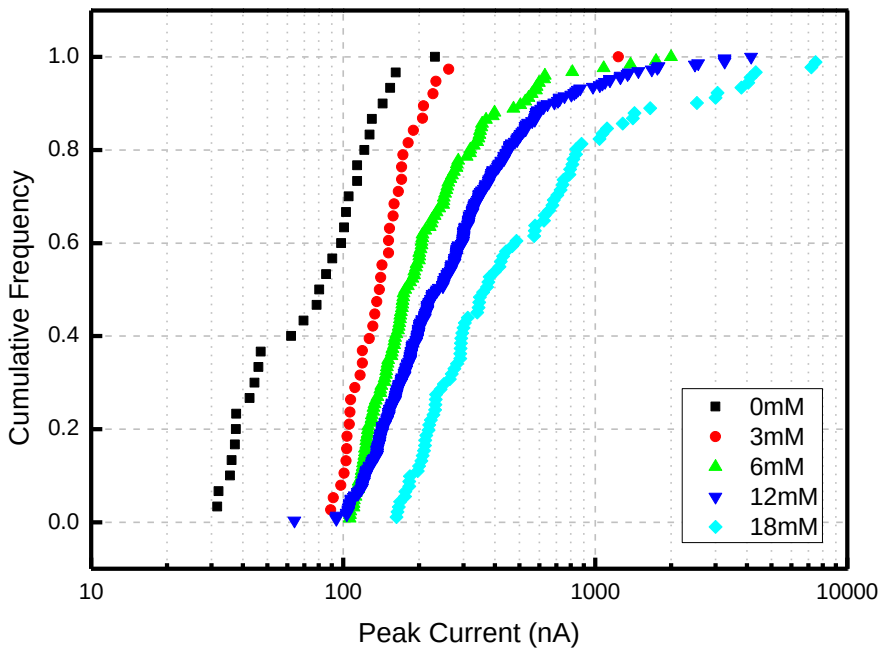

Figure 5-5. Cumulative frequencies of peak current for 304L specimens polarized

at 0V vs. SCE (Concentration of thiosulfate ions added to the base solution are indicated in the legend.)

It can be observed from the graphs that in all solutions, the cumulative frequency curves have a linear region. However, at large peak current values, there is a “turning point”, after which the tendency for pit growth is much higher. The curves shifted to the right (higher peak current) with the addition of thiosulfate. This means that either pit growth was enhanced or the repassivation of pits was hindered with an increase in the thiosulfate concentration. The pit growth time distribution for 304L specimens is given in Figure 5-6.

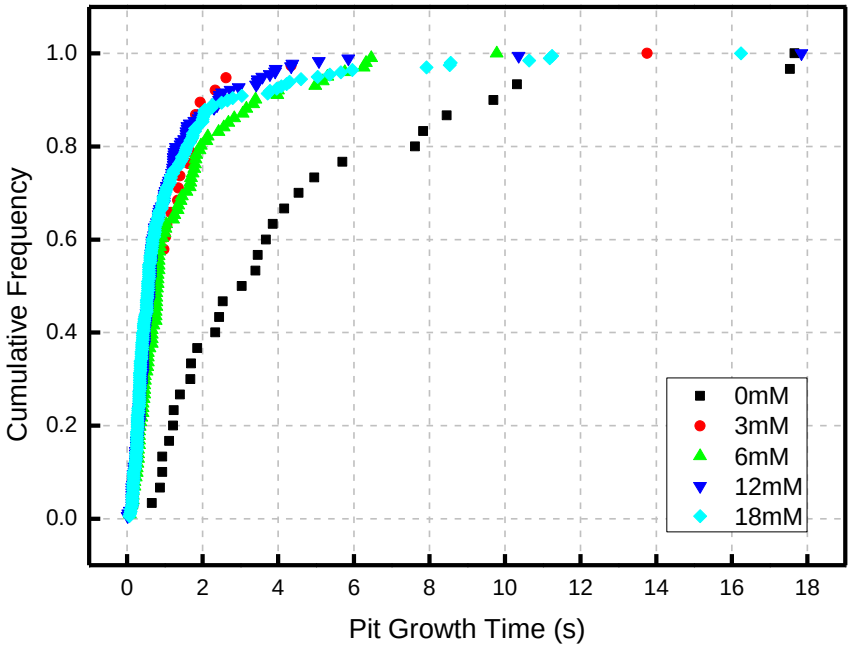

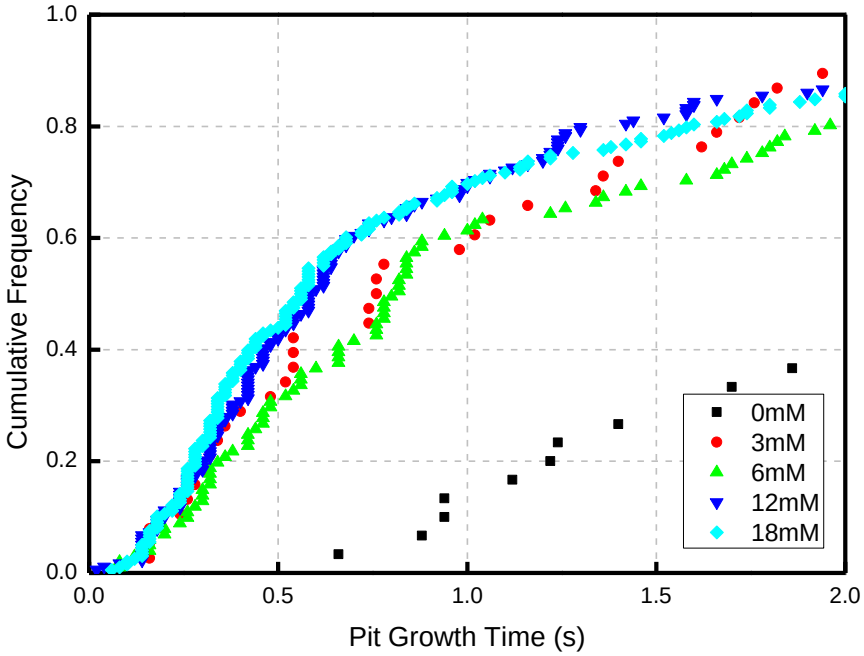

Figure 5-6. Growth time distribution and a magnified graph for 304L specimens polarized at 0V vs. SCE (Concentration of thiosulfate ions added to the base solution are indicated in the legend.)

It can be observed from the graphs that in chloride only environments the percentage of pits that grew for longer periods than 1 second is much higher than in thiosulfate-containing environments. As thiosulfate concentration increased, the percentage of pits growing for longer times decreases. This means that an addition of thiosulfate is promoting occurrence of pits with shorter growth time. As shown in Figure 5-5, the peak currents of the metastable pits are higher for thiosulfate containing environments. One can easily deduce that thiosulfate enhances the growth kinetics of these metastable pits. The occurrence time distribution curves for the pits did not show

a marked difference in tested environments, which is shown in Figure 5-7.

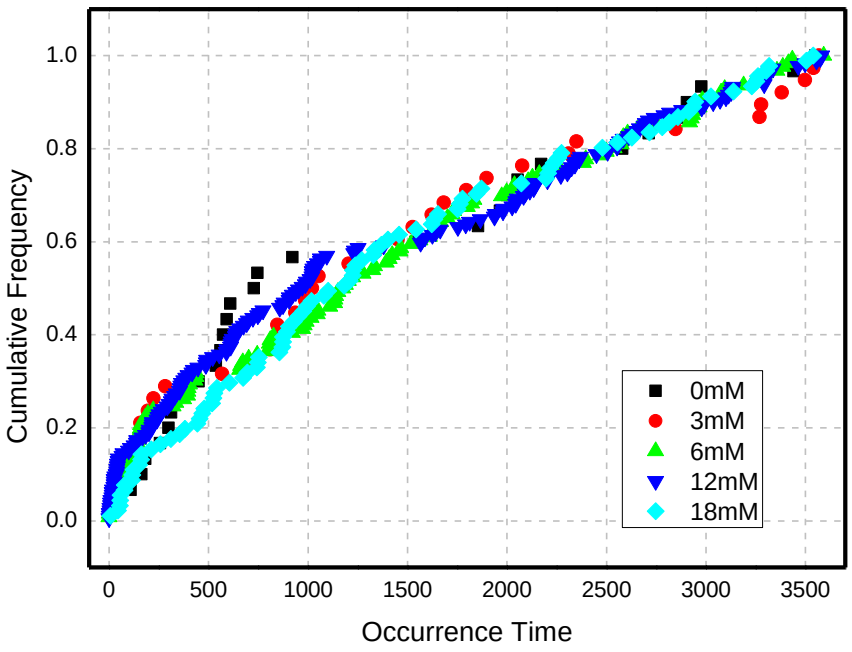

Figure 5-7. Occurrence time distribution for 304L specimens polarized at 0V vs. SCE

Surfaces of 304L specimens before and after tests are shown in Figure 5-8. Metastable pits were not labeled in the graphs due to the fact that it is very difficult to distinguish inclusion and particles in the steel from metastable pitting. However, the number of the black dots clearly increased from the addition of 6mM thiosulfate. Further increase in thiosulfate concentration resulted in more black dots shown on the specimens.

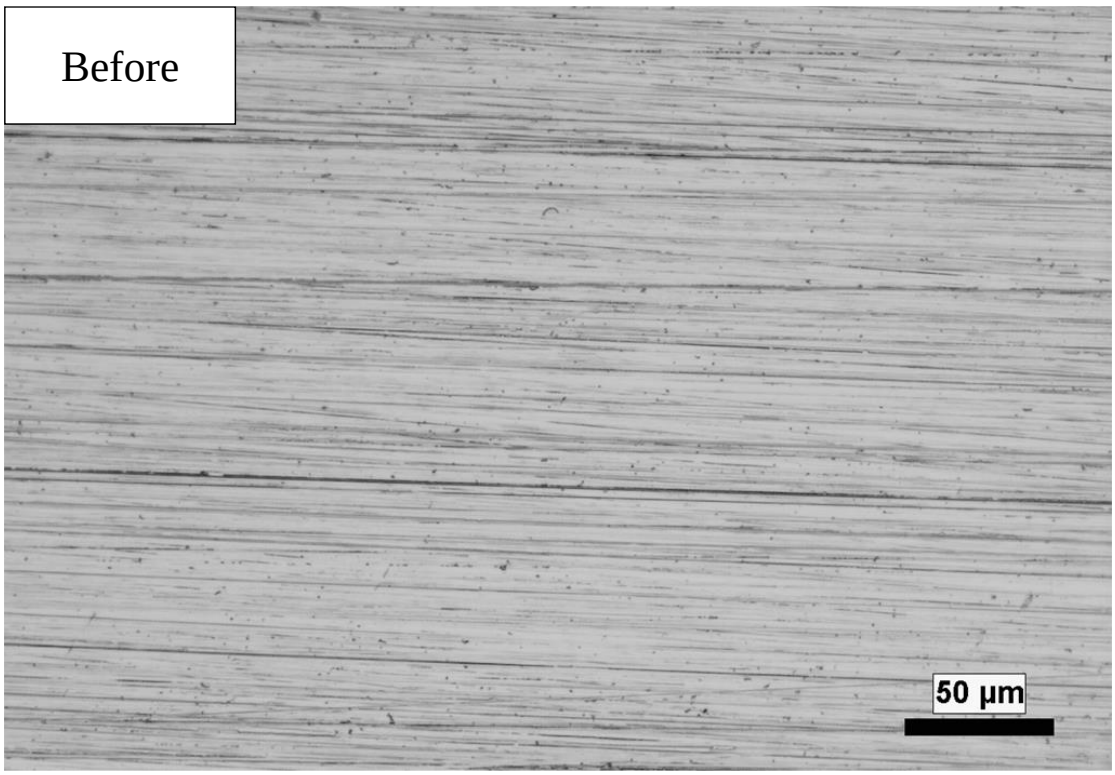
Before
50 µm

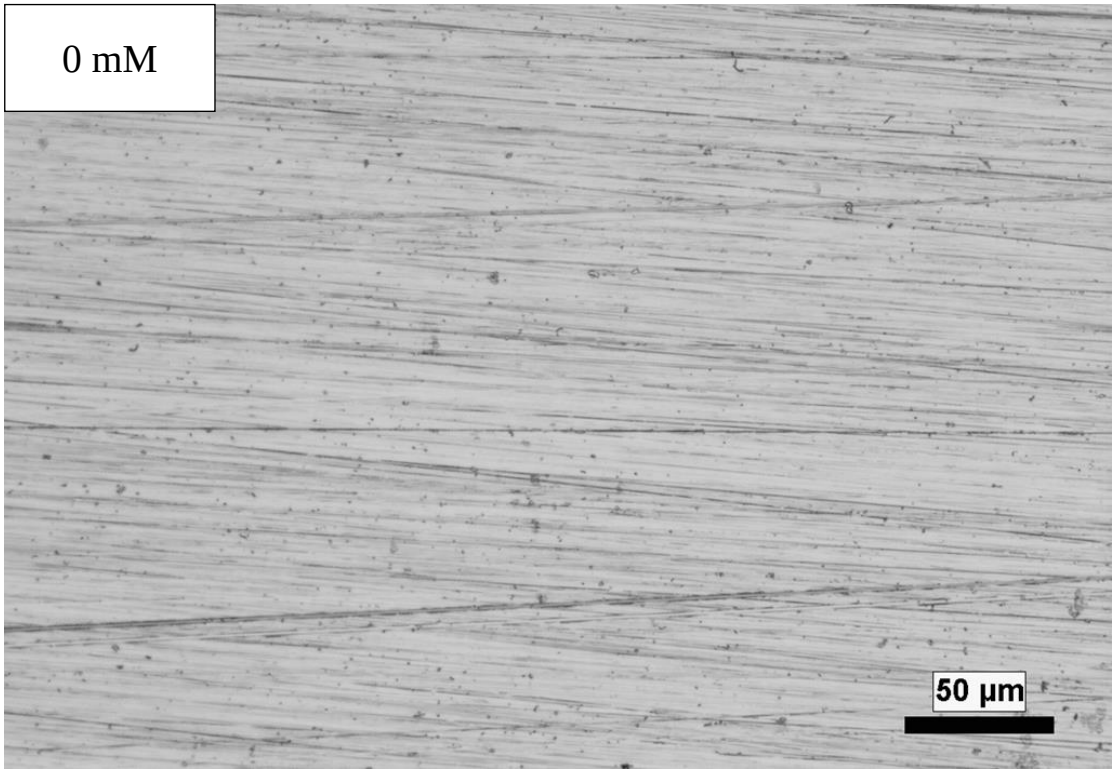
0 mM
50 µm

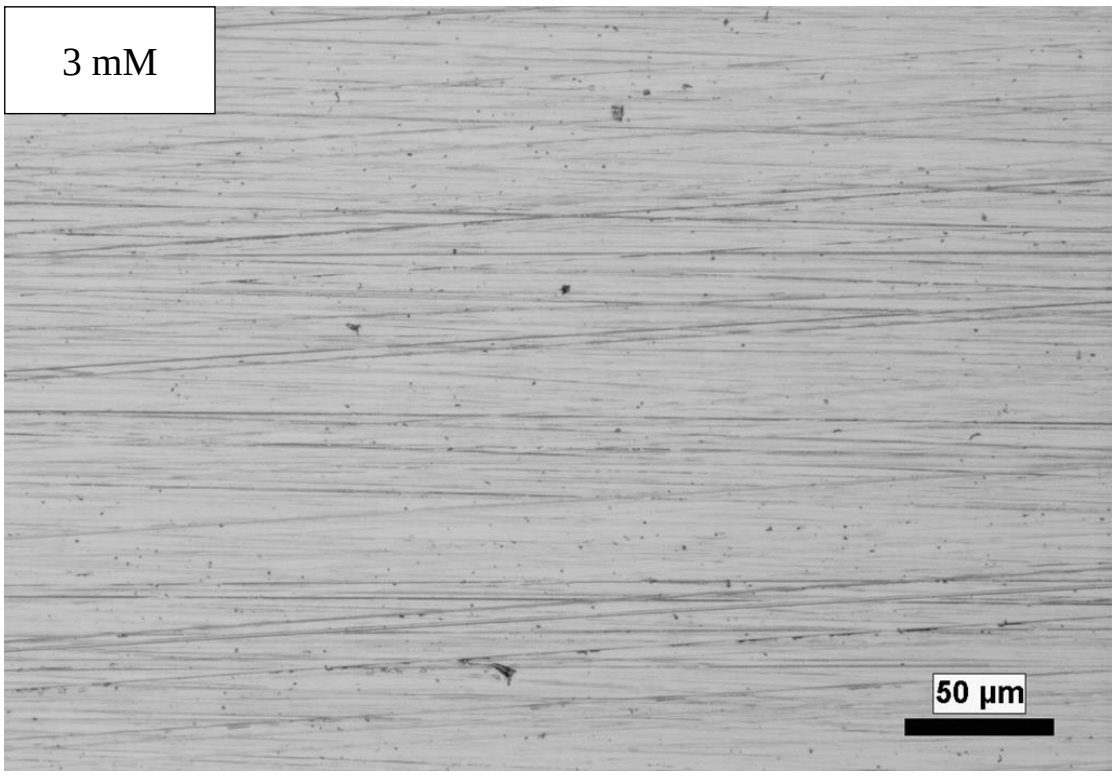
3 mM
50 µm

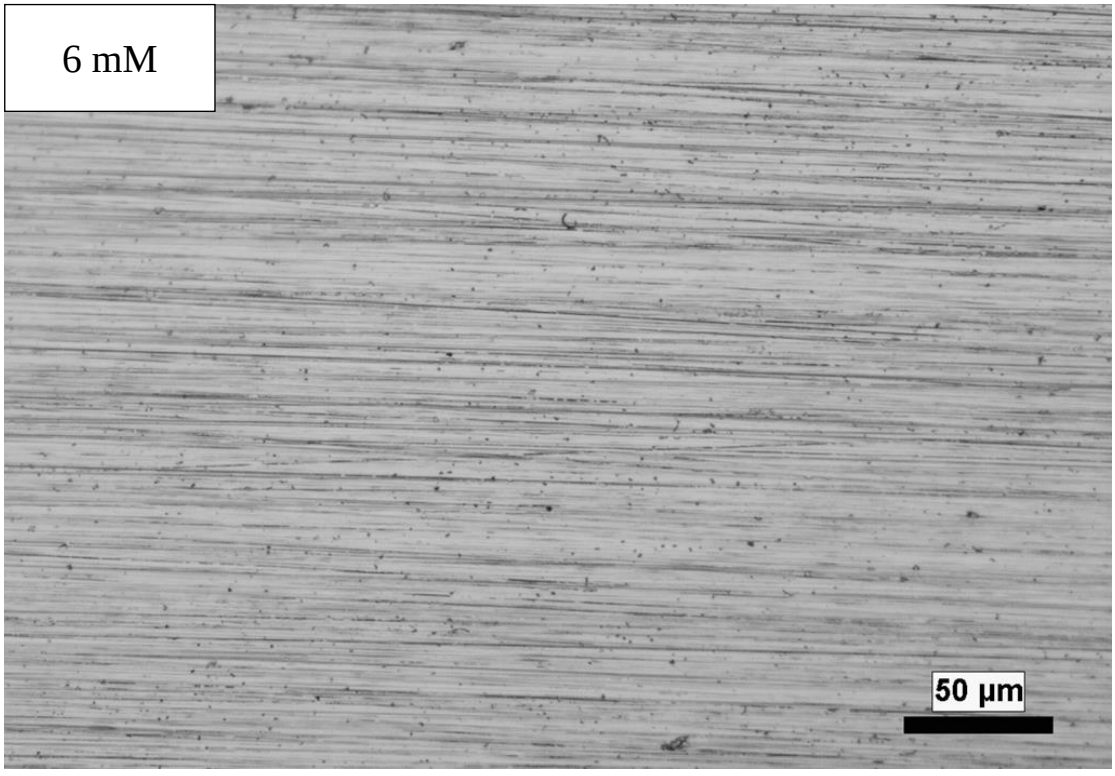
6 mM
50 µm

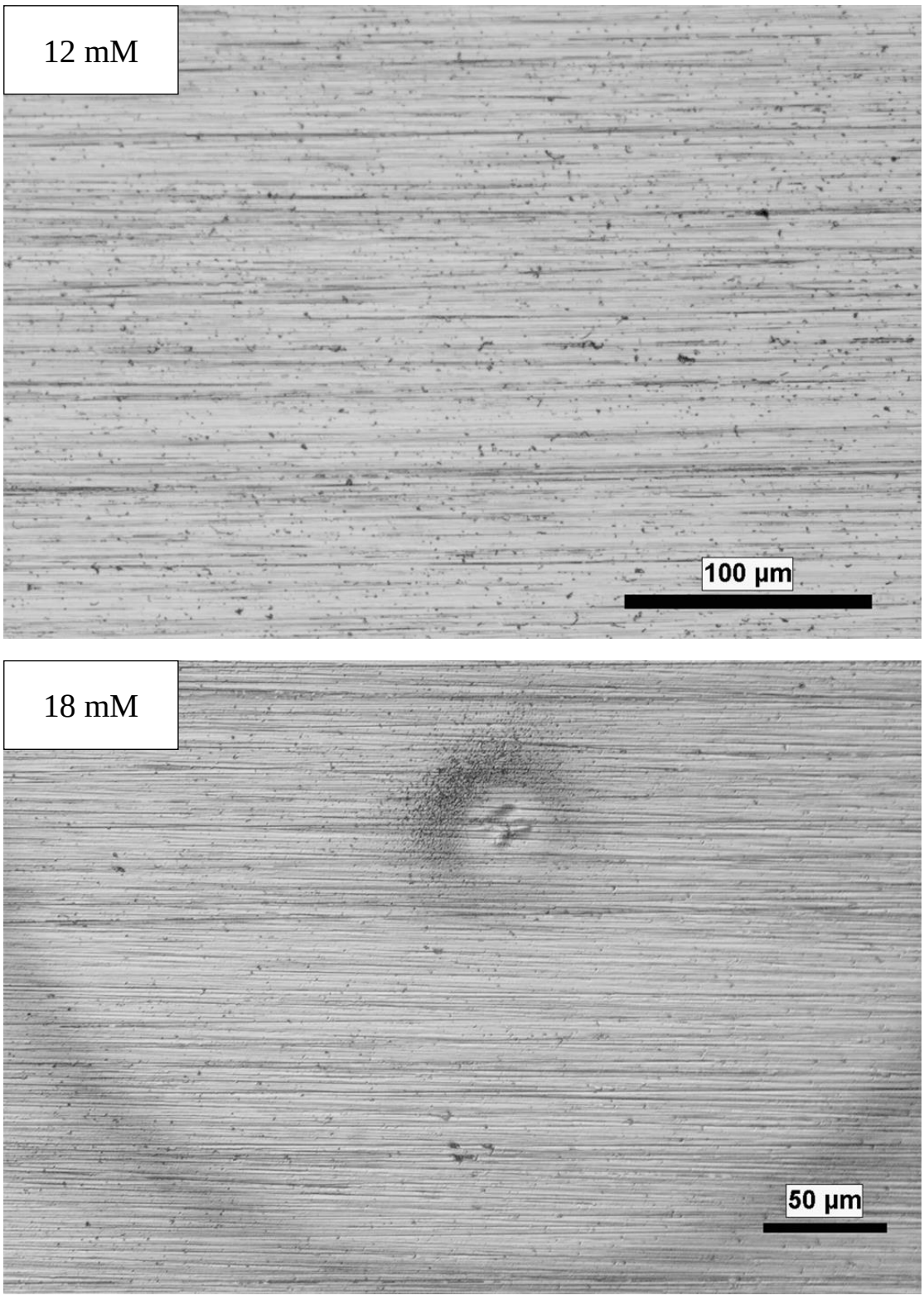

Figure 5-8: Surfaces of 304L specimens before and after potentiostatic polarization in solution with 0mM, 3mM, 6mM, 12mM, and 18mM $S_2O_3^{2-}$

Both the number and the aggressiveness of the pits increase with an increase in the thiosulfate concentration, as shown in Figure 5-8, which correspond well to the metastable pit distribution curves for 304L.

5.3. Effect of Thiosulfate on Pit Initiation and Metastable Pitting of DSS2101

The effect of thiosulfate on pit initiation and metastable pitting for 2101 was studied using specimens of DSS2101 plate, with transvers short surface exposed to the environment. Results from potentiostatic tests have indicated that the addition of thiosulfate in chloride containing environment also promotes pitting initiation in 2101, as shown in Figure 5-9.

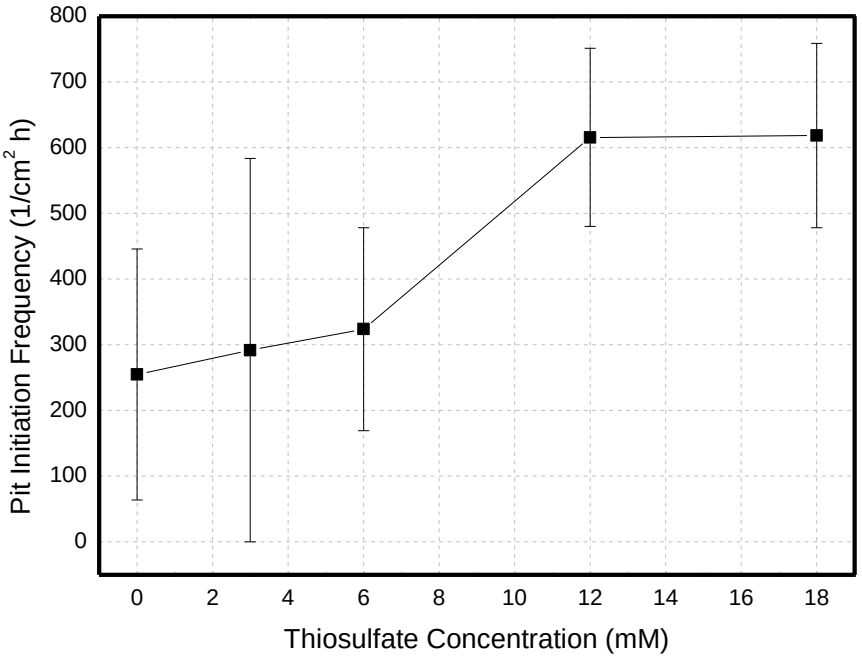

Figure 5-9. Pit initiation frequency for 2101 specimens polarized at 0V vs. SCE

The pit initiation frequency increased from ~200 to ~600 $cm^{-2}h^{-1}$ with the addition of 18mM thiosulfate ions. In the case of 304L, the initiation frequency increased from ~200 to ~1200 $cm^{-2}h^{-1}$. The effect of thiosulfate on peak current distribution for 2101 is shown in Figure 5-10.

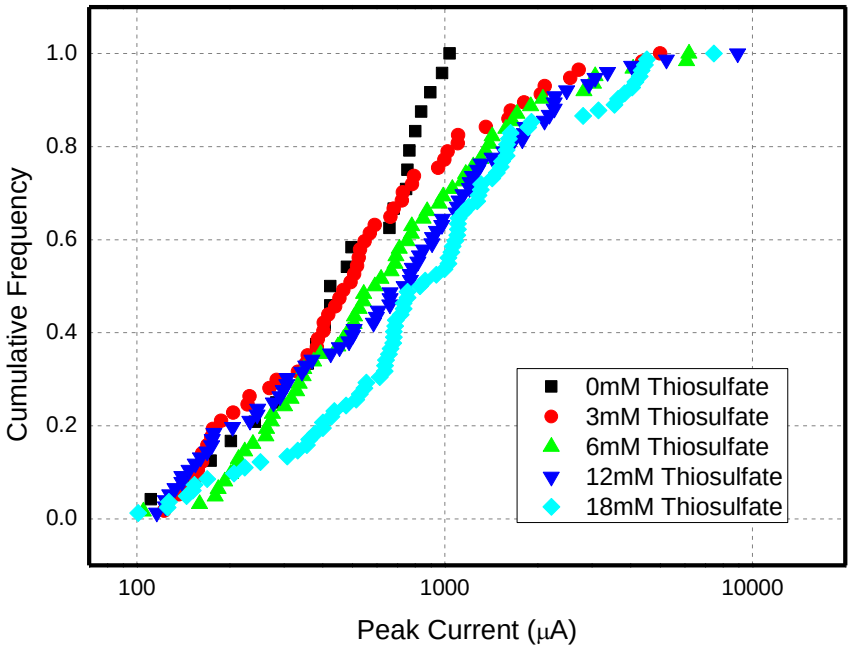

Figure 5-10. Cumulative frequencies for 2101 specimens polarized at 0V vs. SCE

Addition of thiosulfate still resulted in an increase in metastable peak currents for 2101, especially for bigger metastable pits, compared with chloride only environments. However, this effect on peak currents distribution for DSS2101 is much less prominent than 304L.

No definitive influence on growth time and occurrence time for the metastable pitting events was observed with the addition of thiosulfate for 2101, as shown in Figure 5-11.

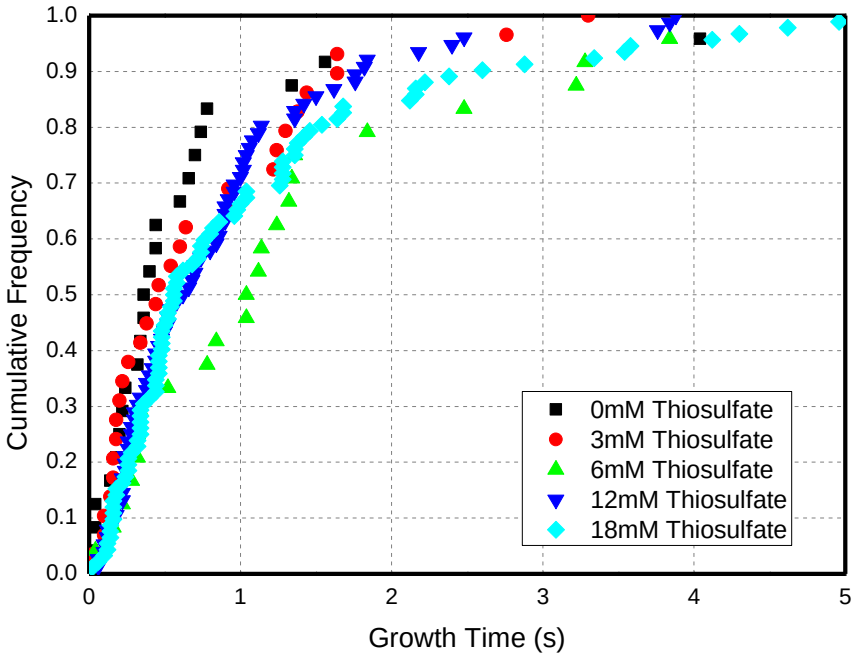

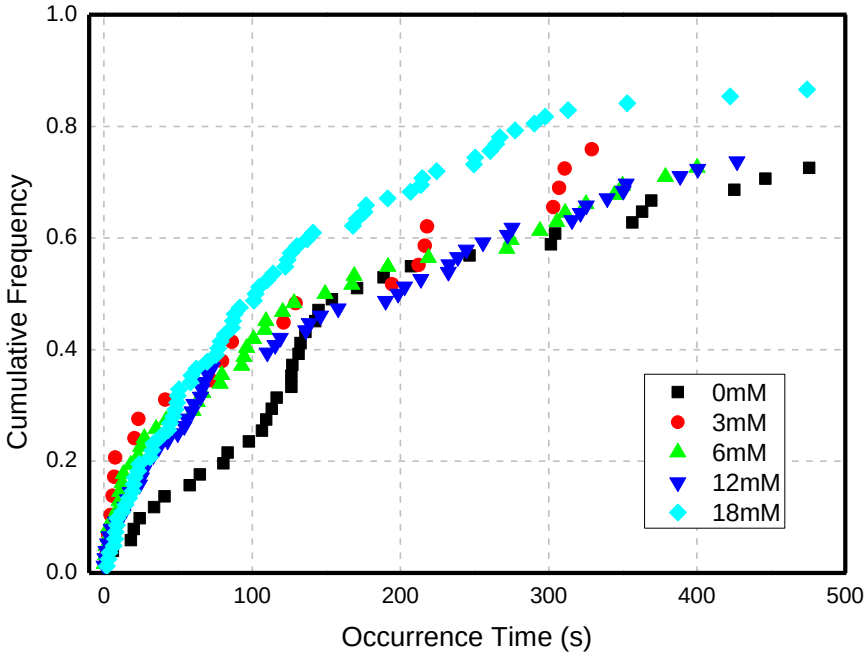

Figure 5-11. Growth time and occurrence time for 2101 specimens polarized at 0V vs. SCE

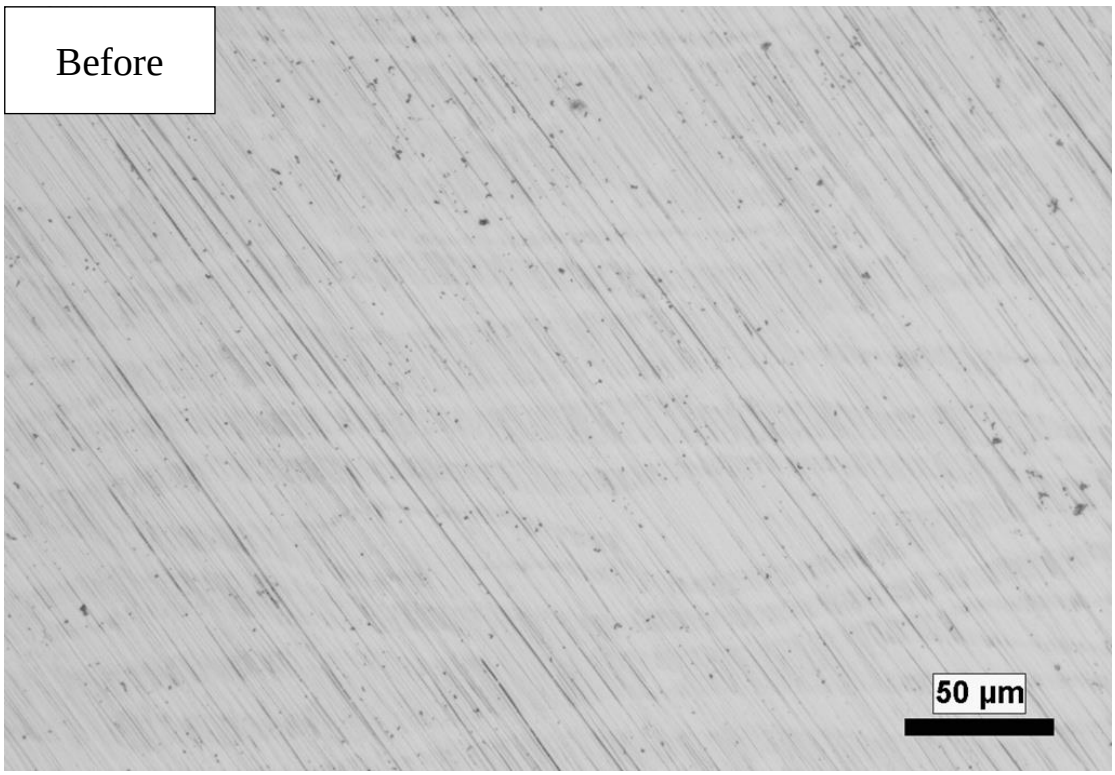
Before
50 µm

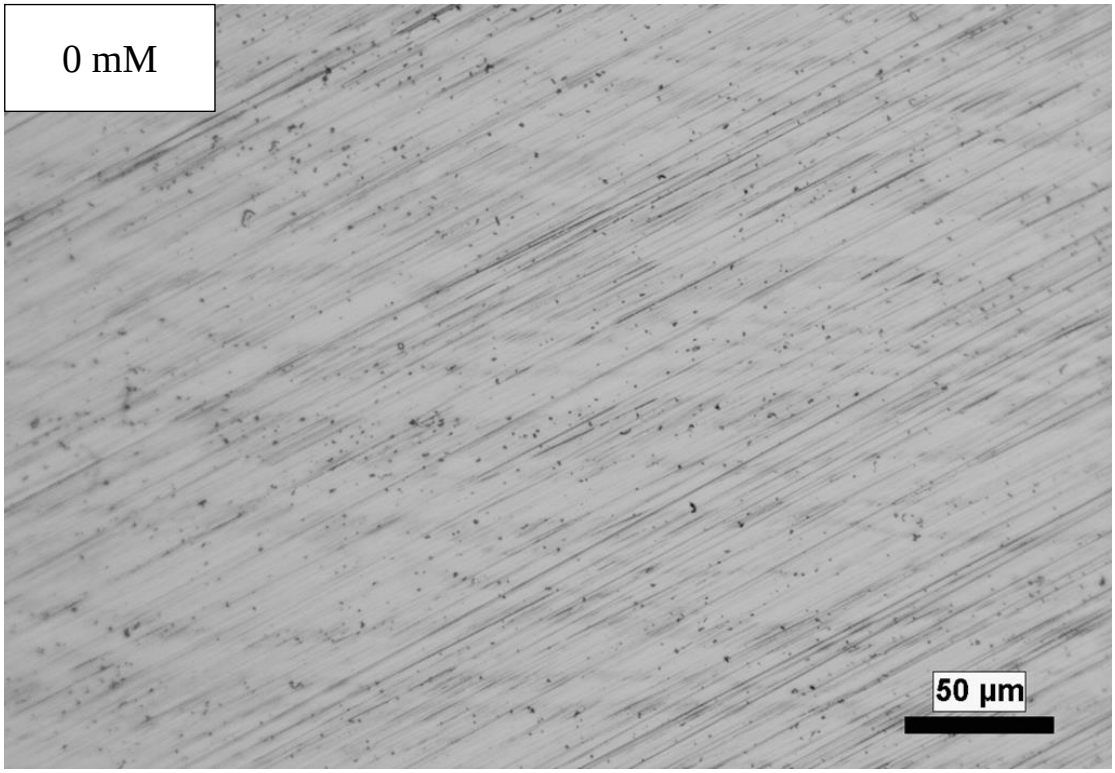
0 mM
50 µm

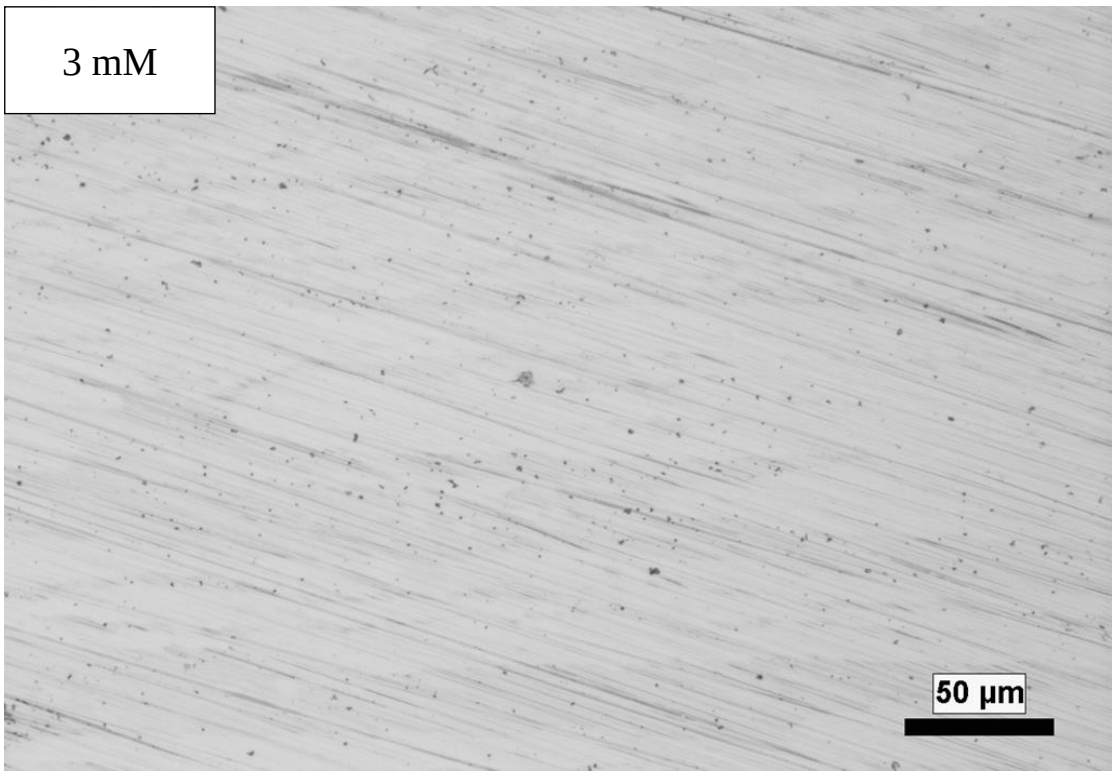
3 mM
50 µm

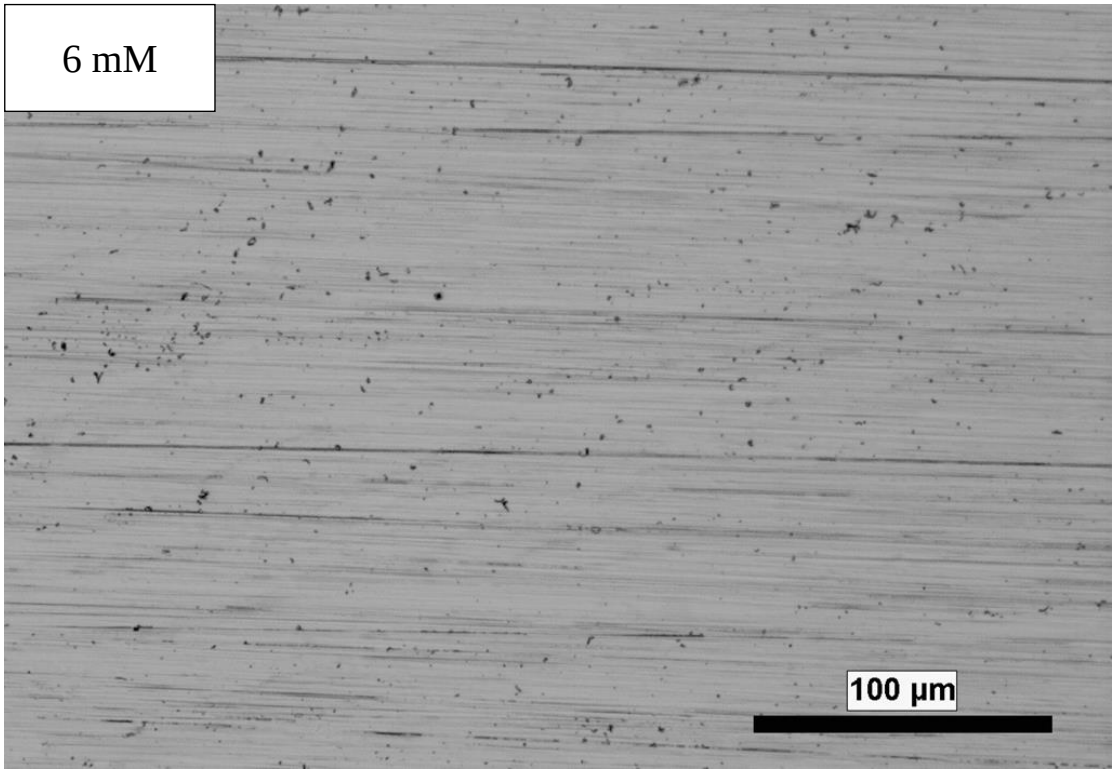
6 mM
100 µm

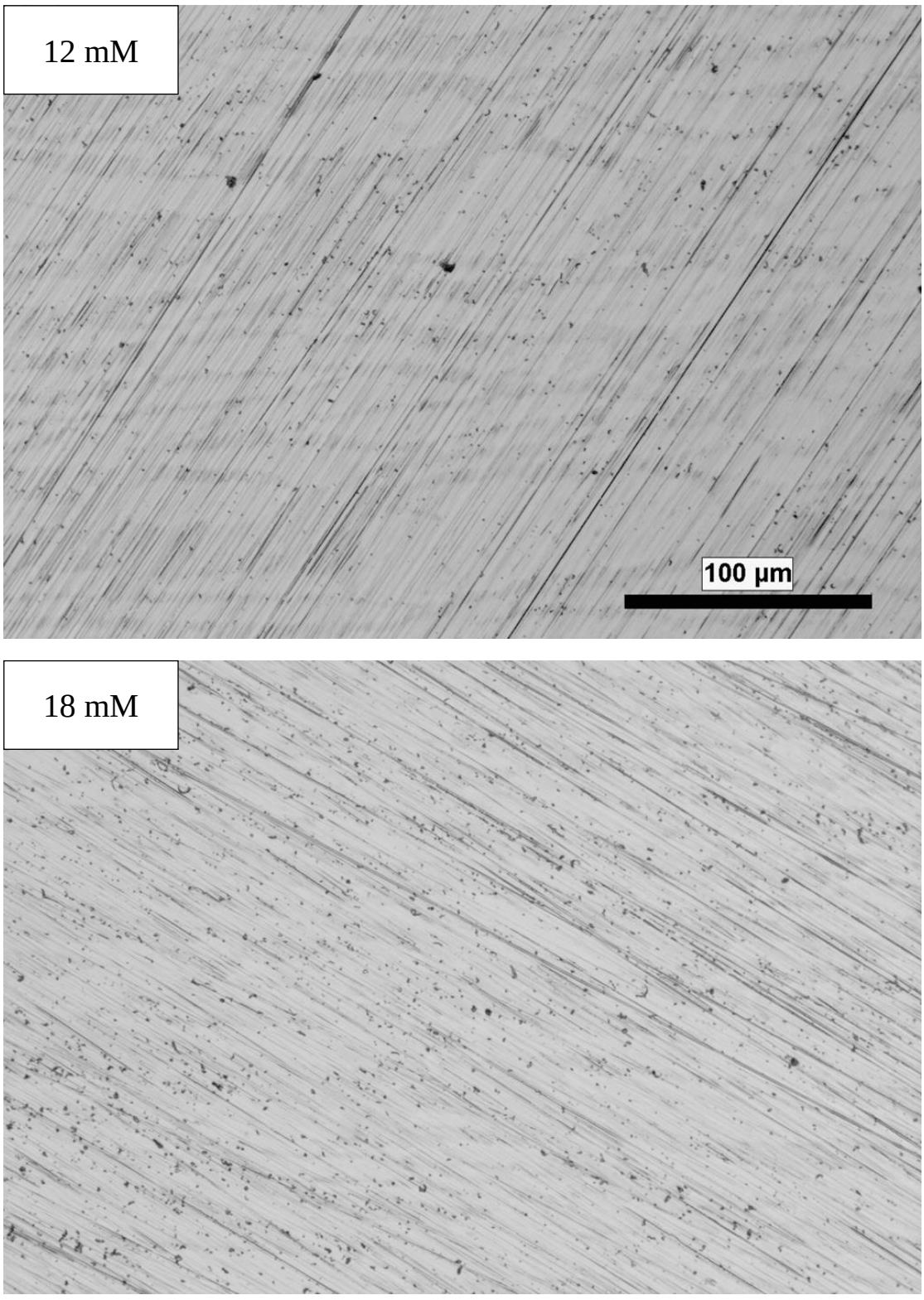

Figure 5-12. Surfaces of 2101 specimens before and after potentiostatic polarization in solution with 0mM, 3mM, 6mM, 12mM, and 18mM $S_2O_3^{2-}$

The surfaces of 2101 specimens before and after tests are shown in Figure 5-12. Again metastable pitting was not labeled on the graph but an increase in number of black dots on the surfaces of specimens was observed after polarization tests.

As can be observed from the images, pit initiation and metastable pit growth was enhanced with the addition of thiosulfate, especially for solutions containing 12mM and 18mM. The metastable pit initiation seems to be preferentially located in the ferritic phase.

To confirm that metastable pitting initiates preferentially on ferritic phase of 2101. Specimens of 2101 were polished to mirror finish and etched to reveal ferritic and austenitic phase. Polarization in 0.6M NaCl at 0V vs. SCE showed that pits indeed preferentially initiates on the ferritic phase and the phase boundary of 2101, a few of which are shown in Figure 5-13.

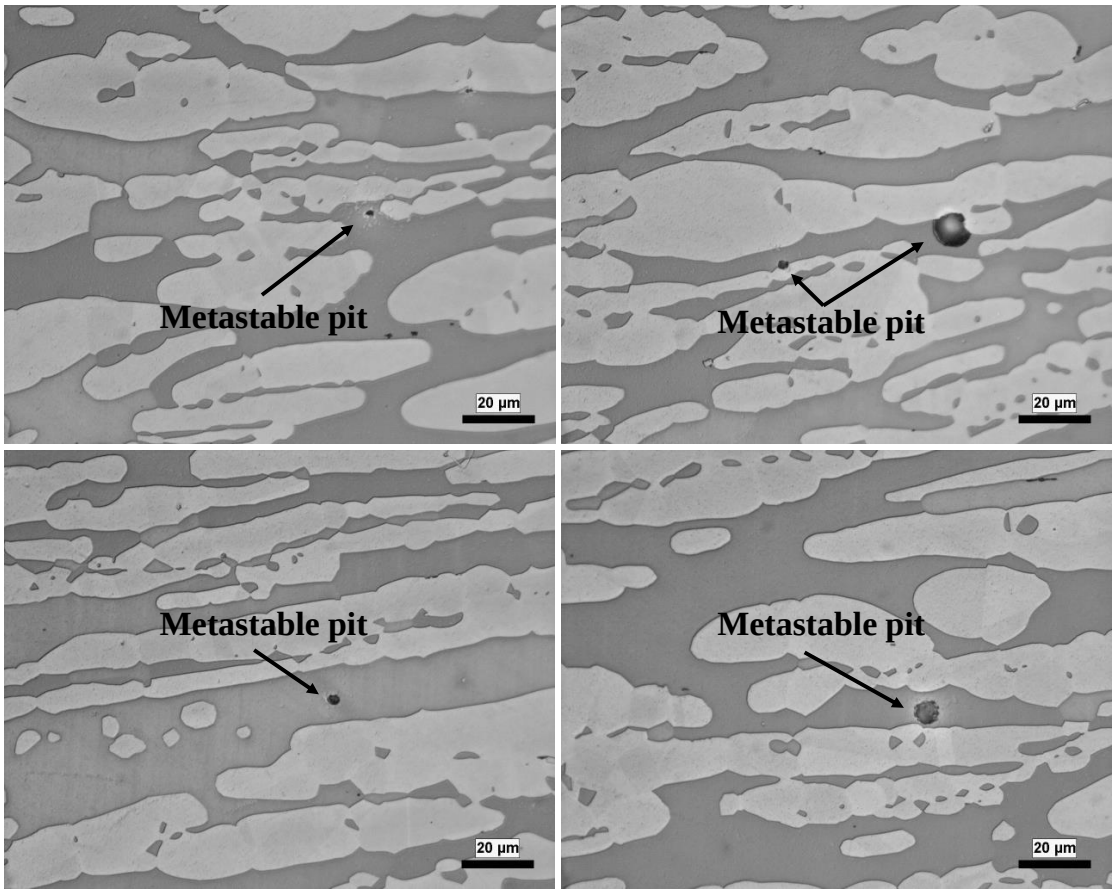

Figure 5-13. Preferential pit initiation on ferritic phase of 2101

5.4. Conclusions

In this chapter, effect of thiosulfate on metastable pitting was investigated. Addition of 3mM, 6mM, 12mM, and 18mM thiosulfate was made to a 0.6M NaCl solution. Potentiostatic polarization measurements were used to obtain the information on metastable pitting events. Effect of thiosulfate on pit initiation frequency, pit occurrence time, pit growth time, as well as peak current distribution for 304L and 2101 was investigated by statistical analysis.

It was shown that the addition of thiosulfate promoted pit initiation in both 304L and 2101. Peak currents shifted to larger values in presence of thiosulfate for both 304L

and 2101. For 304L, the percentage of metastable pits with shorter growth time seem to be promoted with the addition of thiosulfate. However, the effect of thiosulfate on growth time of metastable pits in 2101 and occurrence time in 304L and 2101 was not definitive. Pit initiation preferentially occurred on the ferritic phase of 2101.

6. EFFECT OF MICROSTRUCTURE ON PITTING CORROSION OF 2101 IN CHLORIDE AND THIOSULFATE CONTAINING ENVIRONMENT

From the tests described in Chapter 4, it was observed that ferritic phase of 2101 duplex stainless steel samples was preferentially attacked in chloride and thiosulfate containing environments. Results from potentiostatic tests, discussed in Chapter 5, also confirmed that the metastable pitting was found to initiate preferentially on chromium enriched and nickel deficient ferritic phase of 2101. Since the wrought 2101 is anisotropic, it is expected that the microstructure will influence its pitting behavior depending on which surface is exposed. In this chapter, the effect of microstructure of 2101 on pitting corrosion and the mechanism of thiosulfate-related pitting was further explored.

The surface for rolling direction, transverse short, and transverse long faces of DSS2101 were labeled 2101-X, 2101-Y, and 2101-Z, respectively, as shown in Figure 6-1.

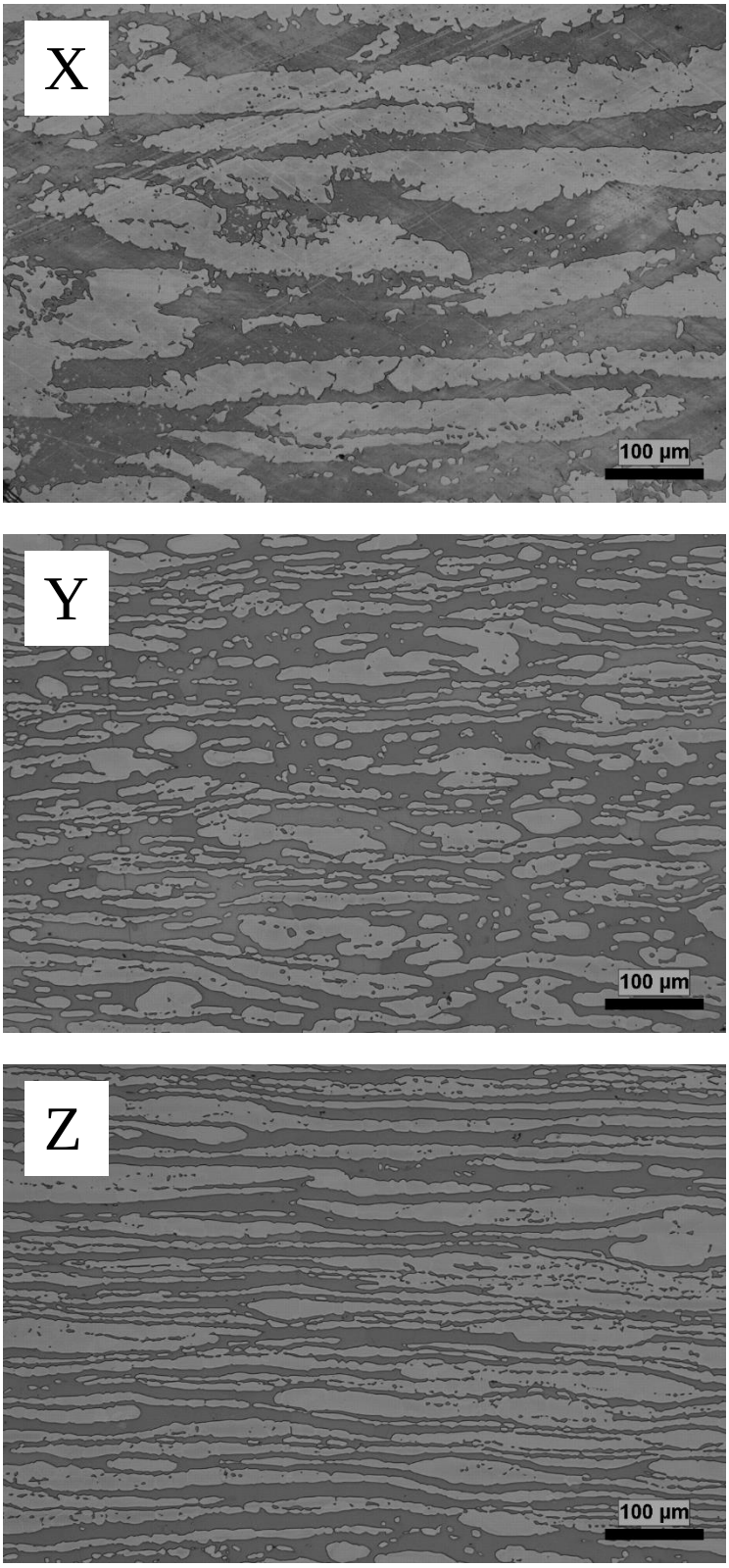

Figure 6-1. Microstructure of the 3 Surfaces of 2101 Specimens

The volume fraction of ferritic phase in 2101 used in this study was evaluated by point counting on 2101-Y surfaces, as shown in Figure 6-2. Three cross-section was made, five field of view (FOV) was taken from each cross-section.

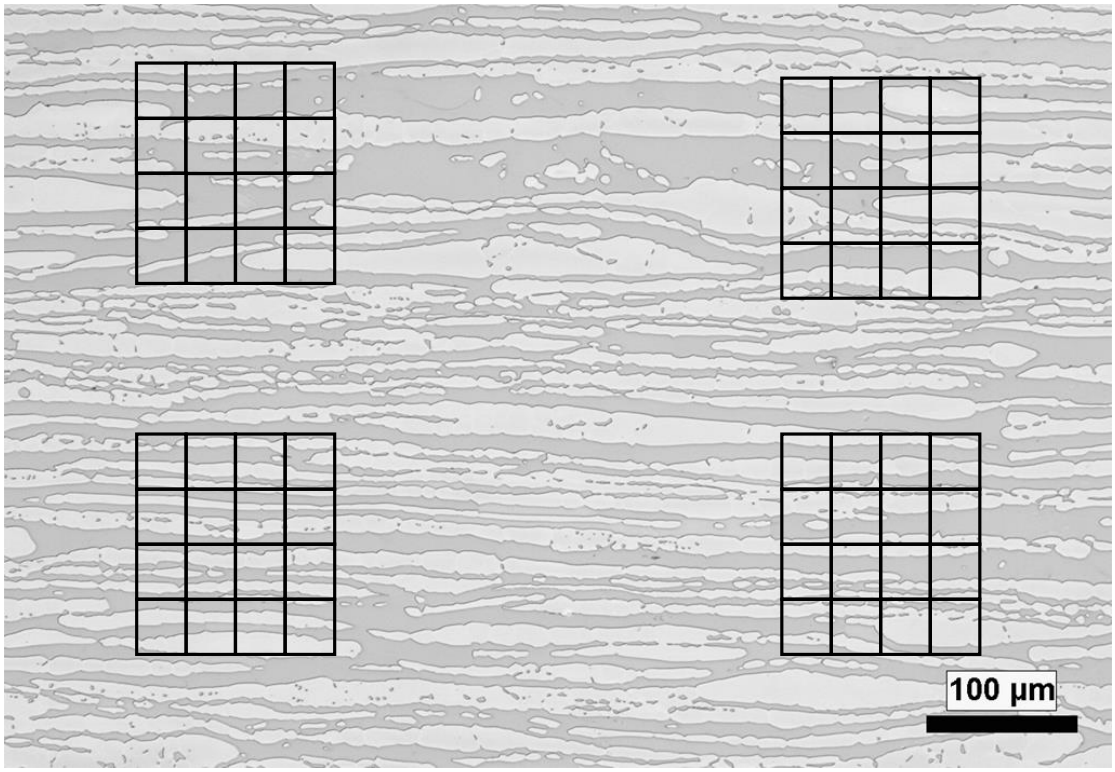

Figure 6-2. Estimation of volume fraction of ferritic phase by point counting

The volume fraction of 2101 from point counting method was estimated to be 45.97±3.22%. The length of phase boundary per unit area was also evaluated by point counting method, as shown in Figure 6-3. Again, 15 FOVs were used in the statistical analysis for each surface orientation, 5 FOV was taken from each cross-section.

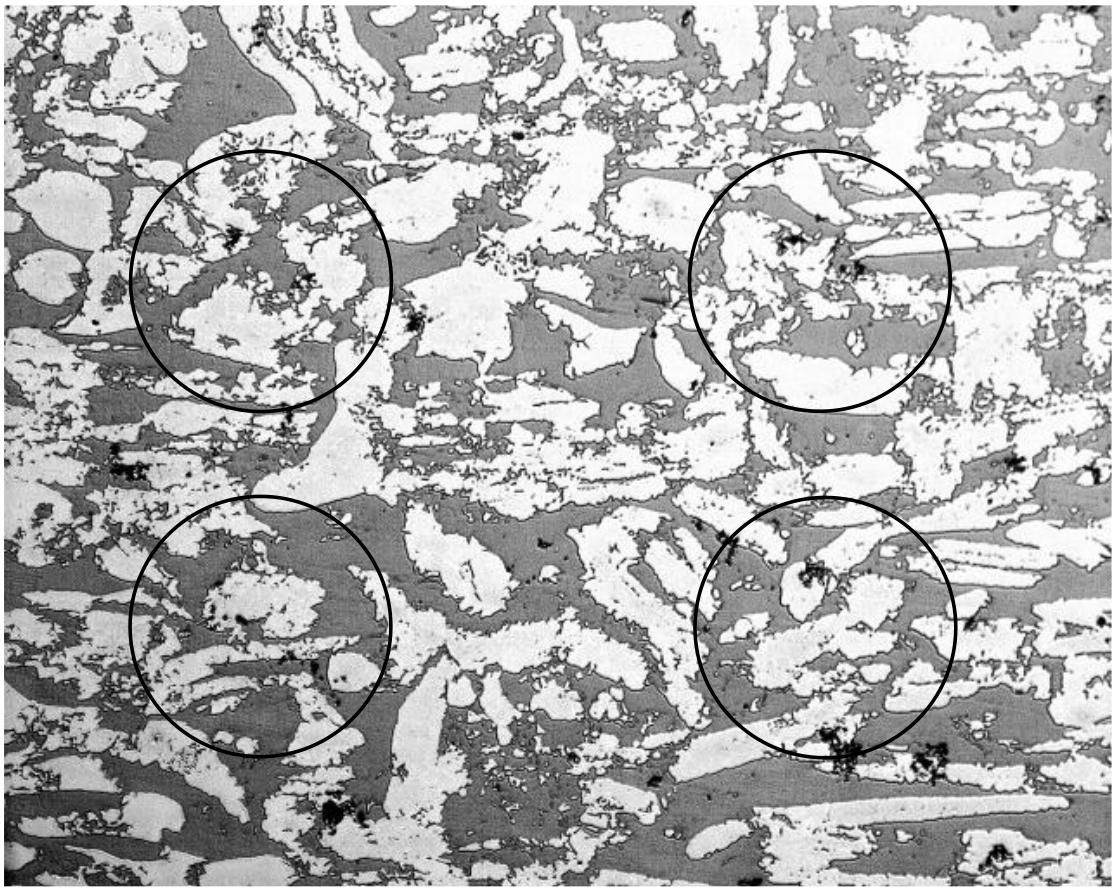

Figure 6-3. Estimation of length of phase boundary per unit volume

The length of phase boundary per unit volume was estimated to be 31.67 ±2.05 mm^{-1} for 2101-X, 119.81 ±6.48 mm^{-1} for 2101-Y, and 116.97 ±6.08 mm^{-1} for 2101-Z. As can be anticipated from the microstructure, 2101-X has shorter inter-phase boundary length per unit volume than 2101-Y and 2101-Z, the two of which are comparable.

6.1. Effect of Microstructure on Pitting and Repassivation Kinetics

Cyclic potentiodynamic polarization measurements were performed in 300ppm Cl^- + 58ppm $S_2O_3^{2-}$ at 50 ℃ for the three surfaces. To observe the morphology of pits formed on the three surfaces, 3 specimens of each surface was ground to mirror finish

and etched in 40% NaOH solution at 2.5V to reveal the austenite and ferrite phases. Pit morphology of the pits formed on the three surfaces after cyclic potentiodynamic measurements is shown in Figure 6-4.

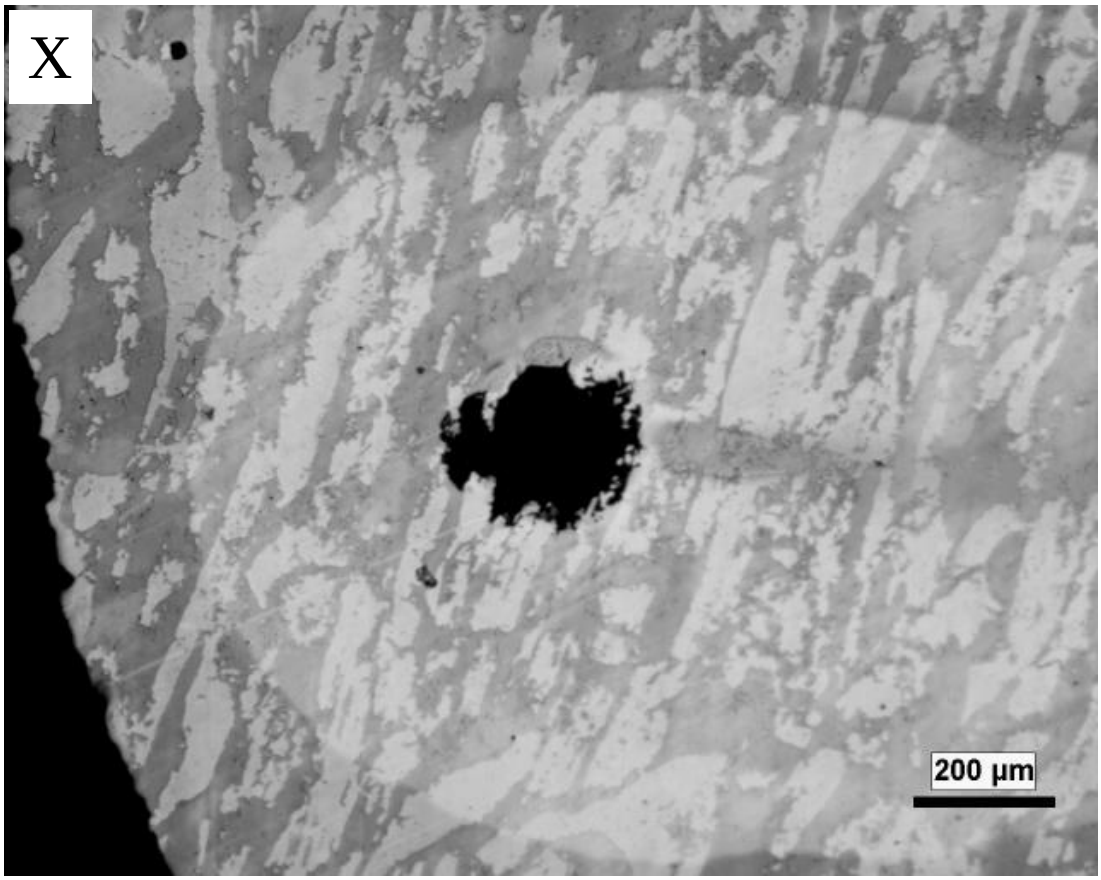

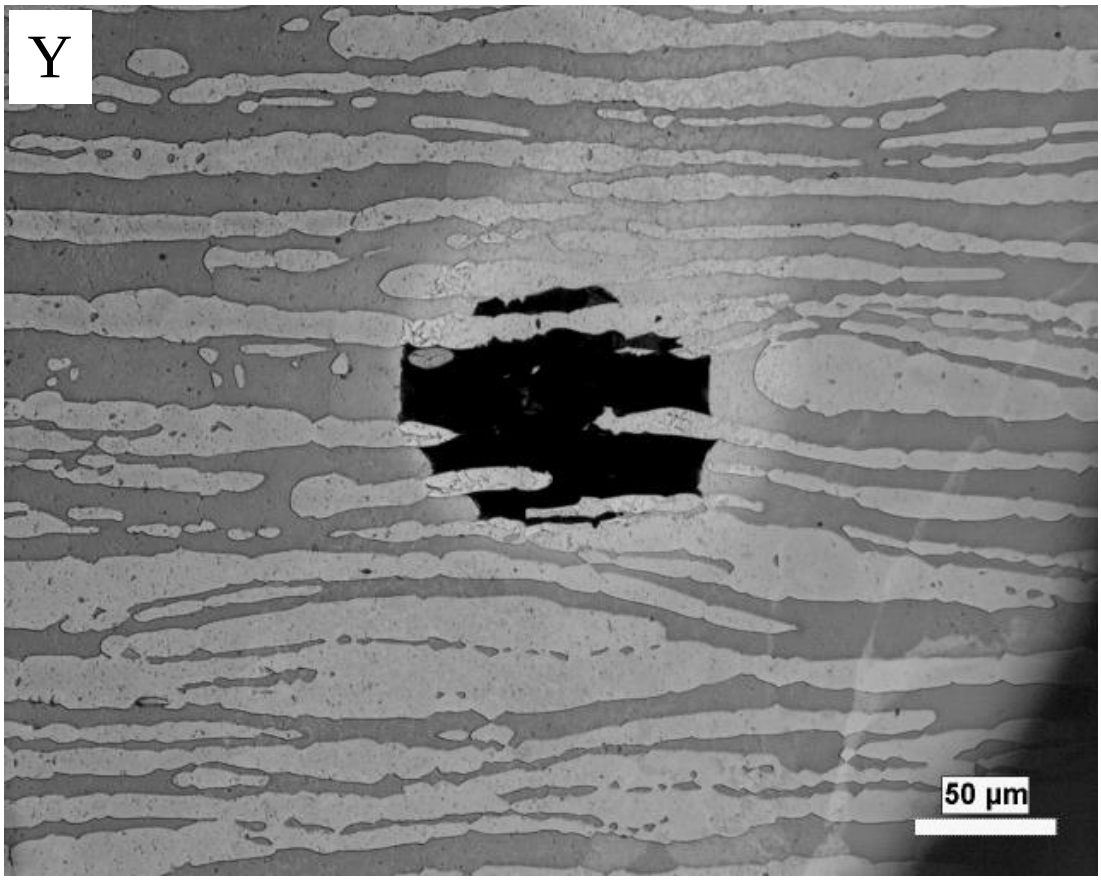
Y
50 µm

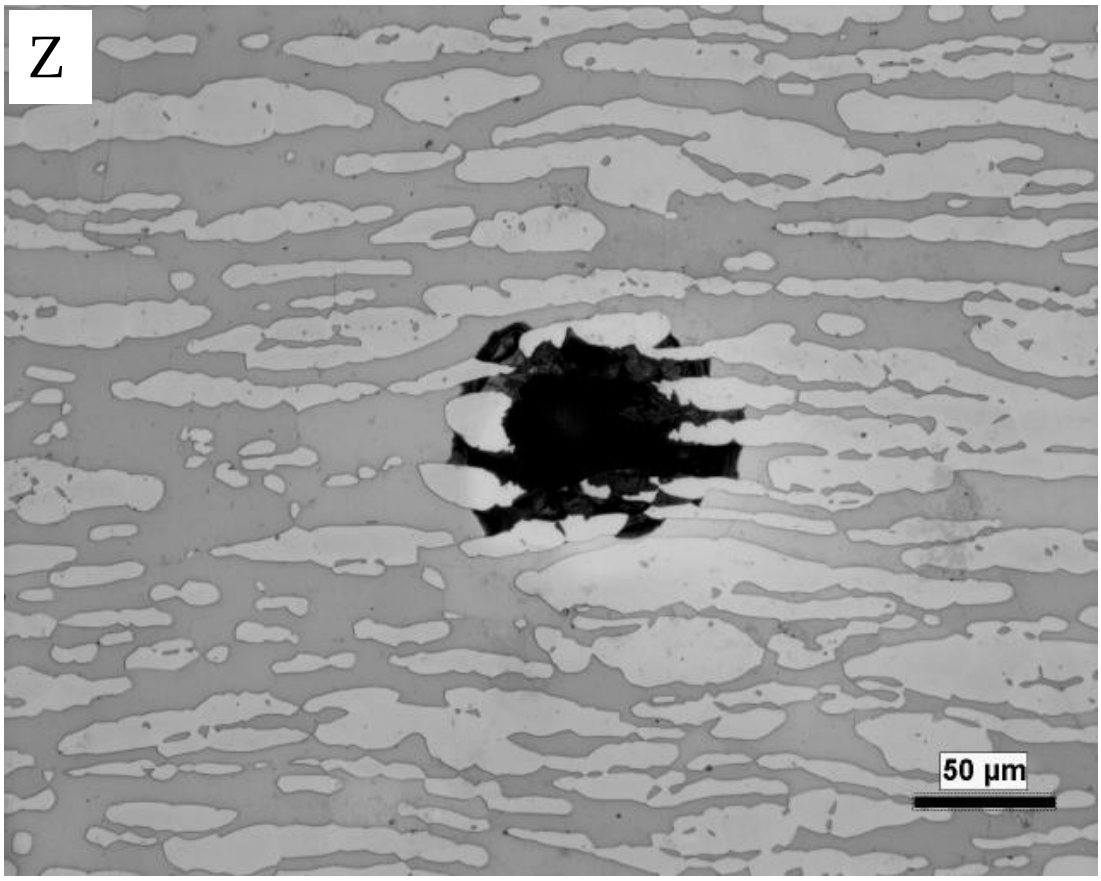

Figure 6-4. Pit morphology on 2101-X, 2101-Y, and 2101-Z etched specimens in

Again, preferential dissolution of ferritic phase was observed for each orientation. However, due to the morphology of the ferritic phase in a particular direction for this wrought stainless steel, pits formed on 2101-Y and 2101-Z tend to be confined by the stripes of ferritic phase, while pits formed on 2101-X were round at the surface.

The pitting potentials and the repassivation potentials for the three surfaces are shown in Figure 6-5.

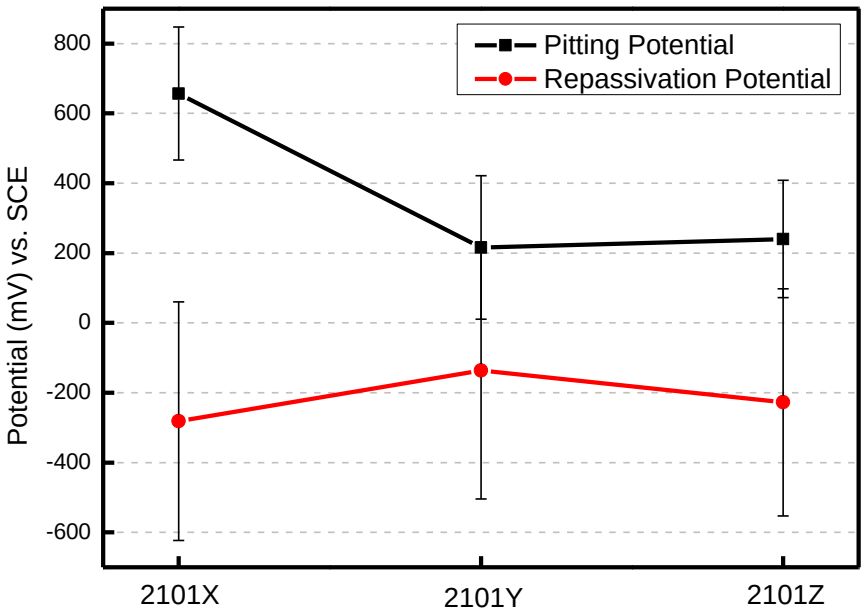

Figure 6-5. Pitting and Repassivation Potentials of 2101-X, 2101-Y, and 2101-Z

As can be observed from the graph, pitting potential of 2101-X is higher than that of 2101-Y and 2101-Z. However, the repassivation potentials of the three surfaces are similar. The scattering of repassivation potentials for the same material was observed to be higher than that of pitting potentials.

The difference of pitting potential between 2101-X and 2101-Y/Z direction was due to pit initiation and/or pit growth. The microstructure of 2101-X could have less pit initiation sites due to less phase boundary length per unit area, which would result in an increase the pitting potential for this surface. On the other hand, if the microstructure of 2101-X favors repassivation of metastable pits, pitting potential would also increase.

6.2. Effect of Microstructure on Metastable Pitting

Effect of thiosulfate on metastable pitting behavior of 2101-Y has been discussed in Chapter 5. In this section, the effect of thiosulfate on metastable pitting of 2101-X and 2101-Z is discussed and compared with the pitting behavior of 2101-Y.

The statistical analysis of metastable pitting behavior for 2101-X and 2101-Z are shown in Figure 6-6 and Figure 6-7, respectively.

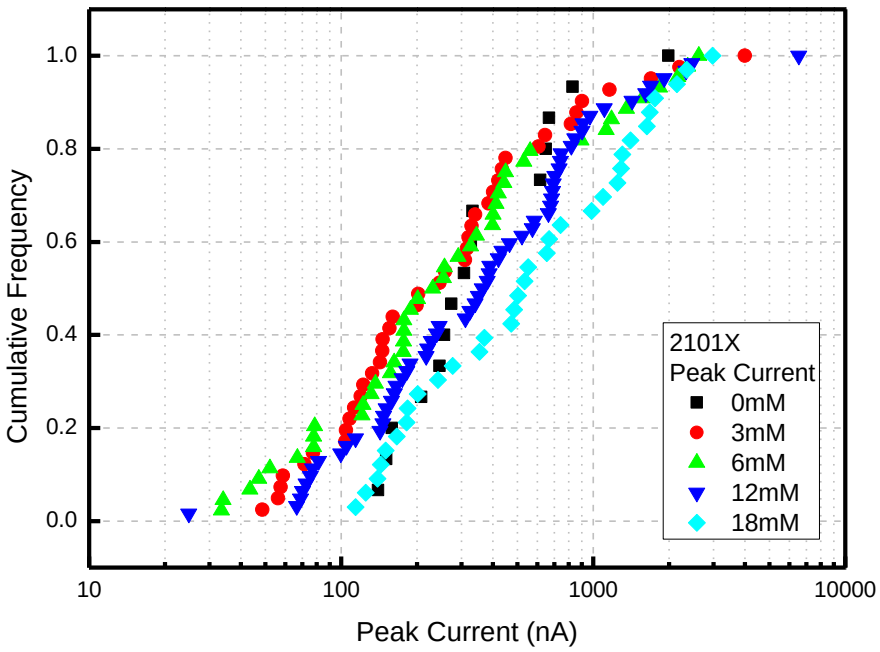

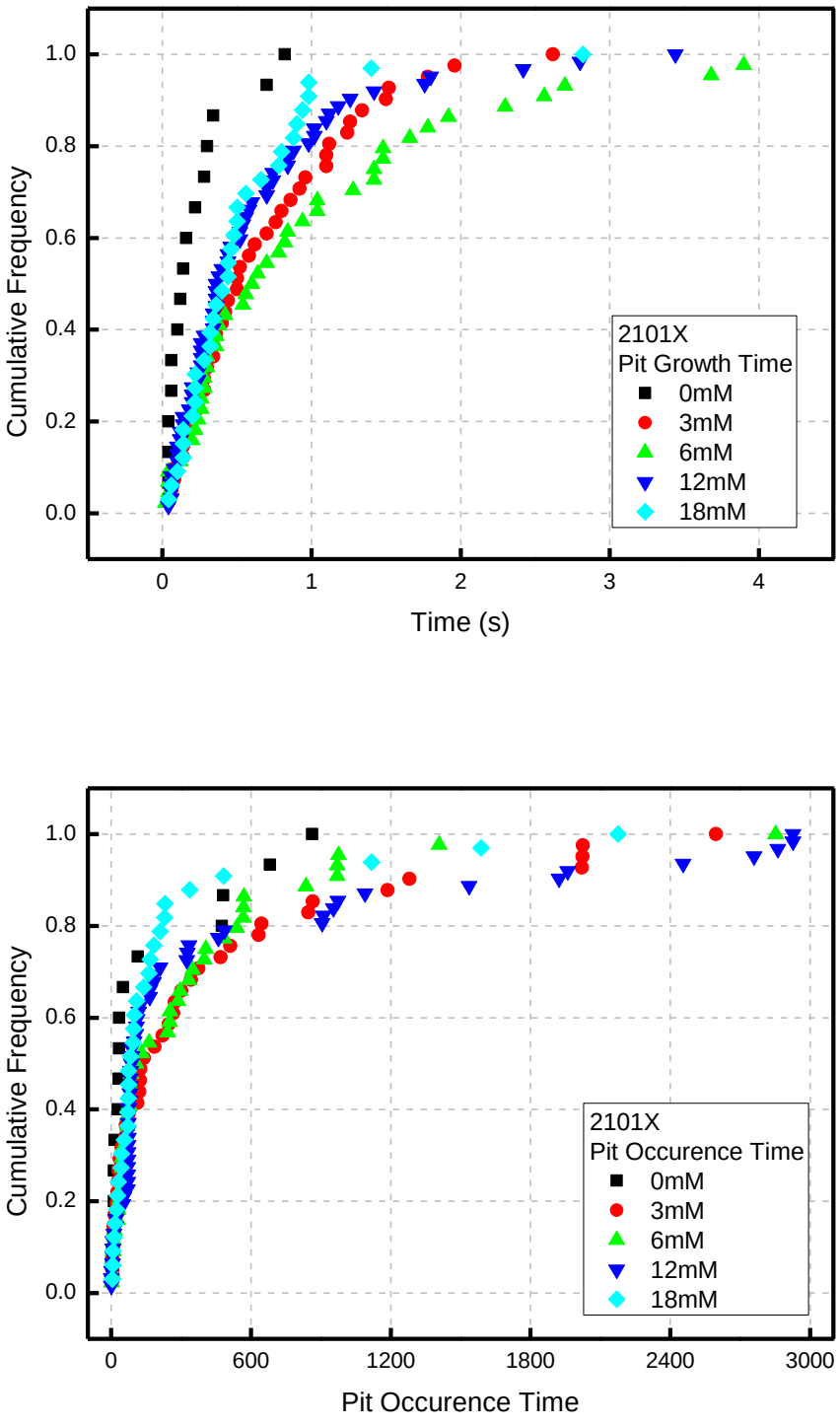

Figure 6-6. Peak current, pit growth time, and pit occurrence time of metastable pitting events for 2101-X in 0.6M NaCl solution with addition of various concentrations of thiosulfate

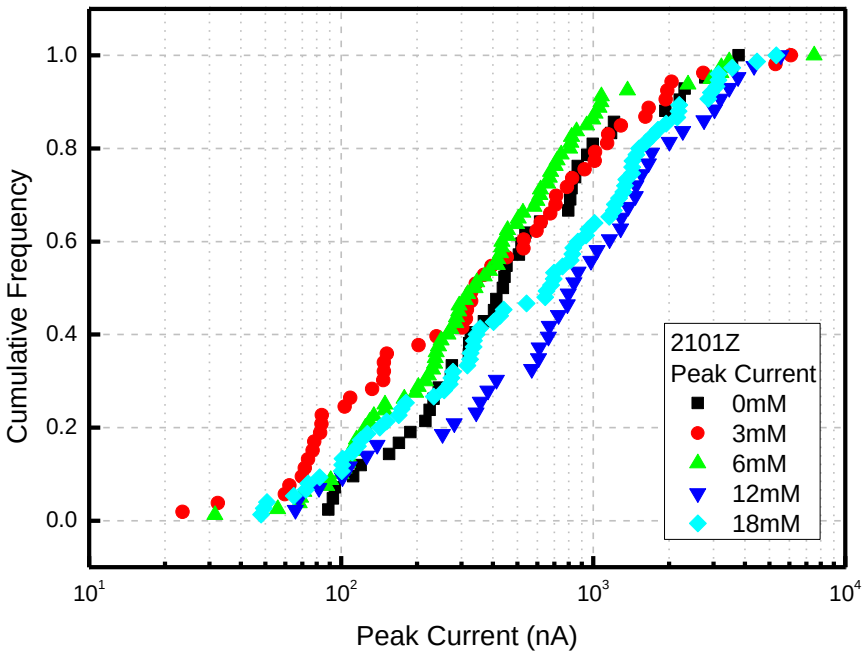
Cumulative Frequency
1.0
0.8
0.6
0.4
0.2
0.0
10^1
10^2
10^3
10^4
Peak Current (nA)
2101Z
Peak Current
0mM
3mM
6mM
12mM
18mM

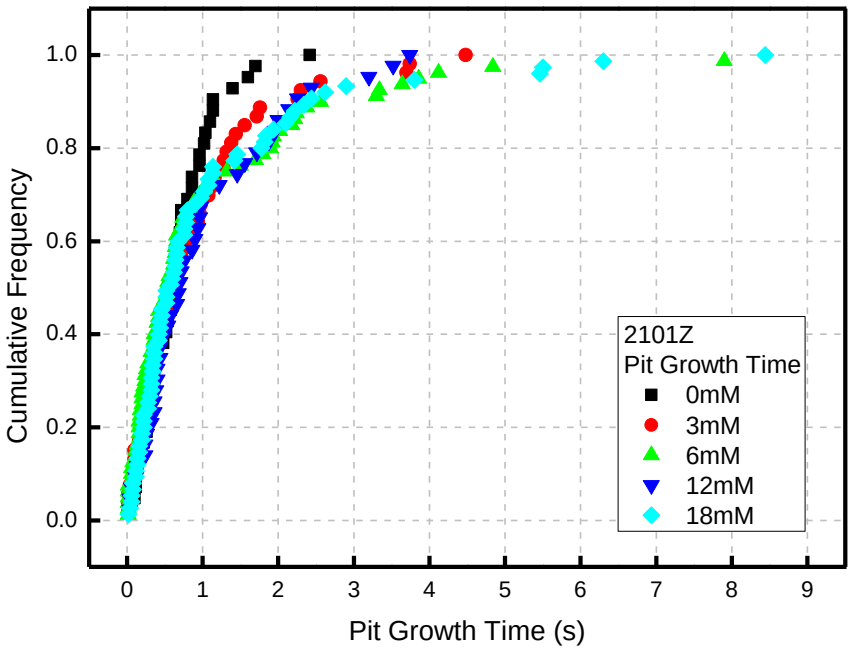
Cumulative Frequency
1.0
0.8
0.6
0.4
0.2
0.0
0
1
2
3
4
5
6
7
8
9
Pit Growth Time (s)
2101Z
Pit Growth Time
0mM
3mM
6mM
12mM
18mM

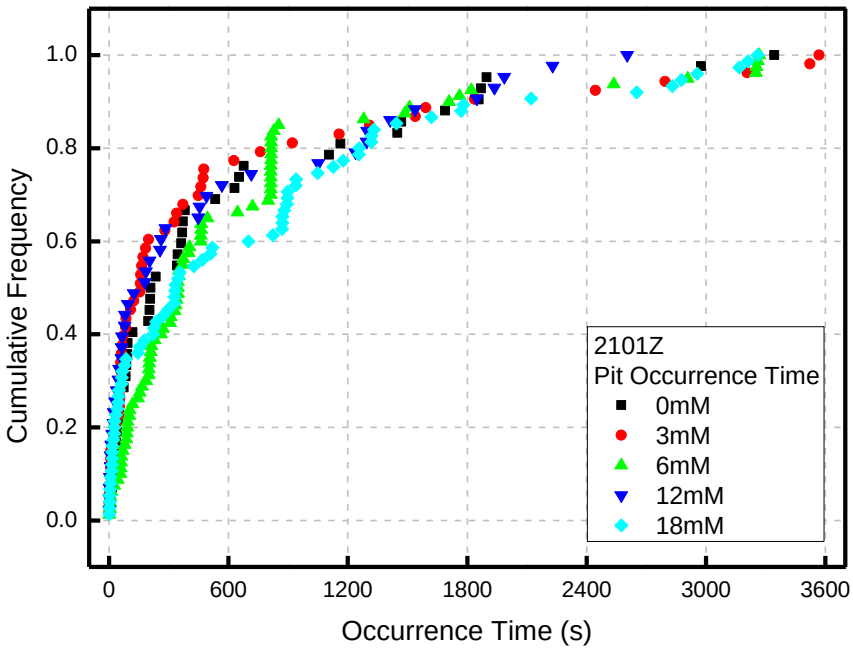

Figure 6-7. Peak current, pit growth time, and pit occurrence time of metastable pitting events for 2101-X in 0.6M NaCl solution with addition of various concentrations of thiosulfate

Pit growth time is the time span between the onset of pitting to the peak current. Pit occurrence time is the time, with respect to the start of polarization, at which the pit reaches its peak. Similar to 2101-Y, addition of thiosulfate results in an increase in the peak current of the metastable pits for 2101-X and 2101-Z, although the influence was not as big as for 304L, as shown in Figure 5-5 in Chapter 5. Addition of thiosulfate promoted pit with short growth time, but did not influence the pit occurrence time.

A comparison between 2101-X, 2101-Y, and 2101-Z was made for peak current and growth time of the metastable pitting events in environments with 0mM and 18mM

thiosulfate, as shown in Figure 6-8 and Figure 6-9.

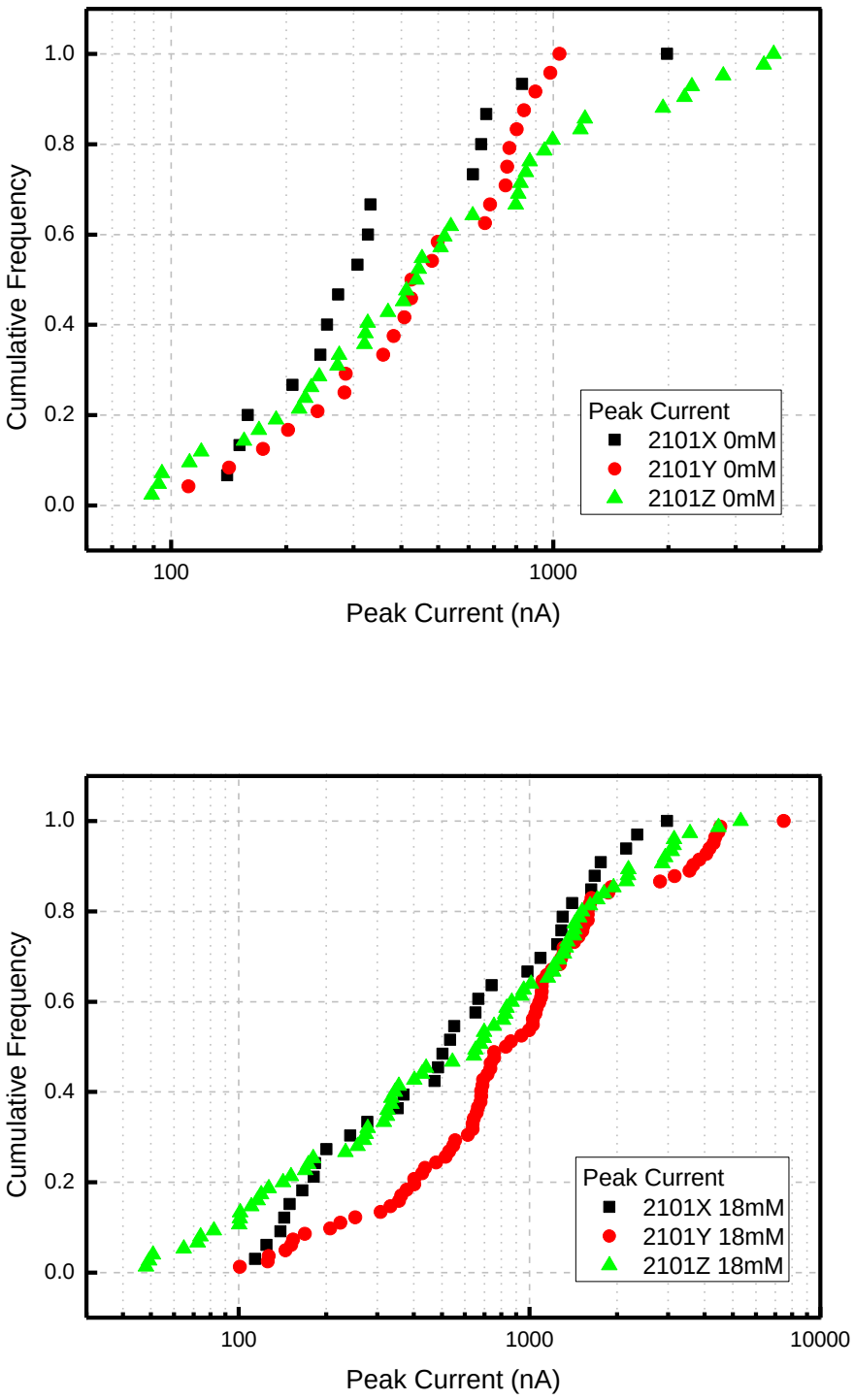

Figure 6-8. Peak current distribution of 2101-X, 2101-Y, and 2101-Z

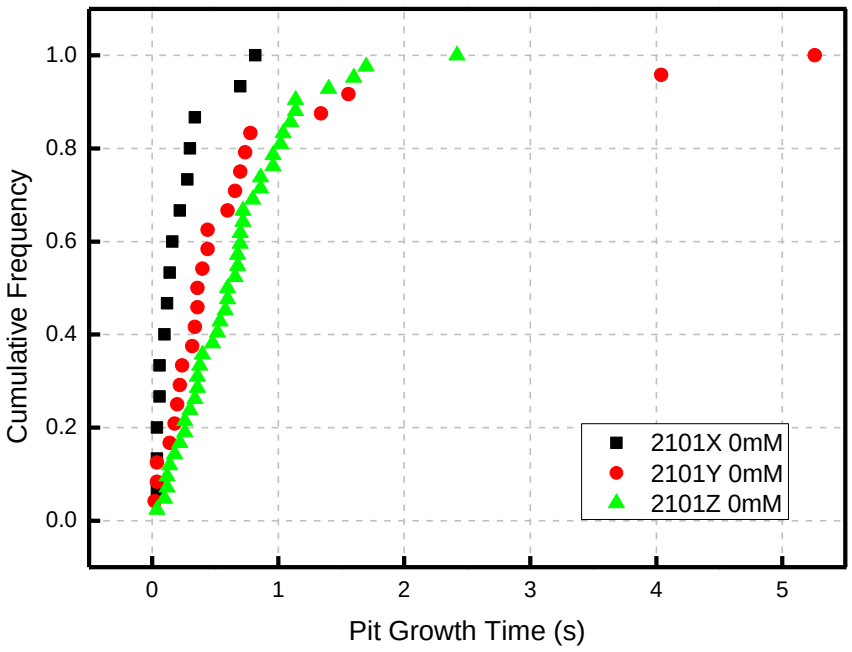

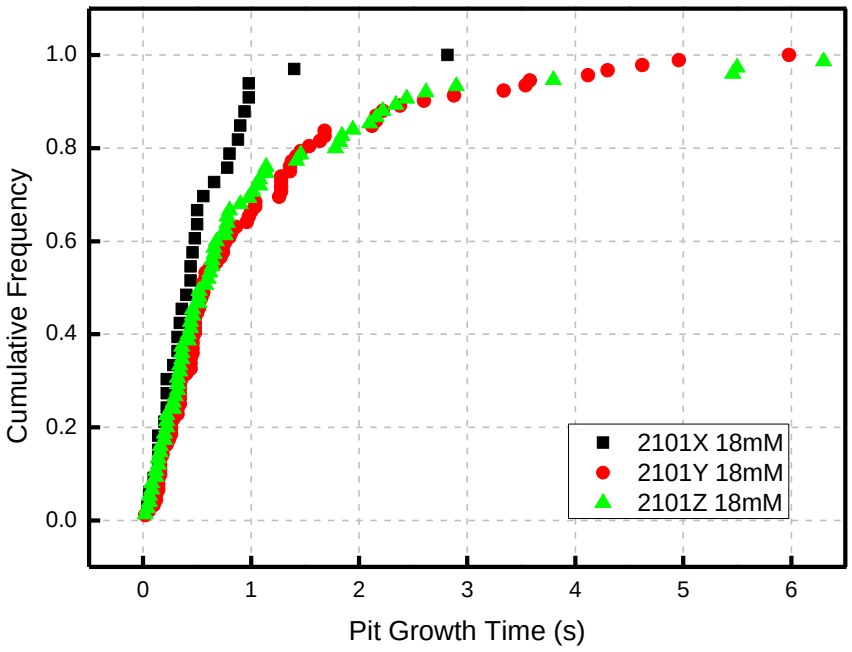

Figure 6-9. Pit growth time distribution of 2101-X, 2101-Y, and 2101-Z

It is clear that 2101-Y and 2101-Z had longer pit growth time, especially for larger values. Pit growth time for 2101-X did not exceed 3 seconds in either environment, while pit growth time for 2101-Y and 2101-Z could be as high as 6 seconds.

The growth of metastable pits for 2101-X and 2101-Y/Z is shown in a cross section view in Figure 6-10.

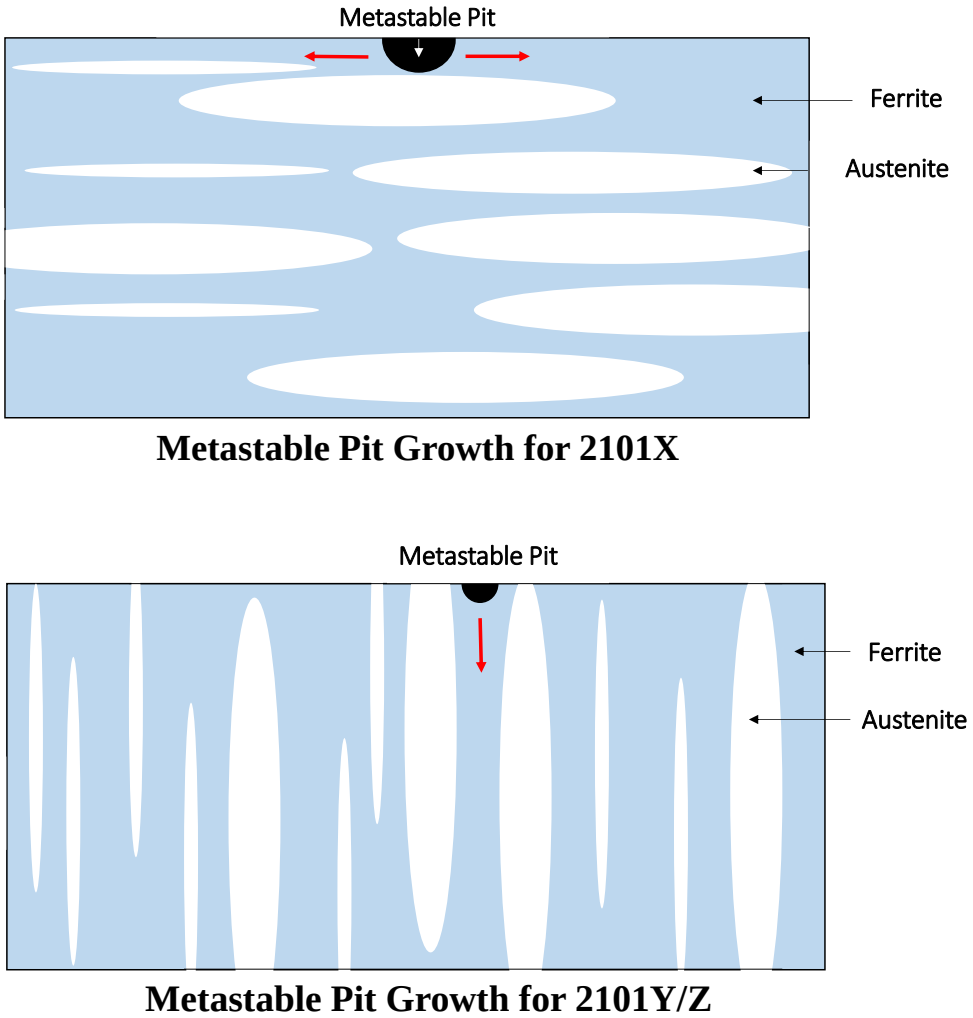

Figure 6-10. Cross section view of metastable pit growth for 2101-X and 2101-Y/Z

Since the austenitic phase of DSS2101 is more corrosion resistant in the same

environment than its ferritic phase in tested environments, the growth of pits would experience a barrier when the front of the pit growth hits the phase boundary. A more aggressive environment is required for the pit to initiate and sustain pit growth in the austenitic phase. Due to the short growth time of metastable pits, most of the existing metastable pits would not have an environment that is aggressive enough to pit through the austenitic phase. For 2101-X, therefore, the pit growth is within the ferritic phase, which extends horizontally. The pit growth is essentially a 2-D pit growth. Once passive film breaks for the pit on 2101-X, the enhanced diffusion would quickly destroy the aggressive pit environment and result in the repassivation of the metastable pits. On the other hand, for 2101-Y and 2101-Z, the metastable pits formed would extend vertically into the ferritic phase. If the pit cover breaks, the enhanced diffusion is limited due to the small pit opening, thus growth time of pits tend to be longer than that in 2101-X specimens.

The discussion in this section could also be used to explain the observed phenomena in the former section. Since it's easier for metastable pits on 2101-X specimens to repassivate, because of the large pit opening areas exposed upon pit cover breaks, a higher driving force to pitting is required to sustain the pit growth and transition of metastable pitting to stable pitting. This is the reason 2101-X why has higher pitting potential than 2101-Y and 2101-Z.

The scattering of the repassivation potentials could also be explained with a similar argument. A stable pit which only grows within the ferritic phase of 2101 may undergo repassivation, assisted by the "pitting barrier" provided by the phase boundary, as

shown in Figure 6-11.

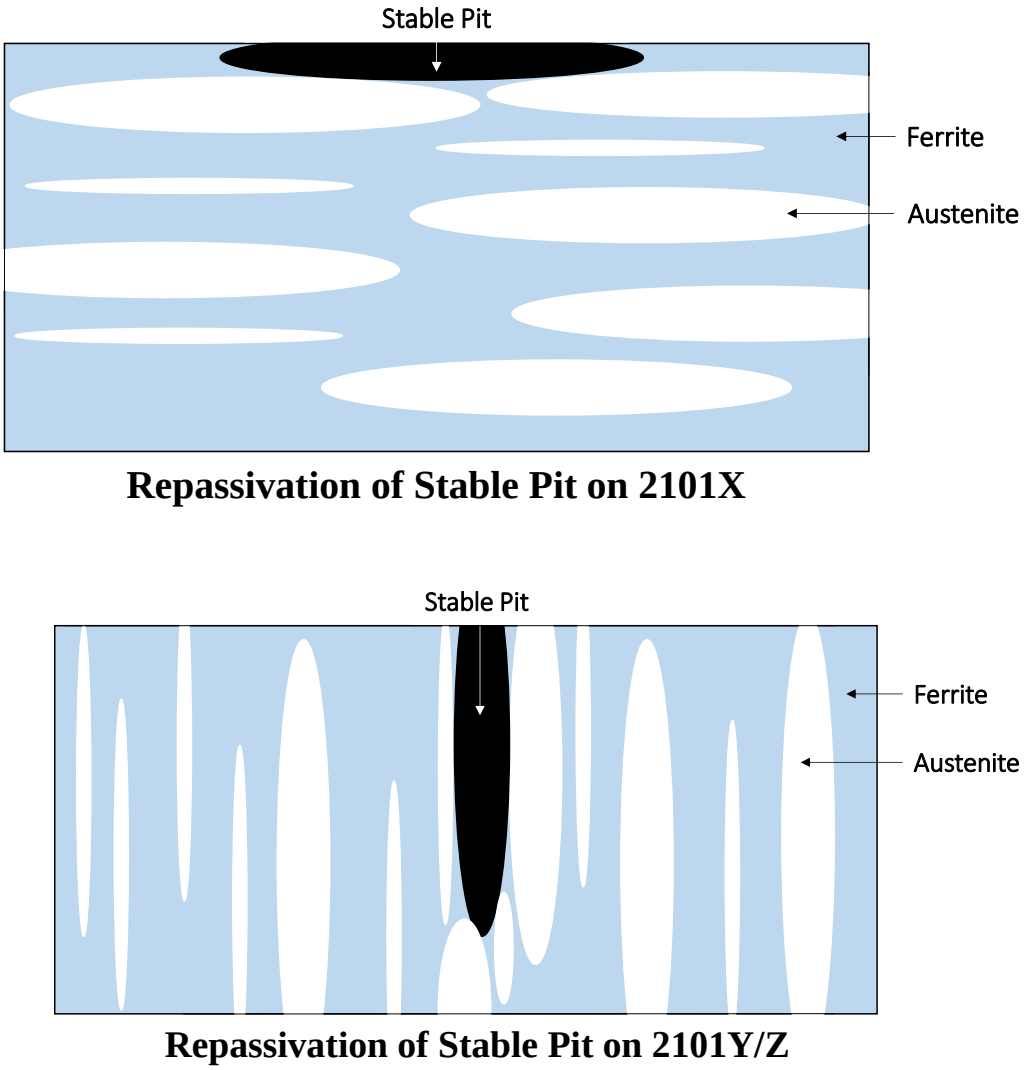

Figure 6-11. Repassivation of stable pits on 2101-X, 2101-Y, and 2101-Z formed in ferritic phase only

The reason for the scattering of repassivation potential is that a stable pit in the ferritic phase may not be a stable pit in the austenitic phase. If the pit in the ferritic phase is large enough to form an aggressive environment that is able to pit through

austenitic phase, the repassivation potentials would be very low. Otherwise, the repassivation potential could be relatively high, depending on how much room for growth is left in the ferritic phase before the pit growth is arrested by phase boundary.

Setting a considerably large limiting current, 2mA/cm^2, at which the potential sweep is reversed, would result in the formation of a stable pit which can grow in both phases, thus remove the large scattering of the repassivation potential, as is shown in Figure 6-12.

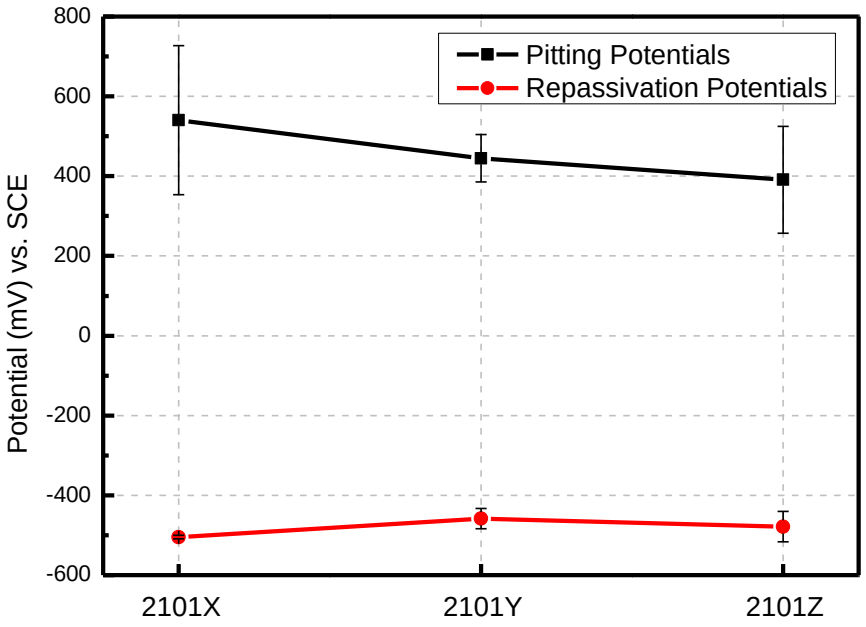

Figure 6-12. Pitting and repassivation potentials of 2101-X, 2101-Y, and 2101-Z in experiments with large limiting current

6.3. Effect of Microstructure on Pit Growth Kinetics

Aside from metastable to stable pit transition and repassivation, microstructure of duplex stainless steels could also influence the growth kinetics of the pits. Scratch tests of two 3-mm thick 2101-Y specimens were performed in solutions with 6000ppm NaCl with addition of 12000ppm Na_2SO_4, and 4000ppm $Na_2S_2O_3$ at 50 ℃. For one specimen, 2101-Y-1, scratch orientation is parallel to the long axis of the "ferritic pancakes". For 2101-Y-2, scratch orientation is perpendicular to the long axis of the "ferritic pancakes", as shown in Figure 6-13.

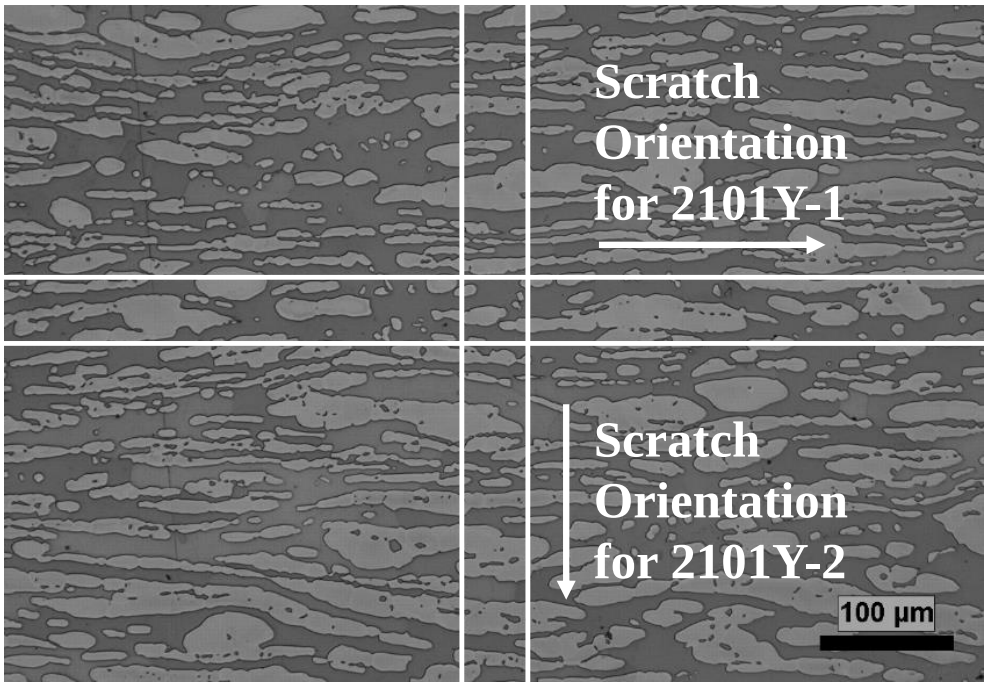

Figure 6-13. Scratch orientations for 2101-Y-1 and 2101-Y-2

The current transients after scratch test on the specimens in the two directions polarized at -300/-200/-100mV vs. SCE are shown in Figure 6-14.

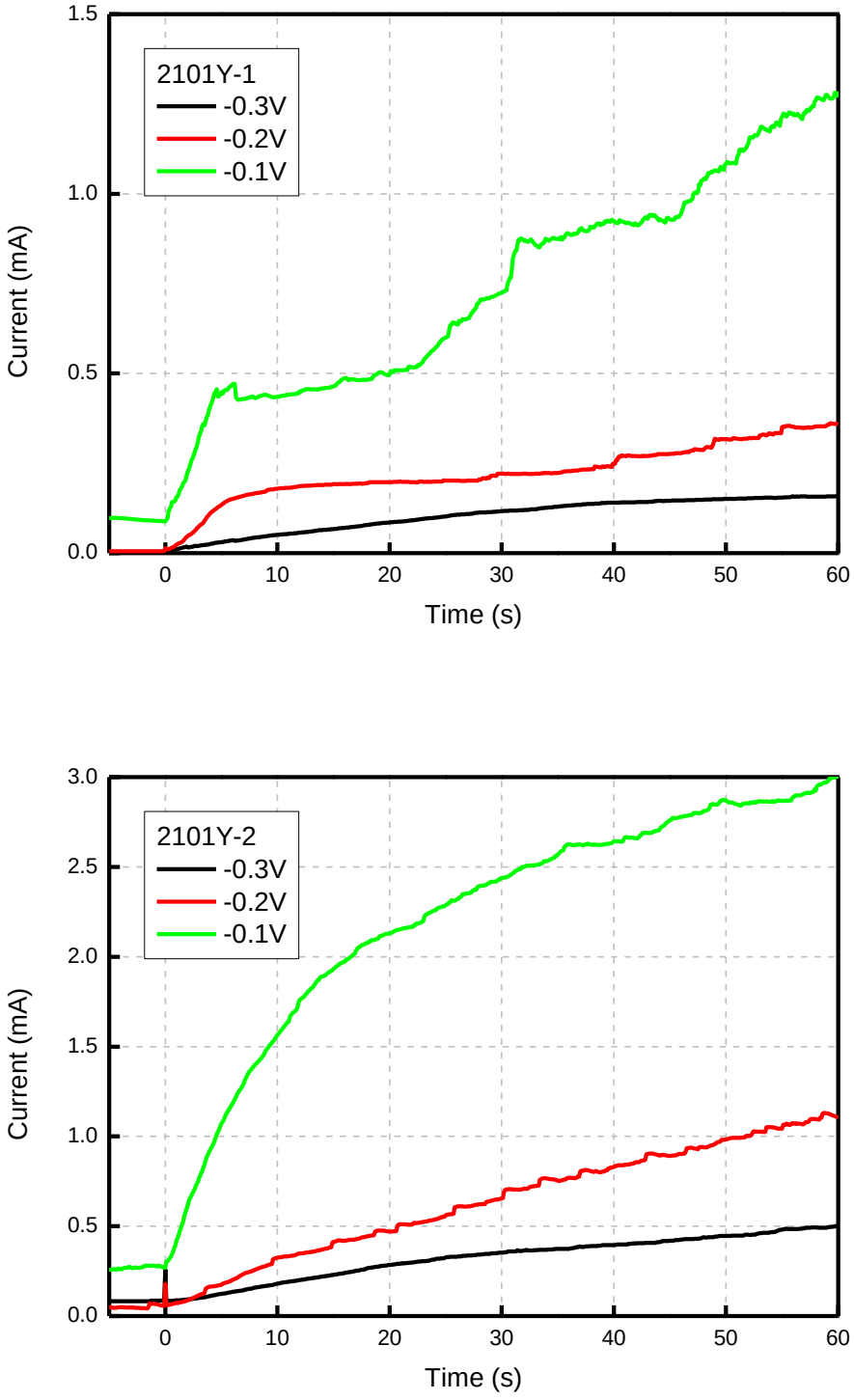

Figure 6-14. Current transients of the 2101-Y-1 and 2101-Y-2 after scratch, polarized at -300/-200/-100mV vs. SCE in 6000ppm NaCl, 12000ppm Na_2SO_4, and 4000ppm $Na_2S_2O_3$ solution at 50 ℃

As can be observed from Figure 6-14 that an increase in the applied potential resulted in an increase in the current at 60 seconds after scratching. It can also be observed that for the two set of scratch tests are done in different directions but on the same surface of the same material, 2101-Y-2 had a much higher current transient than 2101-Y-1 under each applied potential. The optical microscope image for the specimens polarized at -0.1V vs. SCE are shown in Figure 6-15.

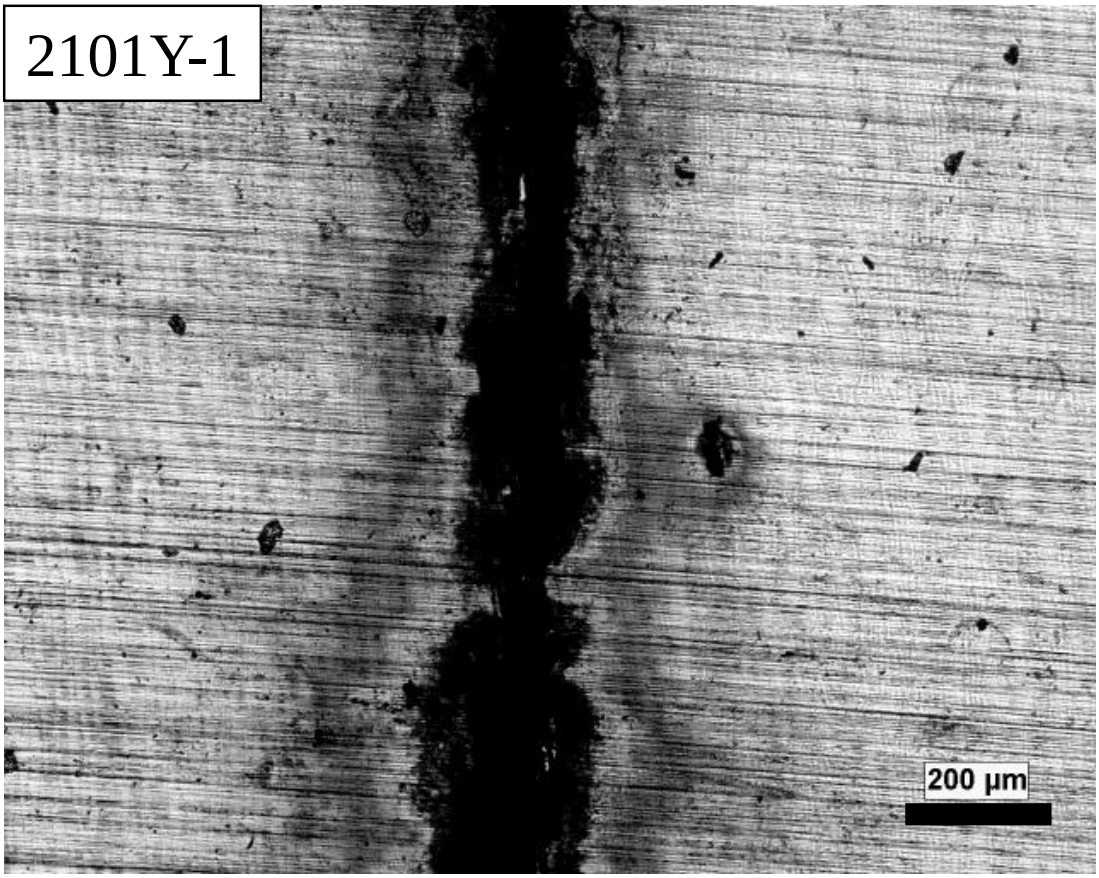

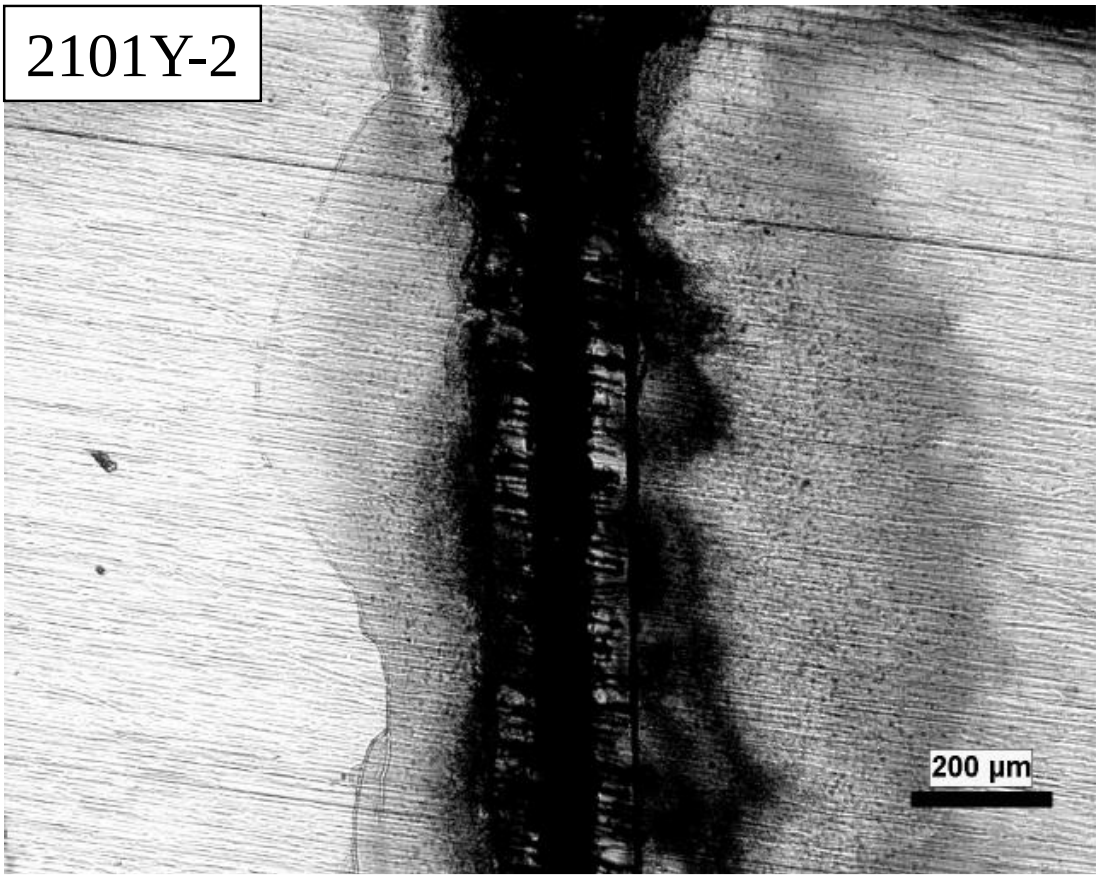

Figure 6-15. Scratch test specimens of 2101-Y-1 and 2101-Y-2 polarized at -0.1V vs. SCE in 6000ppm NaCl, 12000ppm Na_2SO_4, and 4000ppm $Na_2S_2O_3$ solution at 50 ℃

As is shown in the optical images in Figure 6-15, the pit grew preferentially along the ferritic phase of 2101. Similar results to 2101-Y-2 was shown in chapter 4. For 2101-Y-1, because the longer axis of the "ferritic pancakes" oriented parallel to the scratch, the pit formed were within the scratch. A schematic in Figure 6-16 reveals the reason why the current on 2101-Y-2 was much larger than 2101-Y-1.

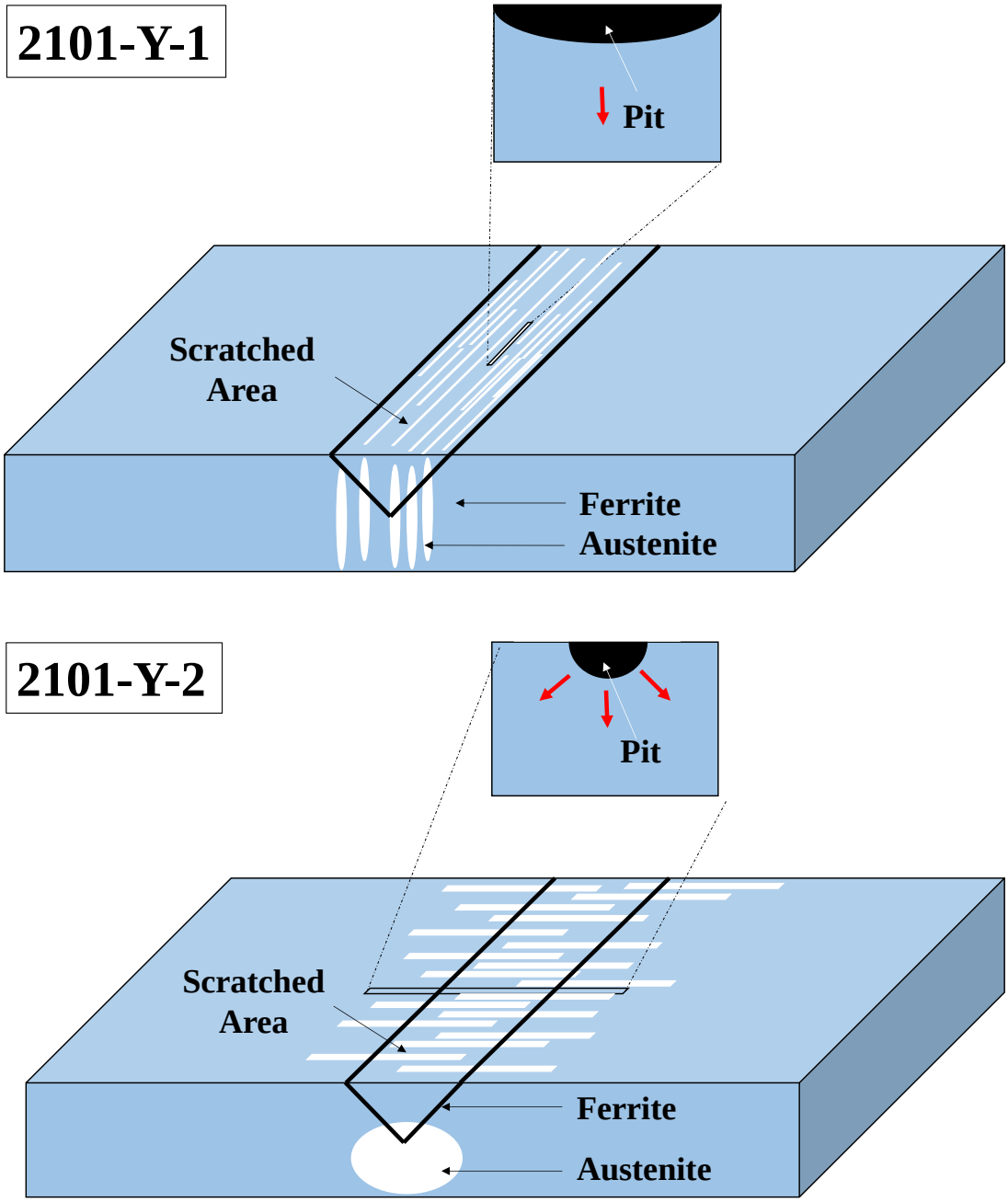

Figure 6-16. Schematic showing pit growth in 2101-Y-1 and 2101-Y-2

In 2101-Y-1, all ferritic phase underneath the scratched area were exposed to the environment, the pit growth is essentially a 1-D pit growth until the front of pit growth meet the austenitic phase boundary. On the other hand, in 2101-Y-2, ferritic phase

within the scratched area were only a fraction of the ferritic phase underneath the scratch, thus the pit growth is a 2-D pit growth, as depicted in the schematic. Therefore the current from pitting corrosion is higher for 2101-Y-2 than for 2101-Y-1.

6.4. Conclusions

In this chapter, the effect of microstructure on the pitting corrosion of duplex stainless steel 2101 was discussed. Quantitative analysis of the volume fraction of the ferritic phase as well as phase boundary per unit area were made and this data was correlated with the pit initiation and growth on surfaces with different orientations with respect to the rolling direction. Effect of microstructure on the pitting and repassivation potentials was evaluated, pitting potential of 2101-X was found to be higher than 2101-Y and 2101-Z. A large scatter in repassivation potentials was seen from the experimental results. Metastable pitting events on the three surfaces of 2101 was analyzed statistically, pits formed on 2101-X was found to have shorter pit growth time than those on 2101-Y and 2101-Z. Combined with the microstructure and the fact that the pits preferentially initiate in ferritic phase, the effect of microstructure on 2101 was revealed. Since the austenitic phase requires more aggressive environment for pit growth, the phase boundary becomes a barrier for pit growth. This explains the easier repassivation of metastable pits on 2101-X surface and its higher pitting potentials. Pit growth was also found to be favored in ferritic phase. It is because of this selective phase preference in which pits grow that the direction of the scratch also determines the pitting kinetics.

7. INTERACTION BETWEEN THIOSULFATE AND INDIVIDUAL ALLOYING ELEMENTS

Understanding the interaction between thiosulfate ions and individual alloying elements in a stainless steel is crucial to mechanistic understanding of thiosulfate related pitting corrosion. In this chapter, equilibrium phase stability diagrams (Pourbaix diagrams) were constructed and used along with the cyclic potentiodynamic polarization measurement results to understand the interaction between alloying elements and the environment. Scratch tests and X-ray photoelectron spectroscopy were used to investigate the interaction between thiosulfate and stainless steels and formation of reaction products at the steel surface, as well as the role of thiosulfate in the growth stage of pitting.

7.1. Potentiodynamic Polarization Measurements

In order to understand the role that individual alloying elements play in the overall pitting corrosion process of stainless steels, corrosion behavior of each alloying element was individually studied through cyclic potentiodynamic polarization measurements using pure metal electrodes. Testing environments were naturally aerated 300ppm Cl^- and 300ppm Cl^- + 58ppm $S_2O_3^{2-}$ solutions at 50 ℃. Experimental procedures were the same as for the cyclic polarization tests carried out on stainless steels specimens.

A background potentiodynamic scan was made on platinum foil for both environments. The polarization curve for both scans are shown in Figure 7-1.

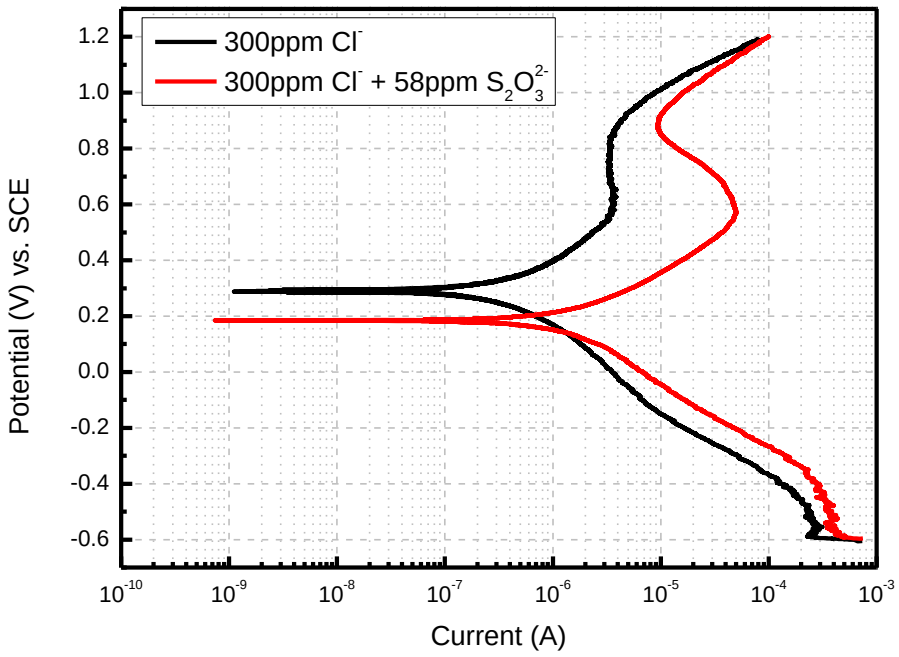

Figure 7-1. Background scan for 300ppm Cl^- and 300ppm Cl^- + 58ppm $S_2O_3^{2-}$ solutions at 50 ℃

In the thiosulfate containing environment, the cathodic current is higher due to the reduction of thiosulfate. According to the mixed potential theory, an increased cathodic current would result in an increased open circuit potential, which is probably why the open circuit potential increased by approximately 100mV. The increased current of anodic polarization curve is due to the oxidation of the sulfur species.

Polarization curves for chromium, nickel, iron, and molybdenum in the two environments at room temperature are shown in Figure 7-2.

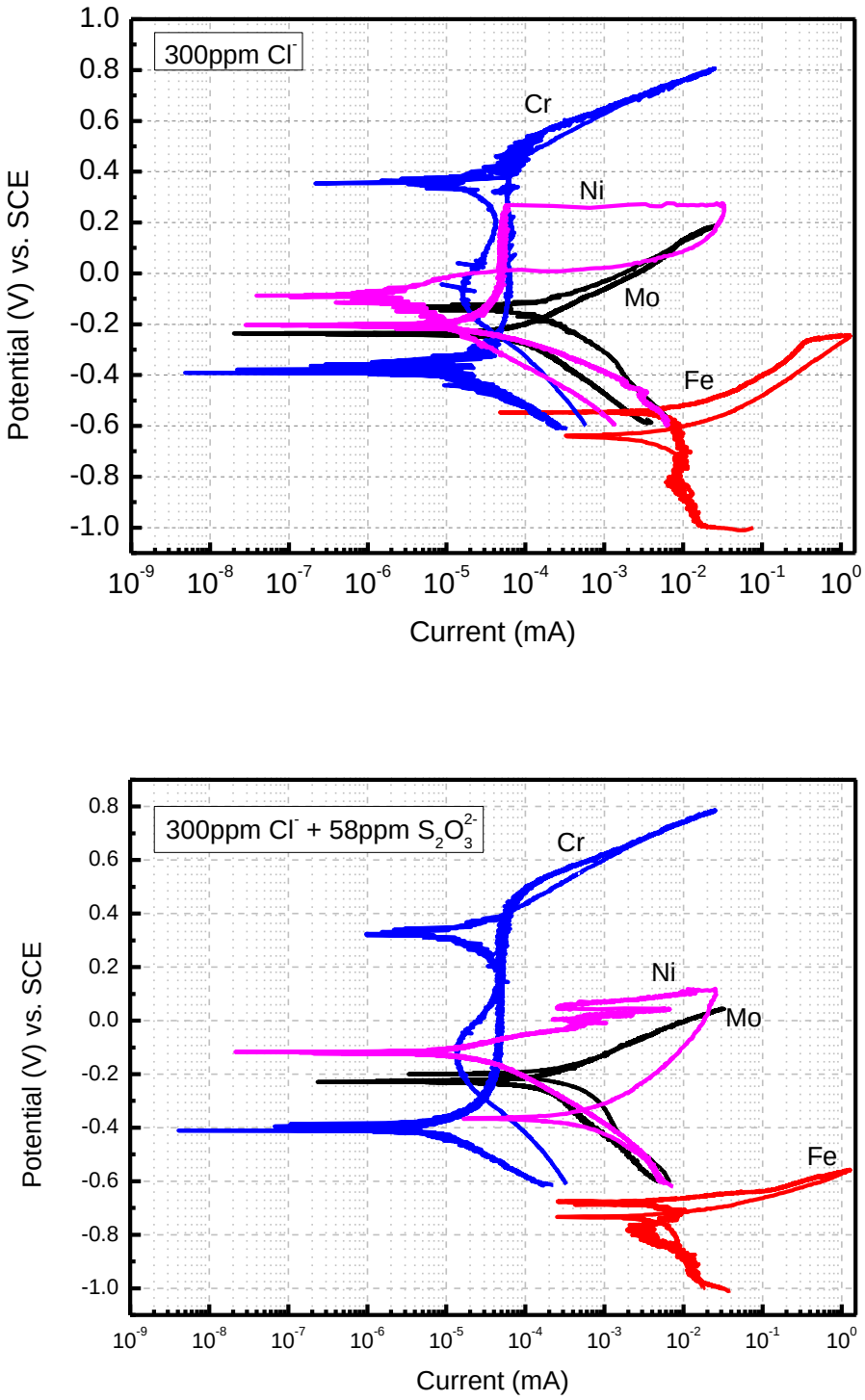

Figure 7-2. Cyclic polarization curves of pure elements in tested environment

As is shown in the graph, chromium showed passive behavior in a larger range of

potentials in both environments, whereas the nickel specimens showed positive hysteresis indicating susceptibility to pitting corrosion. Iron and molybdenum specimens did not show any passive behavior under tested conditions. Comparison of individual elements in the two environments were provided in the following section.

(1) Electrochemical behavior of Chromium:

Polarization behavior of pure chromium in the two environments is compared in Figure 7-3. The addition of thiosulfate to the chloride solution did not change the polarization behavior of chromium much, except for a slight shift in the open circuit potential as well as the transpassive potential. Chromium remained passive from roughly -0.3 V (SCE) to almost 0.4 V (SCE), where the chromium oxide is expected to be the main component in the passive film and thiosulfate is not expected to affect the composition of the passive film. Change in redox behavior due to the addition of sulfur species was not reflected on chromium, which means there is limited interaction between sulfur species and chromium oxide.

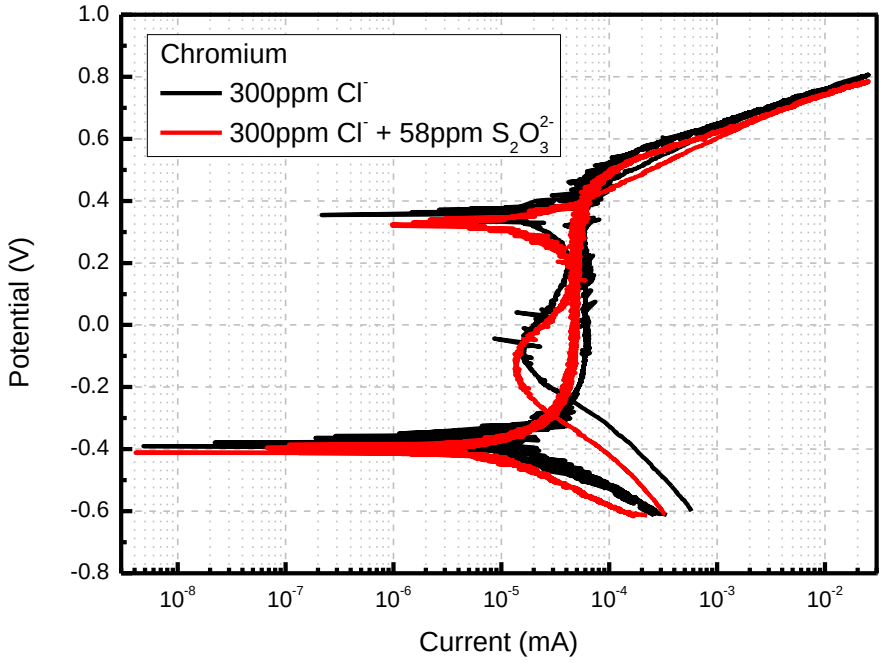

Figure 7-3. Cyclic Polarization Curves of Chromium in 300ppm Cl^- and 300ppm Cl^- + 58ppm $S_2O_3^{2-}$ Solutions

(2) Electrochemical behavior of Nickel:

Results in Figure 7-4 compare the polarization behavior of pure Nickel in the two environments. Positive hysteresis in the cyclic polarization curves during the reverse potential scan indicates that the Nickel specimens were susceptible to the localized corrosion in both environments. Hemispherical pits were observed on nickel electrodes after these tests, as shown in Figure 7-5. In thiosulfate containing environment, compared with chloride only environment, many more pits formed on the surface of the nickel specimen. However, the pits formed in thiosulfate containing environment were smaller than those in chloride only environment.

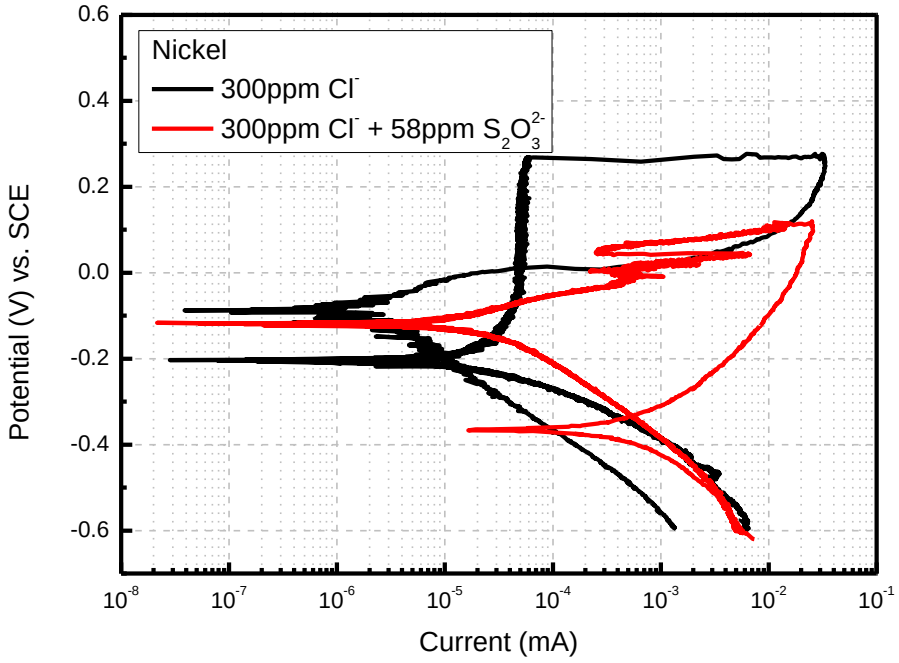

Figure 7-4. Cyclic Polarization Curves of Nickel in 300ppm Cl^- and 300ppm Cl^- + 58ppm $S_2O_3^{2-}$ Solutions

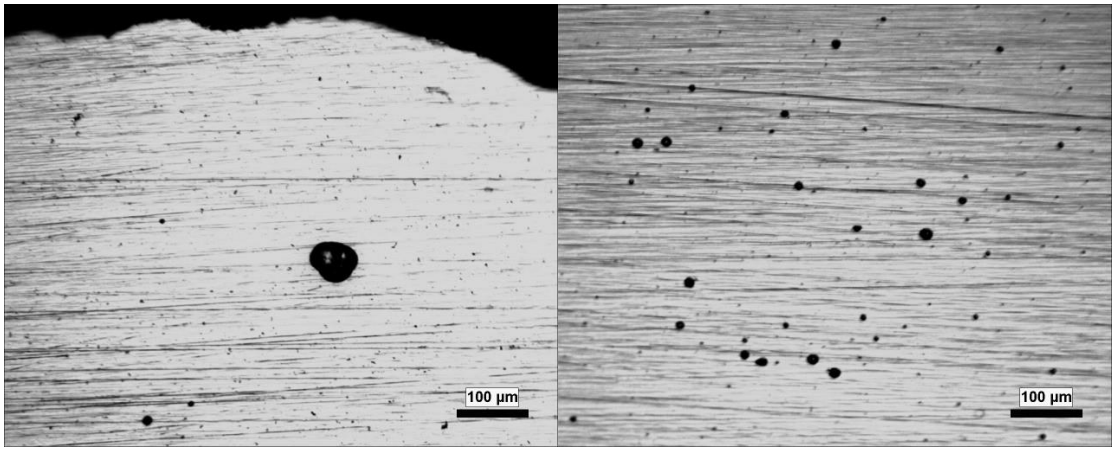

(a) (b)

Figure 7-5. Pits formed on nickel specimen in environments containing (a) no thiosulfate (b) 58ppm thiosulfate

The change in the shape of the polarization curves by addition of 58 ppm of thiosulfate ions in the chloride solution is very noticeable. With the addition of thiosulfate, the open circuit potential of nickel was raised by approximately 100mV. The addition of thiosulfate seemed to destroy the passive region for nickel, as is shown in Figure 6-3. Both pitting and repassivation potentials were lowered with the addition of thiosulfate, which means that the addition of thiosulfate promotes pitting corrosion and inhibits repassivation of pure nickel in chloride environments.

(3) Electrochemical behavior of Iron:

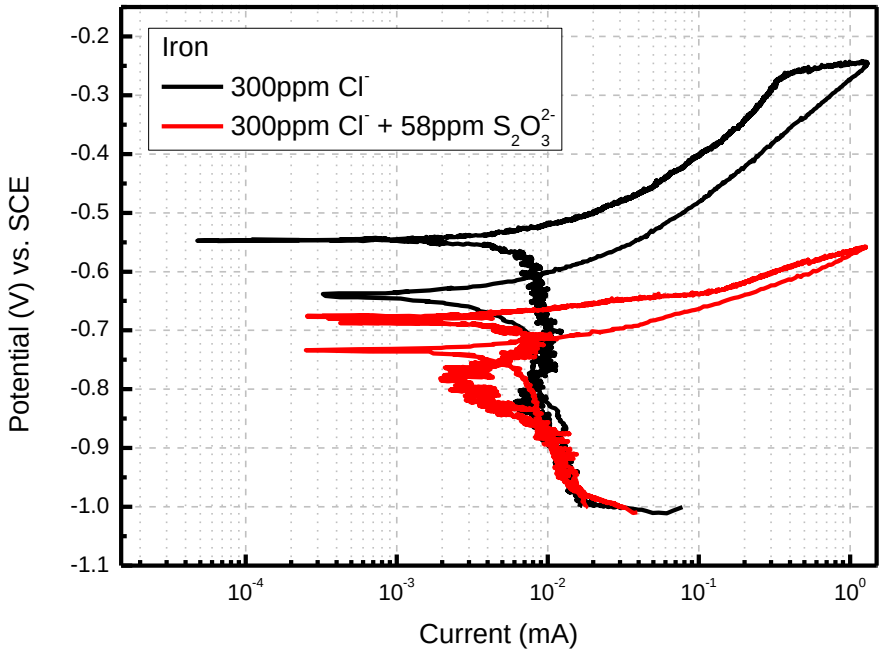

Figure 7-6. Cyclic Polarization Curves of Iron in 300ppm Cl^- and 300ppm Cl^- + 58ppm $S_2O_3^{2-}$ Solutions

Polarization results for pure iron in the two environments are shown in Figure 7-6. Polarization curves for iron displayed active corrosion upon anodic polarization. No passive behavior was seen for iron electrode in both environments. However, in contrast to nickel, the open circuit potential decreased by approximately 200mV by addition of thiosulfate ions.

(4) Electrochemical behavior of Molybdenum:

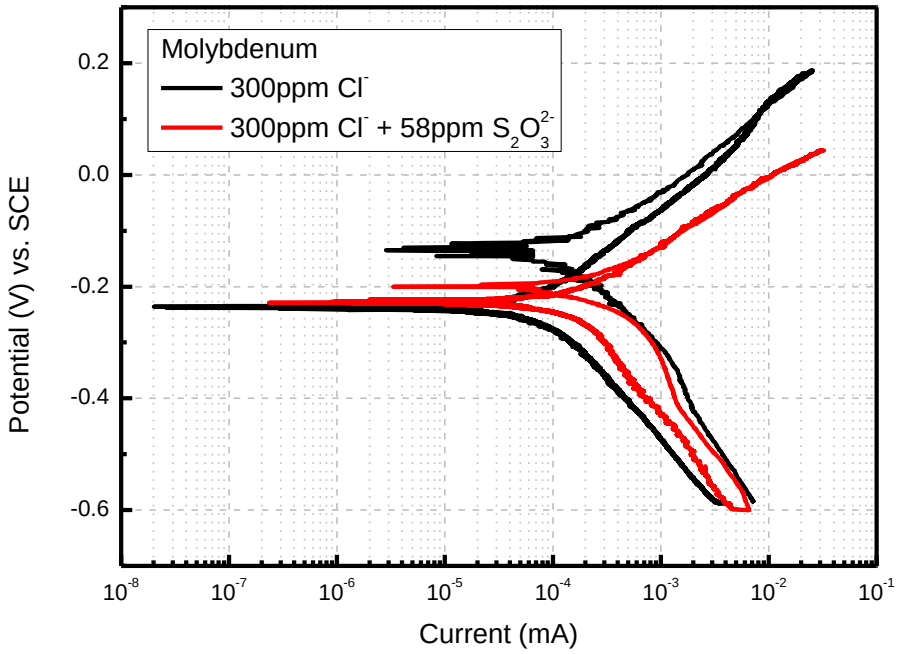

Figure 7-7. Cyclic Polarization Curves of Molybdenum in 300ppm Cl^- and 300ppm Cl^- + 58ppm $S_2O_3^{2-}$ Solutions

Results in Figure 7-7 shows an increase in the anodic polarization current with the addition of thiosulfate. No passive behavior was observed on the molybdenum surface

under tested conditions. There was no change in the open circuit potential of Mo with the addition of thiosulfate. Otherwise the change in the polarization curve for molybdenum with the addition of thiosulfate was less prominent compared to pure iron.

7.2.Thermodynamic Analysis of Pure Elements in Tested Conditions

Equilibrium phase stability diagrams, also called E_H-pH diagrams or Pourbaix diagrams, of sulfur species, as well as chromium, nickel, iron, and molybdenum in presence of hydrogen, oxygen, and sulfur were calculated and drawn by using a chemical reaction and equilibrium software, HSC Chemistry®. Results from these phase stability calculations are discussed in the following sections for each element individually.

7.2.1. Stability of Sulfur Species

The Pourbaix diagram showing stable species under given pH and electrochemical potential (E_H) for sulfur in presence of oxygen and hydrogen at 50 ℃ is given in Figure 7-8.

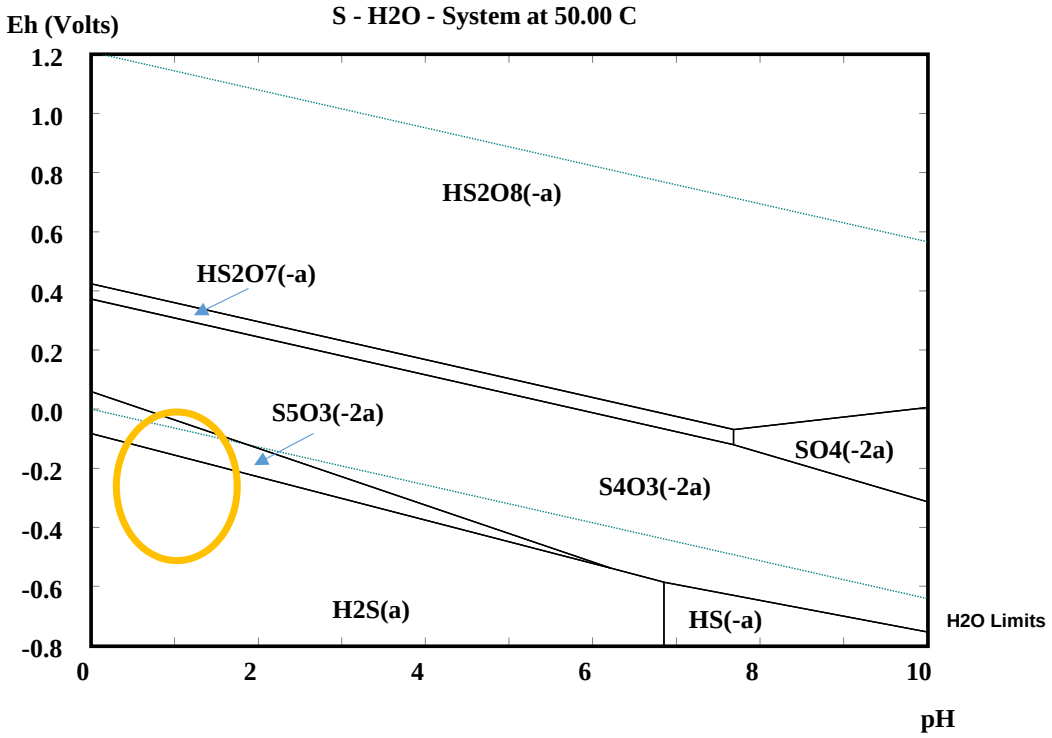

Figure 7-8. Pourbaix diagram of S-H_2O system at 50 ℃

As is shown in the Poubaix diagram, thiosulfate is a thermodynamically unstable species under environmental conditions of interest. Reference [113] gave the pH and potential in a stable pit for 304L formed in chloride only environment at 70 ℃ to be 0.6 – 0.8 and -0.31 – -0.32 V vs. SCE, respectively. Considering the pits formed in this study were at 50 ℃, the saturation concentration would be lower, resulting in higher pH. The environment within a stable pit would fall in the circled area on the diagram. The stable ionic species for sulfur in most of the circled area would be S^{2-}, which is most probably the chemical state of the reduced sulfur species formed in a stable pit.

Pourbaix diagram of the four alloying elements (Fe, Cr, Ni, and Mo) in presence of hydrogen, sulfur, and oxygen along with their polarization curves in 300ppm Cl^- and

300ppm Cl^- + 58ppm $S_2O_3^{2-}$ solutions will be discussed in the following section.

7.2.2. Polarization Behavior of Pure Element Specimens

Pourbaix diagrams of pure elements in presence of Cl-H-O and Cl-S-H-O were constructed with molarity of ionic species assumed to be 10^{-3} M. The pH for 300ppm Cl^- and 300ppm Cl^- + 58ppm $S_2O_3^{2-}$ are very close to 5. A line was drawn at pH=5, which intersects with different regions in the Pourbaix diagrams. Polarization curves were adjusted to the same potential scale so that reactions due to change in the most stable species can be read easily.

(a) Chromium:

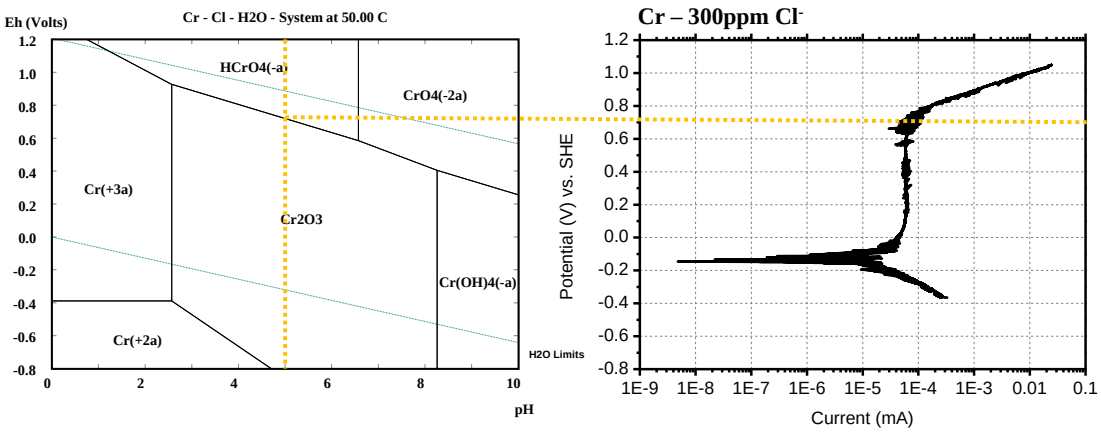

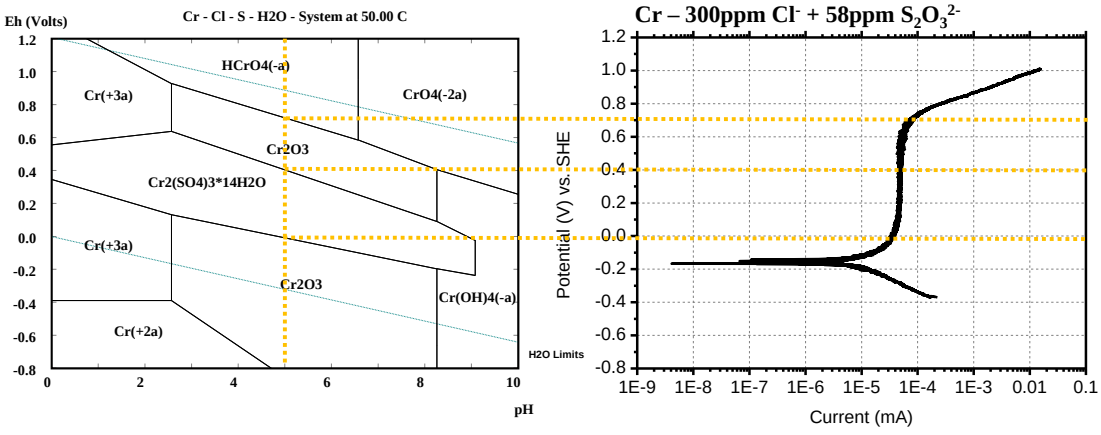

Figure 7-9. Polarization Curves for Chromium in 300ppm Cl^- and 300ppm Cl^- + 58ppm $S_2O_3^{2-}$ Solutions

In the test environment with 300 ppm chloride only, formation of a protective oxide film (Cr_2O_3) resulted in the passive behavior of the chromium specimen. The passive region came to an end as the potential reached the transpassive region with the formation of $HCrO_4^-$ ions, as is indicated by the Pourbaix diagram in Figure 7-9. In 58 ppm thiosulfate containing chloride environment, although chromium sulfate formation is thermodynamically favored in the presence of sulfur in the scanned potential range but the presence of 58 ppm thiosulfate ions did not alter the polarization behavior of pure chromium. This is probably because chromium sulfate is insoluble [114], which did not destroy the passive film that has already formed. The passive region came to an end when potential reached transpassive potential.

(b) Nickel:

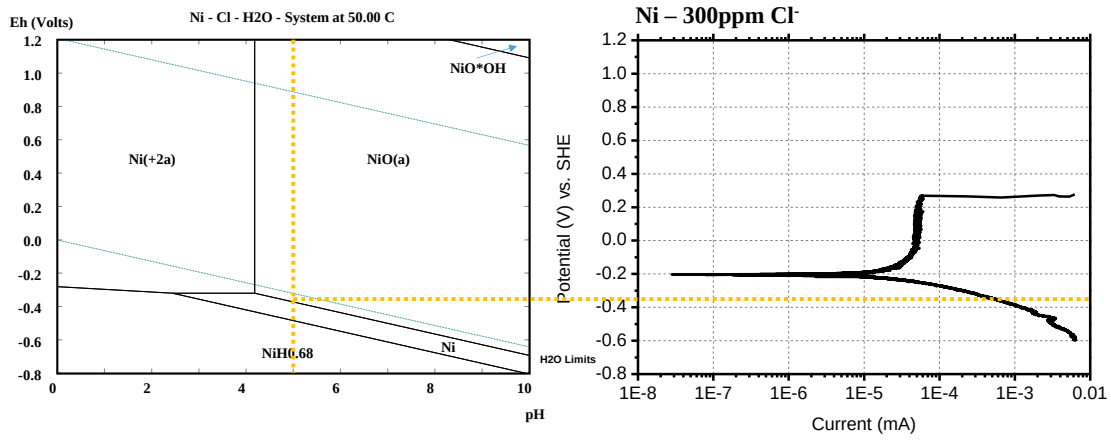

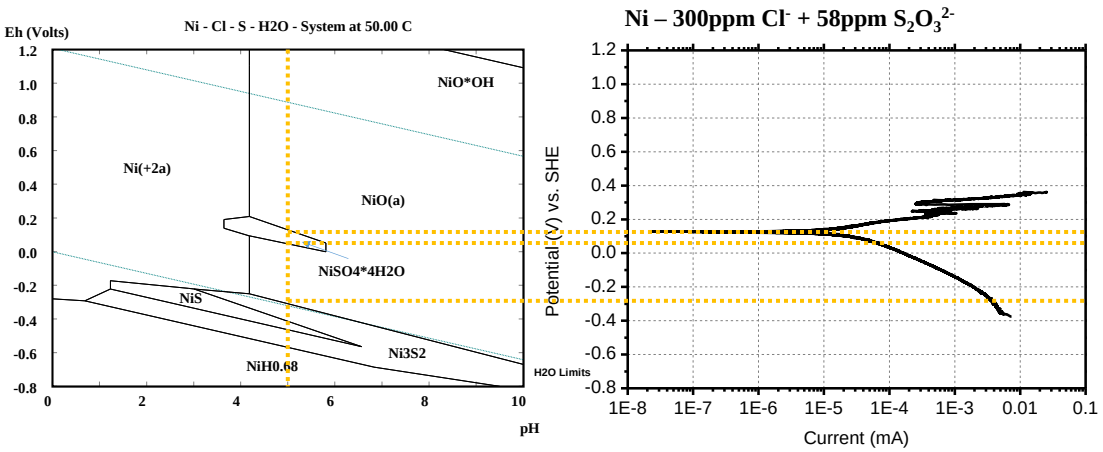

Figure 7-10. Polarization Curves for Nickel in 300ppm Cl^- and 300ppm Cl^- + 58ppm $S_2O_3^{2-}$ Solutions

In the thiosulfate-free solution, nickel oxide start to form above approximately -350mV, which explains the passive behavior of nickel in chloride only environment. The passive region for pure nickel was disrupted at applied anodic potentials due to the formation of pits. On the other hand, formation of soluble [115] $NiSO_4$ may destroy the passive film formed on nickel, which explains the lack of passive region for nickel specimen in solution containing thiosulfate, as well as the formation of more, smaller pits.

(c) Iron

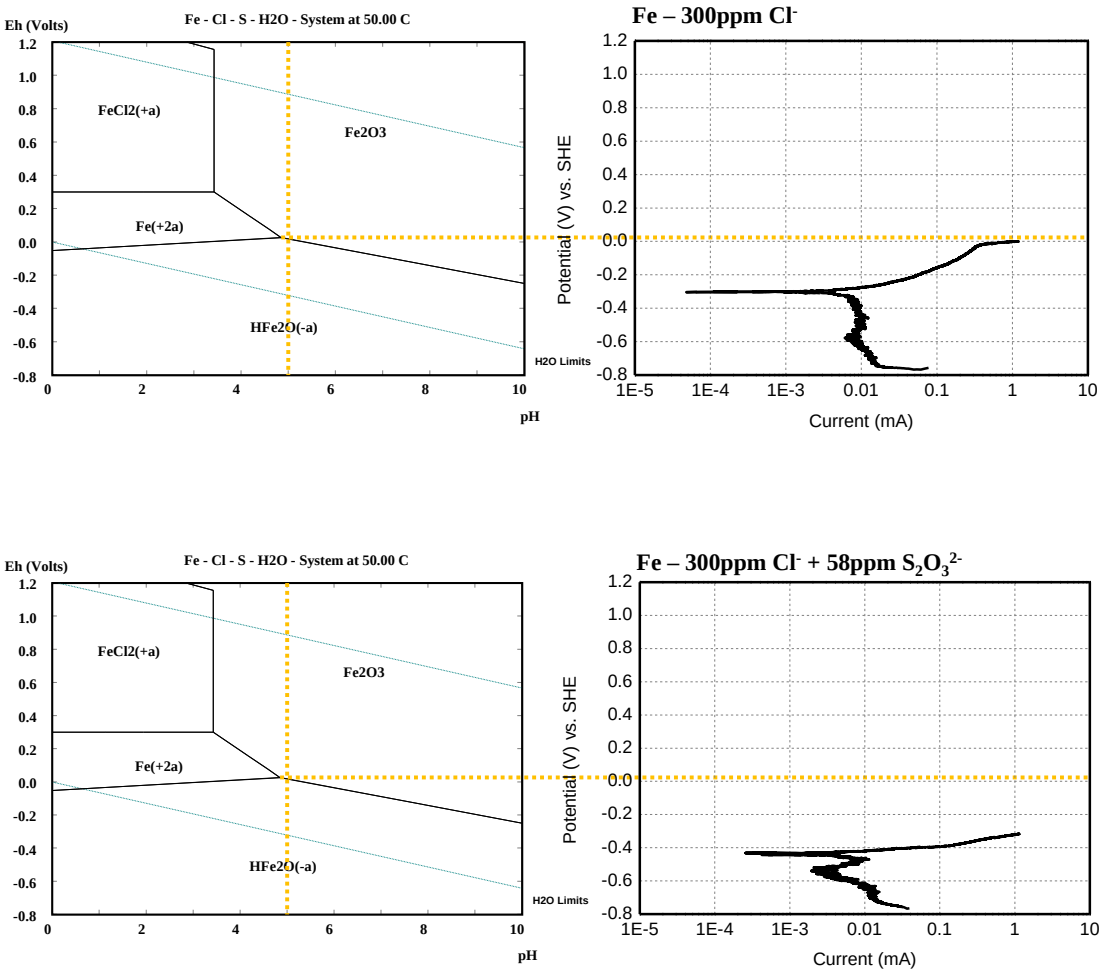

Figure 7-11. Polarization Curves for Iron in 300ppm Cl^- and 300ppm Cl^- + 58ppm $S_2O_3^{2-}$ Solutions

The Pourbaix diagram of iron did not change with the addition of sulfur element for the assumed conditions. However, an increased corrosion rate was observed with the addition of thiosulfate. The iron under scanned anodic potential range was in active corrosion state. The open circuit potential decreased from approximately -300mV to -450mV with the addition of thiosulfate. This is due to an increased anodic current, since the cathodic current should not be reduced with the addition of thiosulfate. Optical

microscope images of two iron specimens is given in Figure 7-12.

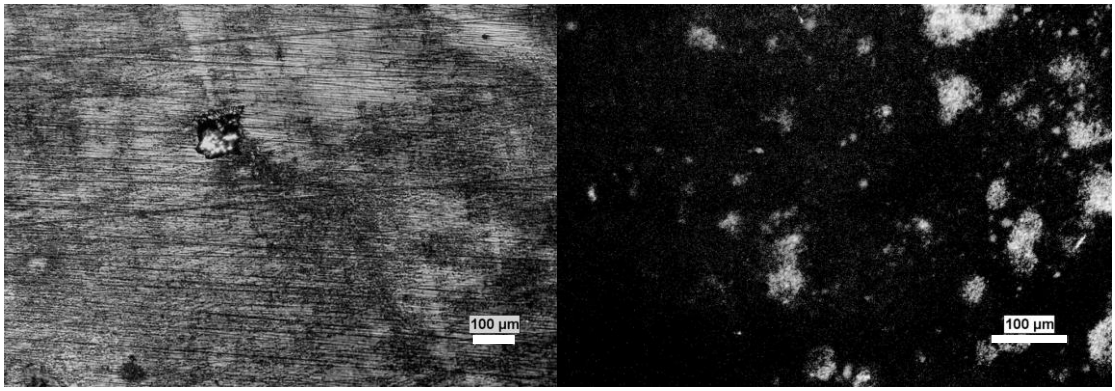

(a) (b)

Figure 7-12. Optical microscope images of iron specimen after polarization tests in (a) chloride only environment (b) environment containing thiosulfate

Pits were found on iron specimen after test in chloride-only environment, which means there was a combination of pitting and uniform corrosion. On the other hand, black corrosion products were found on specimen tested in thiosulfate-containing environment, which is probably because of enhanced anodic dissolution of iron due to the presence of S^{2-} formed in the cathodic sweep.

(d) Molybdenum

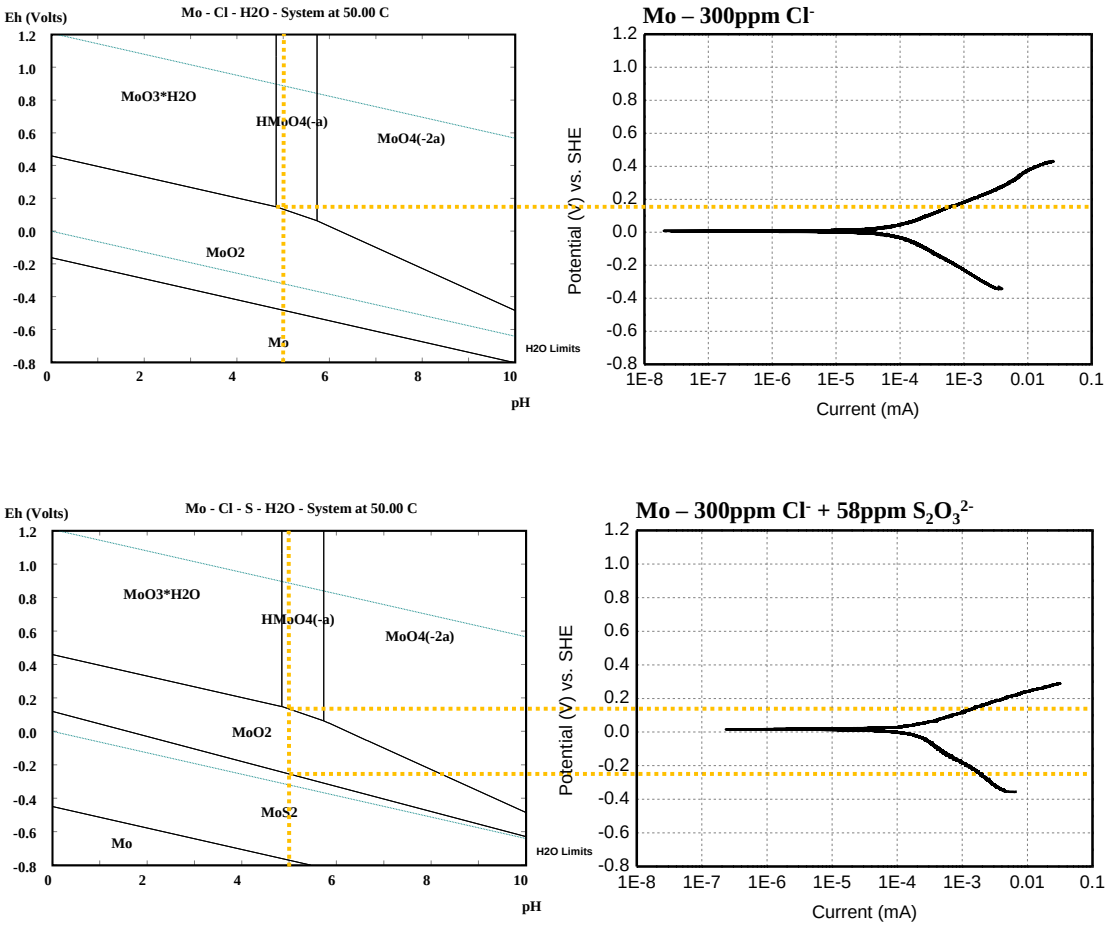

Figure 7-13. Polarization Curves for Iron in 300ppm Cl^- and 300ppm Cl^- + 58ppm $S_2O_3^{2-}$ Solutions

The anodic polarization curve for molybdenum was mostly in the active dissolution zone with the formation of $HMoO_4^-$. Active dissolution of molybdenum starts at -200mV vs. SHE, before possible active-passive transition for molybdenum. Addition of 58ppm thiosulfate also results in a region where MoS_2 is the most stable species. Oxidation of the sulfur species may be the reason for the increased anodic current in the thiosulfate-containing environment.

7.2.3. Thermodynamic Analysis of Stable Pits Environments

In a stable pit, cathodic reaction has already transferred to outside the pit due to the absence of oxygen or other species that enables cathodic reaction. Positive metal cations due to the metal dissolution start to accumulate. As a result, anions electro-migrate into the pit environment. In the tested environment, these anions are chloride and thiosulfate (or other sulfur containing anions formed by oxidation or reduction actions). The subsequent hydrolysis of the metal cations increases the acidity of the pit environment.

Pourbaix diagram of stable pits formed in 304L and 316L were constructed according to the information given in reference [113]. For 304L in a non-sulfur-containing environment, the Pourbaix diagrams are shown in Figure 7-14.

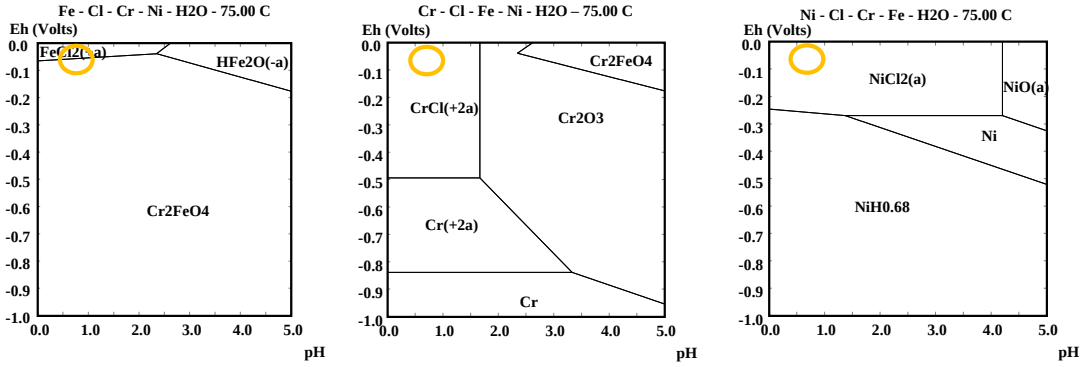

Figure 7-14. Pourbaix Diagram of Fe, Cr, and Ni in Fe-Ni-Cr-Cl-H_2O System

Iron takes the form of $FeCl_2$ or Cr_2FeO_4. When chromium is not available, it is $FeCl_2$ and hydroxylated HFe_2O^-. Nickel is present as Ni^{2+} while chromium as Cr^{3+}. With the addition of sulfur (considering concentration and mobility of $S_2O_3^{2-}$ ion, molarity of sulfur is estimated to be 1% of M_{Cl^-}), the Poubaix diagram for iron remains the same,

while diagrams for chromium, nickel, and sulfur are given as following.

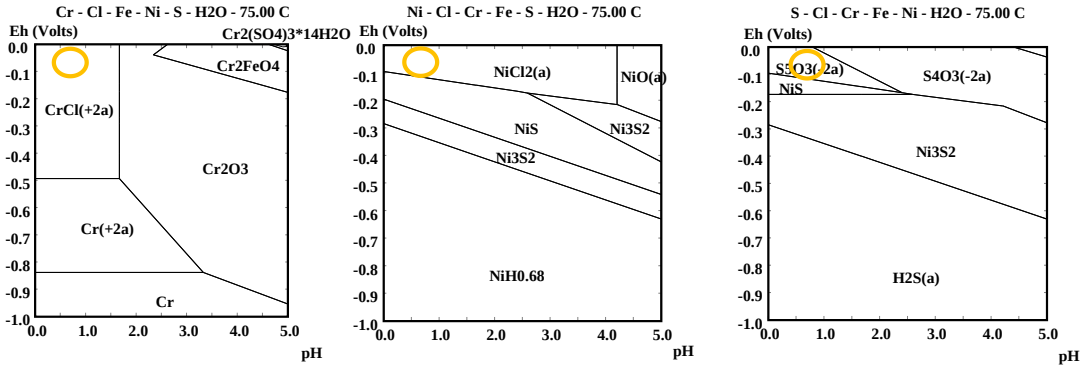

Figure 7-15. Pourbaix Diagram of Cr, Ni, and S in Fe-Ni-Cr-Cl-S-H_2O System

The Pourbaix diagram of chromium remains the same in pit environment. However, nickel may involve in the formation of NiS, especially when the polarization was at lower potentials. If the sulfur species added is thiosulfate, it would be partially reduced or even fully reduced to S^{2-} depending on the potential. It can also be observed that sulfur has highest affinity with nickel in this environment.

For molybdenum containing stainless steels, Pourbaix diagram (constructed according to stable pit in 316L from reference [113]) for sulfur and molybdenum is shown in Figure 7-16.

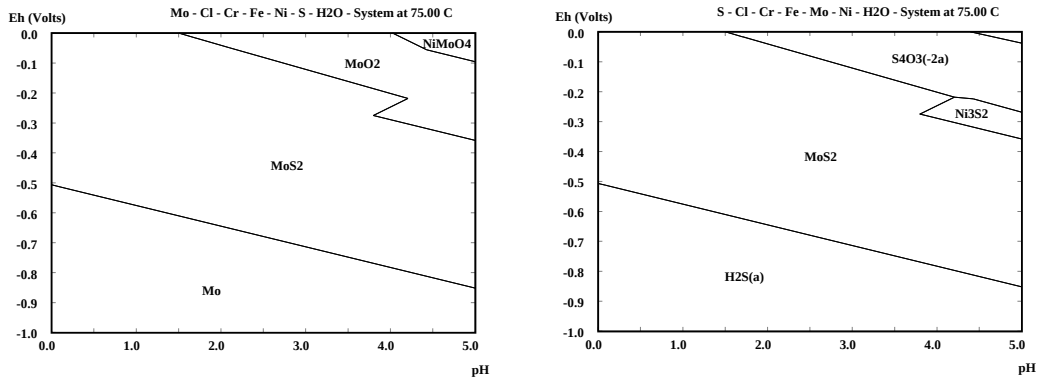

Figure 7-16. Pourbaix Diagram of Mo and S in Fe-Ni-Cr-Mo-Cl-S-H_2O System

The most thermodynamically stable form of sulfur is MoS_2 in the pit environment, as shown in Figure 7-16. This may explain why addition of molybdenum increases the pitting resistance in chloride and thiosulfate containing environment. Instead of forming the aggressive H_2S, sulfur binds to molybdenum preferentially, which also eliminate the possible hydrolysis due to Mo, which provides acidity in the pit environment [113].

7.3. Chemical Analysis

To understand the role of thiosulfate, scratch tests were combined with X-ray photoelectron spectroscopy (XPS) for chemical analysis of corrosion products. The scratch was made by a ceramic rod rather than a diamond scriber, so that the bottom of the scratch is better suited for XPS analysis. Specimens were polarized to -0.1V vs. SCE.

7.3.1. XPS Analysis of Corrosion Product

In order to identify the chemical state of sulfur in the corrosion product formed on the stainless steel surface, sulfate was not added to the test solution to avoid confusion. The tested environment was 6000ppm Cl^- + 1160ppm $S_2O_3^{2-}$.

Pits were found within the scratched area for 304L and 316L specimens. Without ion etching, the XPS sulfur peaks for a pit formed in 304L is shown in Figure 7-17.

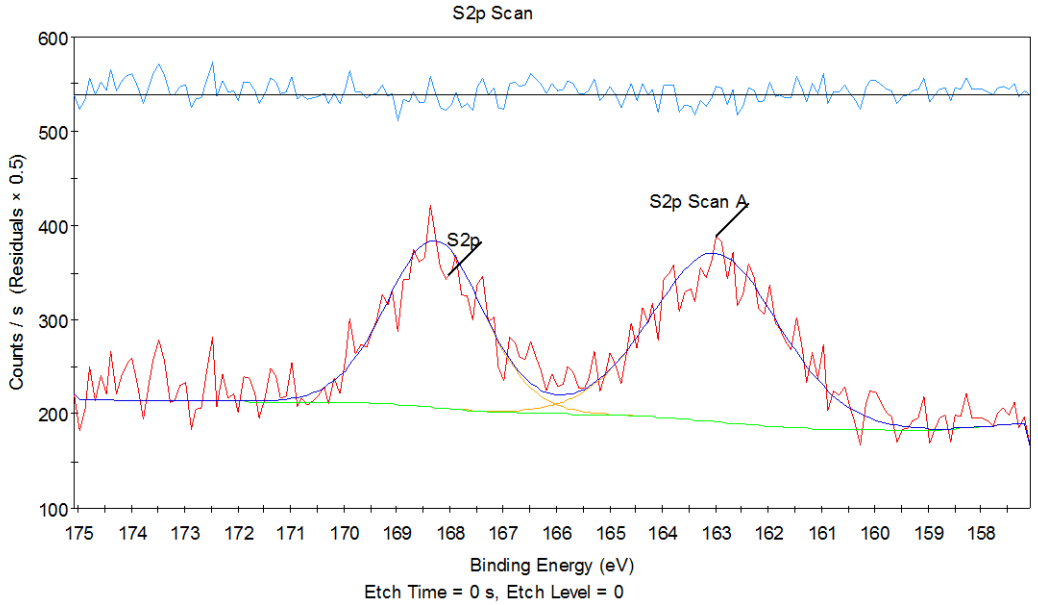

Figure 7-17. XPS Sulfur Peaks for a Pit Formed in 304L (Without Ion Etching)

The two major peaks shown in Figure 7-17 had binding energy of 168.29 eV and 163.00 eV, respectively. According to NIST XPS data base [117], the two 2p peaks for sodium thiosulfate show up in the range of 161.65-162.9 eV and 167.6-168.5 eV. It is highly possible that these were the peaks of the thiosulfate within the pit, or some other surface contamination. After 5 seconds of argon ion etching, the sulfur peaks along with all other elements are given in Figure 7-18 (doublet peaks of chromium and nickel were not fitted).

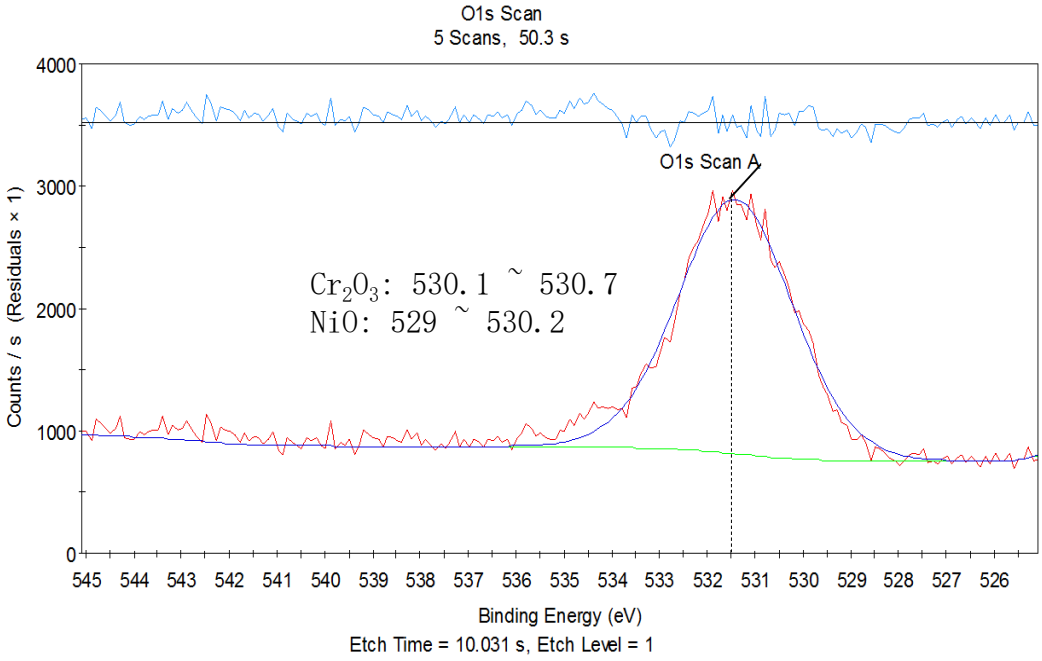
O1s Scan
5 Scans, 50.3 s
O1s Scan A
Cr_2O_3: 530.1 ~ 530.7
NiO: 529 ~ 530.2
Counts / s (Residuals × 1)
Binding Energy (eV)
Etch Time = 10.031 s, Etch Level = 1

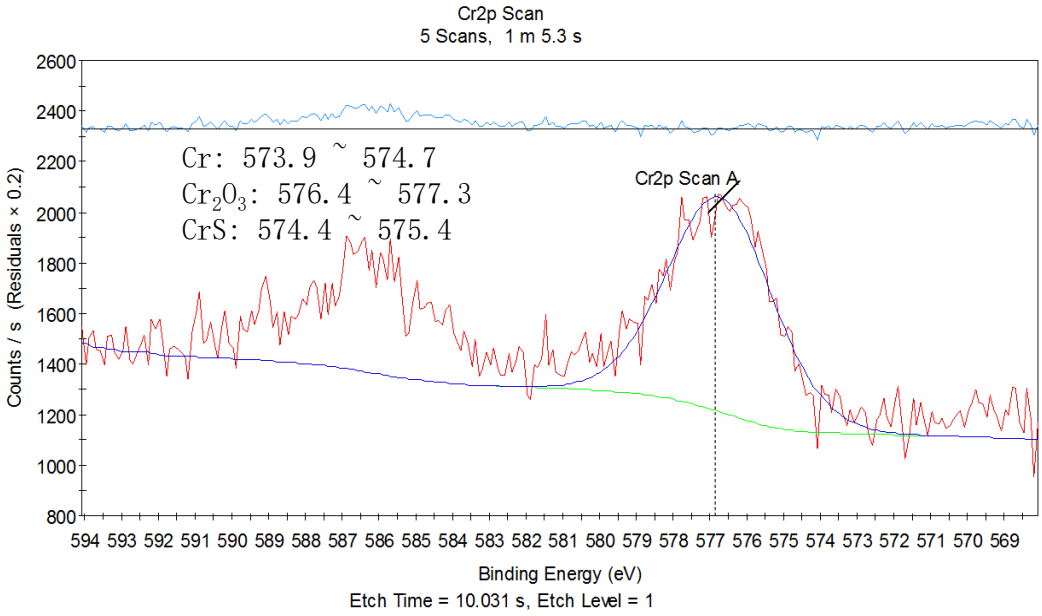
Cr2p Scan
5 Scans, 1 m 5.3 s
Cr: 573.9 ~ 574.7
Cr_2O_3: 576.4 ~ 577.3
CrS: 574.4 ~ 575.4
Cr2p Scan A
Counts / s (Residuals × 0.2)
Binding Energy (eV)
Etch Time = 10.031 s, Etch Level = 1

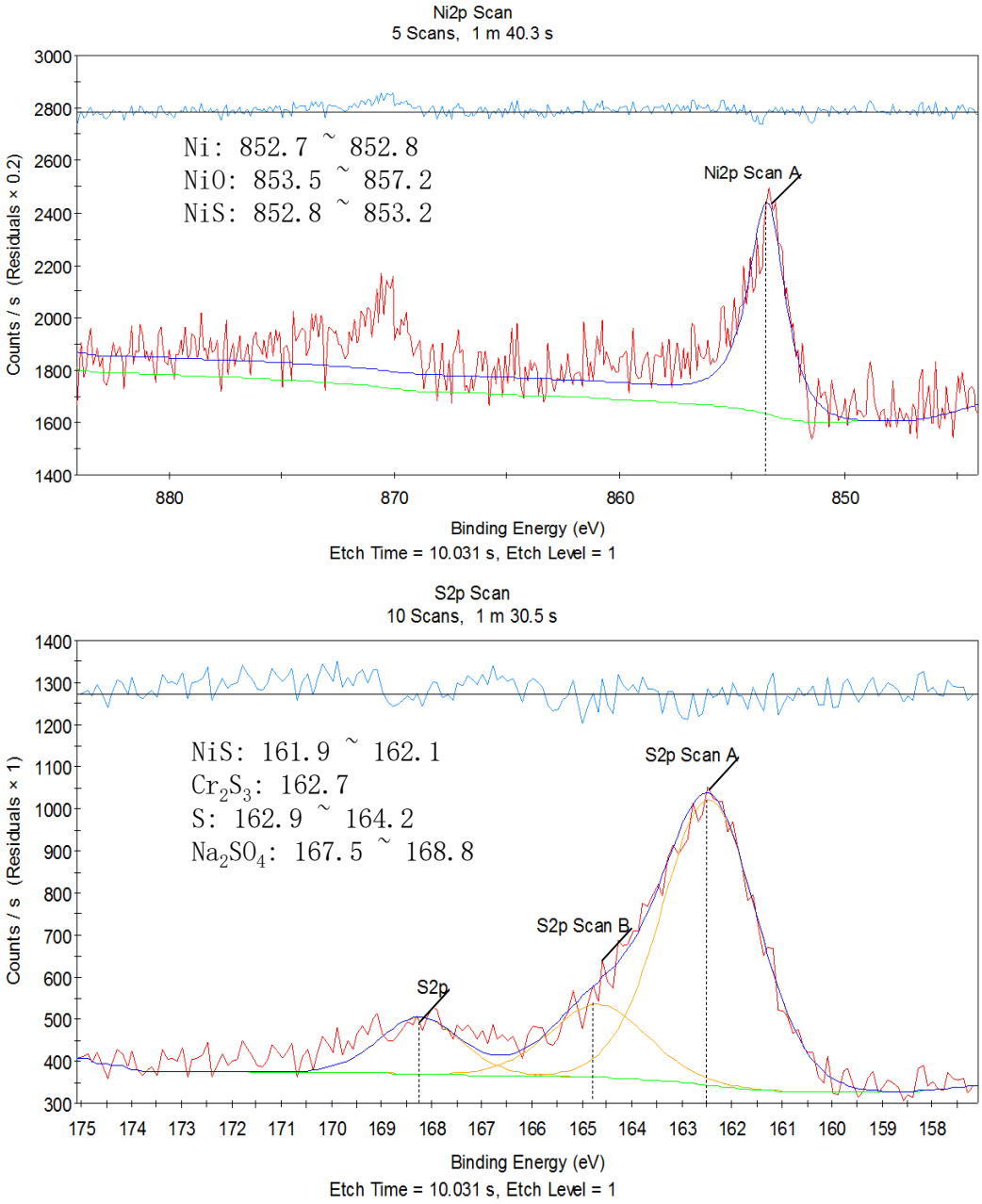

Figure 7-18. XPS analysis of the pit formed in 304L

It is clearly seen from these XPS results that reduced sulfur species formed within the pit for 304L. The three peaks for sulfur had binding energy of 162.45 eV, 164.67 eV, and 168.23 eV, which most probably correspond to the chemical state of sulfur in S^{2-}, S, as well as SO_4^{2-}. The majority of sulfur species was in the form of S^{2-}. Among oxygen, nickel, and chromium, only nickel and chromium are the possible elements

that S^{2-} binds to. Nickel has a peak with a binding energy of 853.45, which possibly correspond to Ni, NiO, NiS, or NiS_2 [117]. Chromium has a peak with a binding energy of 576.72, which most probably corresponds to Cr_2O_3 [117]. According to the thermodynamic analysis in the former section, the most possible reduced sulfur species formed is NiS.

The XPS scan of a pit formed in the scratch on 316L specimen is given in Figure 7-19, again doublet peaks were ignored in the peak fit.

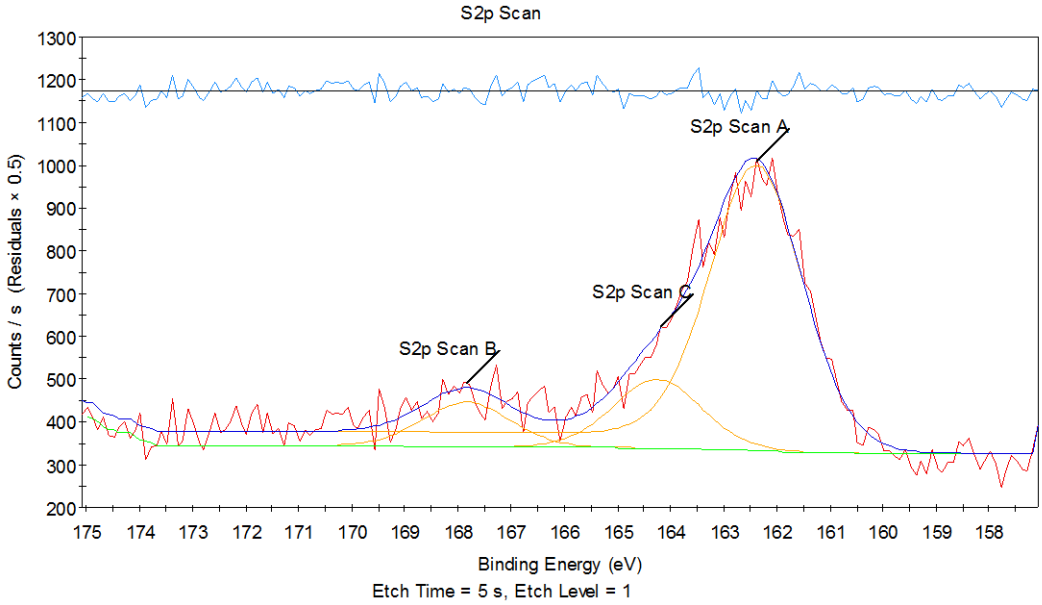

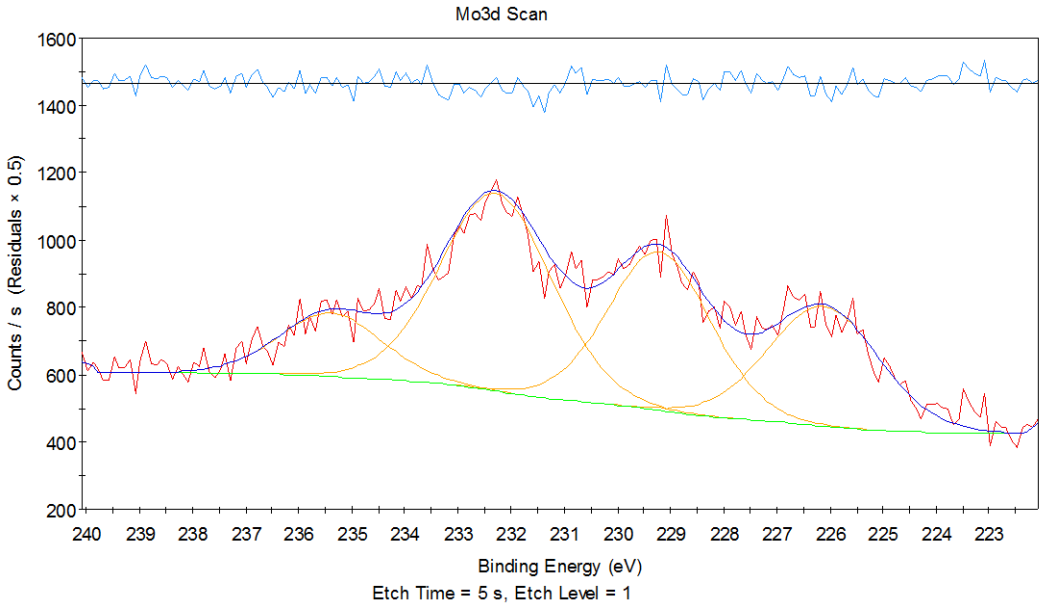
Mo3d Scan
Counts / s (Residuals × 0.5)
1600
1400
1200
1000
800
600
400
200
240 239 238 237 236 235 234 233 232 231 230 229 228 227 226 225 224 223
Binding Energy (eV)
Etch Time = 5 s, Etch Level = 1

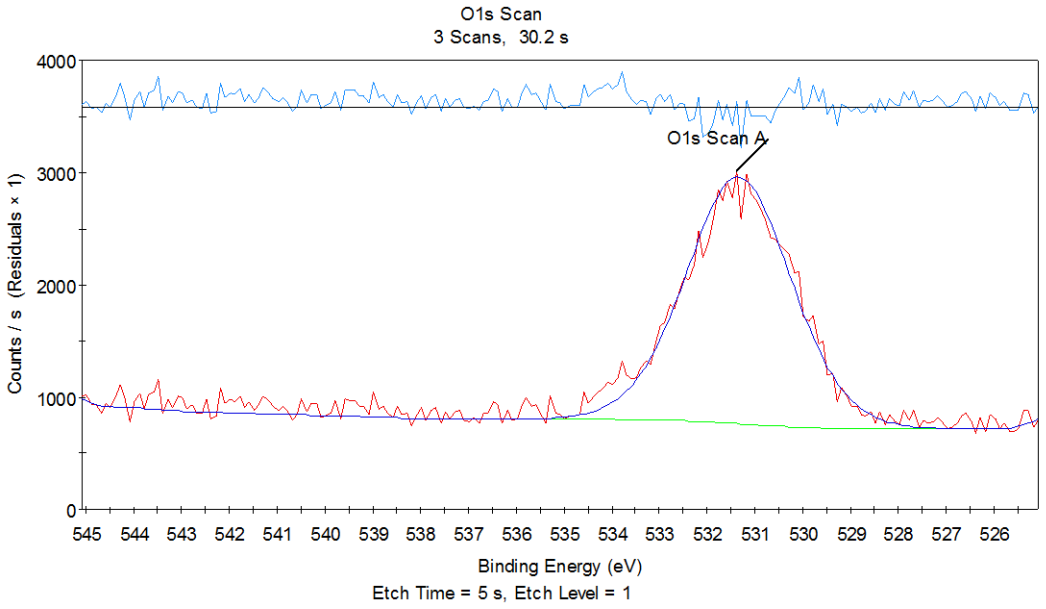
O1s Scan
3 Scans, 30.2 s
O1s Scan A
Counts / s (Residuals × 1)
4000
3000
2000
1000
0
545 544 543 542 541 540 539 538 537 536 535 534 533 532 531 530 529 528 527 526
Binding Energy (eV)
Etch Time = 5 s, Etch Level = 1

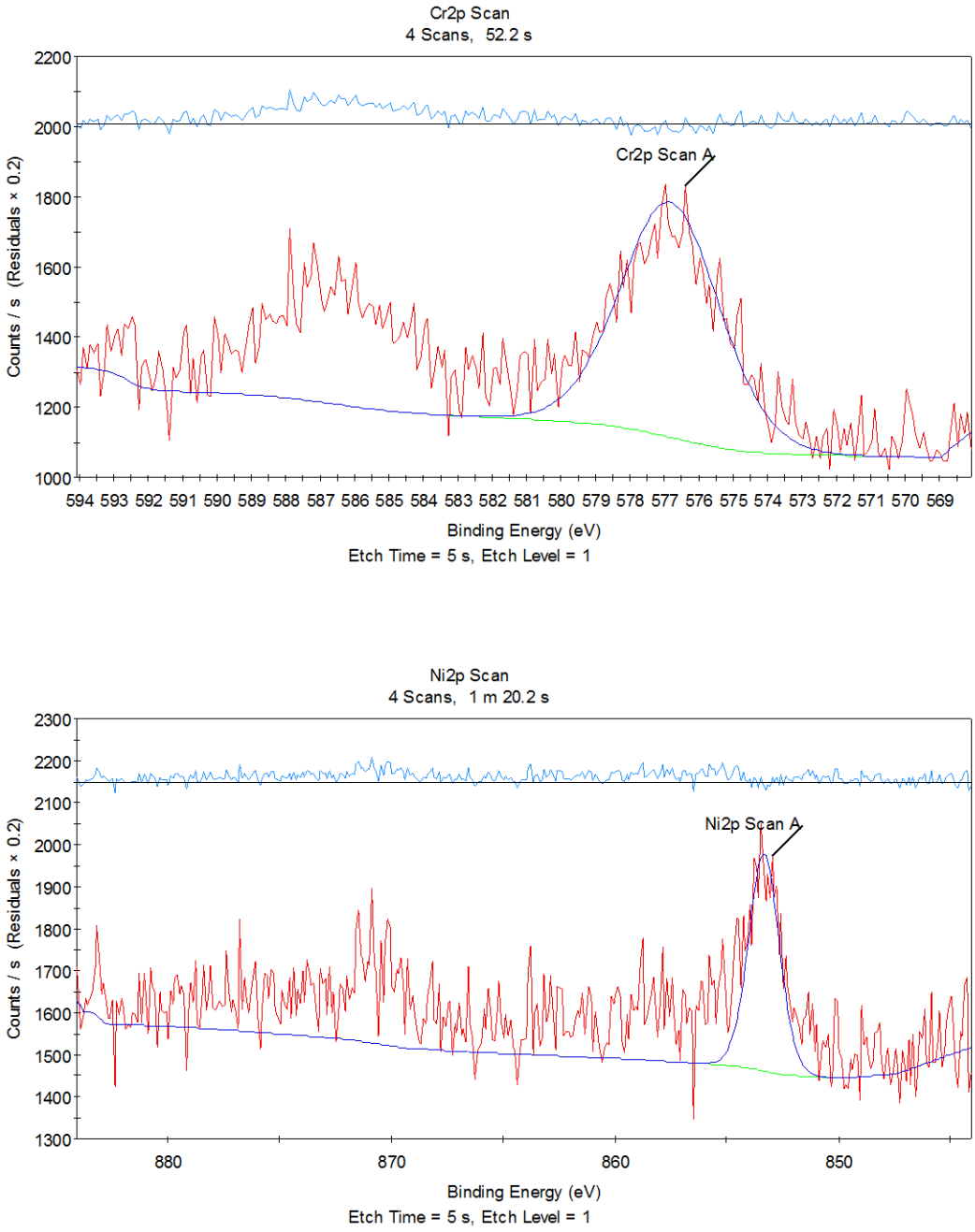

Figure 7-19. XPS analysis of the pit formed in 316L

According to the thermodynamic analysis shown in Figure 7-16, molybdenum has the highest affinity with sulfur, forming MoS_2. Four peaks were observed in the window of 222 – 240 eV. Three of which are most probably 3d5/2 and 3d3/2 peaks of molybdenum in MoS_2 and 2s peak of sulfur in MoS_2. However, there may be presence of oxides and overlapping peaks. Bearing in mind that there may be differences of a

few eV between tests of different researchers, it is difficult to argue exactly what species is present in this region.

7.3.2. Interaction between Thiosulfate Ion with Bare Metal Surface

In chloride containing solution, localized corrosion after mechanical disruption of the passive films was rarely observed at potentials. Only in thiosulfate containing environment did we observe a distinction in the occurrence of localized corrosion. In the meantime, in the scratched area where pit has not formed, formation of small amount of reduced sulfur species was also observed, even with ion etching, as shown in Figure 7-20. On the other hand, no sulfur was observed in unscratched area.

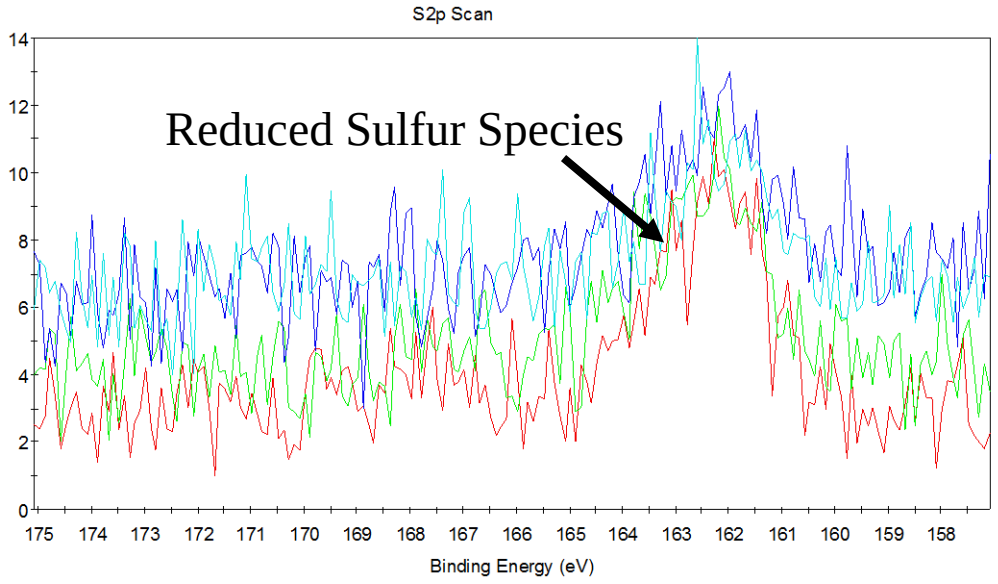

Figure 7-20. Reduced Species was Observed in Scratched Area where No Pitting Occurred for 304L, in 6000ppm Cl^- + 1160ppm $S_2O_3^{2-}$ Solution

To confirm that the reduced sulfur species detected was not from corrosion product formed in the pit, scratch tests were carried out in thiosulfate-only environment, 1160ppm $S_2O_3^{2-}$. No localized corrosion behavior was observed in this environment even after mechanical scratch, the current quickly decreased to passive current after the scratch.

Stainless steel and pure element specimens were polarized at -0.1V and scratch was made in 1160ppm $S_2O_3^{2}$ solution at 50 ℃. The specimen was polarized 10 minutes after the scratch. XPS was carried out in scratched area and unscratched areas. Before XPS analysis, specimens were ion etched for 5 seconds. XPS spectra of sulfur on 304L, 2101, Chromium, Nickel, Iron, and Molybdenum specimens are shown in Figure 7-21. For iron, active corrosion occurs at -0.1V, the spectra given for black corrosion product from the corrosion as well as surface that is not corroded is shown in Figure 7-21.

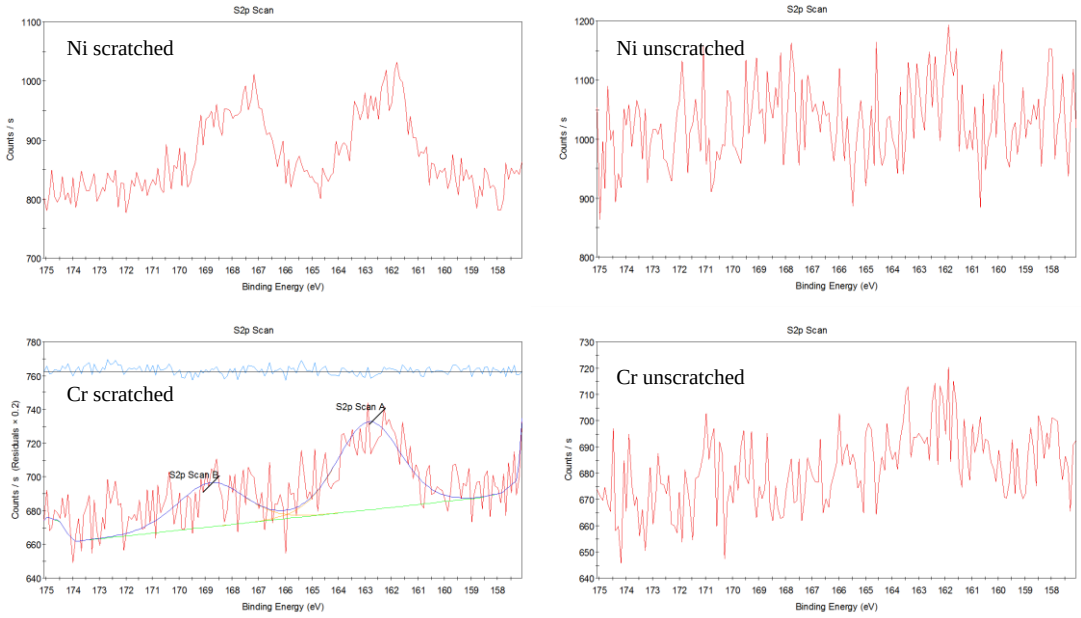

Figure 7-21. XPS spectra for sulfur on 304L, 2101, Fe, Ni, Cr, and Mo specimens in scratched (corroded) and unscratched area

Reduced sulfur species were observed on scratched surfaces of the two stainless steels specimens, chromium specimen and corroded iron specimen, but not on molybdenum or the unscratched surfaces of the same of these specimens. This means that once the native passive film breaks down, thiosulfate helps facilitate the corrosion

in the scratched area by formation of reduced sulfur species, whereas, the sulfur species are not incorporated into the native film in the undisturbed surface areas.

7.4. Conclusions

In this chapter, the interaction of alloying element with thiosulfate was characterized by potentiodynamic polarization measurements and XPS of scratched specimens. Addition of 58ppm thiosulfate ion did not alter the electrochemical behavior of chromium. On the other hand, it destroyed passive region of nickel, due to the formation of soluble $NiSO_4$, as revealed by thermodynamic analysis. It also facilitated the corrosion of pure iron, which was probably due to the formation of S^{2-}.

In the pit environment, reduced sulfur species are formed when thiosulfate is present in the test solution. The most stable form of reduced sulfur species is MoS_2. If no molybdenum is present, formation of NiS is preferred. Otherwise formation of H_2S is preferred, which enhances pit growth. As a result, XPS results showed that the reduced sulfur species formed in the pit is most probably MoS_2 for 316L, NiS for 304L.

Formation of reduced sulfur species occurred not only in the pits, but also on bare metal surfaces where the native passive film was damaged. Reduced sulfur species was found on 304L, 2101, iron, nickel, and chromium specimens when the native passive film was mechanically removed, even if no localized corrosion occurred.

8. REPASSIVATION KINETICS OF STAINLESS STEELS IN PRESENCE OF THIOSULFATE

The stress corrosion cracking susceptibility of a certain material an environment is widely accepted to be associated with the repassivation kinetics of this material in the environment [102].

The presence of thiosulfate could also influence the repassivation kinetics of stainless steel, which could result in an impact on the SCC susceptibility of the stainless steel in thiosulfate containing environment. Stress corrosion cracking (SCC) of stainless steels has been reported in chloride and thiosulfate containing environments. Haruna et al. [118] added 10^{-4} to 10^{-1} M thiosulfate into 4M NaCl solution, and found that stress corrosion cracking of 304L occurred in solutions containing 10^{-3} to 10^{-1} M thiosulfate at 353K. Zanotto et al. [111] demonstrated that in 20% NaCl solution, DSS2101 is susceptible to stress corrosion cracking in solutions containing 10^{-3} to 10^{-2} M thiosulfate. Smaller amounts of thiosulfate did not result in stress corrosion cracking of the stainless steel specimens while for higher thiosulfate concentration pitting corrosion started to compete with SCC. Although it was known that thiosulfate ions affect localized corrosion susceptibility of austenitic and lean duplex stainless steel grades in chloride containing environment but the effect of thiosulfate ions on repassivation kinetics of the stainless steels is not very clear.

The understanding of the influence of thiosulfate ions on the repassivation kinetics of stainless steels is very important for the understanding of the overall corrosion

mechanism and, especially, provide valuable information regarding thiosulfate induced SCC. Formation of reduced sulfur species on surfaces of the stainless steel, where passive film was mechanically disrupted, could be detrimental to passive film formation, which may lead to localized corrosion attack, like pitting corrosion shown in chapter 4. Since repassivation kinetics of stainless steels in presence of thiosulfate was not reported before, it is the aim of this study, as described in this chapter, to investigate the repassivation kinetics of 304L in chloride and thiosulfate containing environment and analyze the data using two existing models for repassivation kinetics on different time scales. The interaction between thiosulfate ions and bare stainless steel surface was systematically evaluated and the results from this study are presented in this chapter.

A number of researchers have studied repassivation behavior of different alloys using film-scratch method, where the current transient after the scratch is carefully monitored and analyzed to model the repassivation events at the alloy surface. Transients have been analyzed based on the physical modes for interaction of reactive species at the metal surface, initial active corrosion reaction, and corrosion-product formation in the area of scratch with one possible outcome being a complete repassivation of the scratched surface. In other cases, general or a localized mode of corrosion attack may start and continue. Data from our scratch tests were analyzed in accordance with two proposed methodologies and the results are discussed in the following sections.

8.1. Dissolution and Passive Film Coverage Model

Lillard et al. [119] modeled current transient with considerations that the total current consists of the dissolution current as well as the film formation current. By adopting film growth kinetics theories from earlier research [120][121][122], they were able to observe an effect of nitrate anions on the dissolution and repassivation current in a scratch test for 304L. The rationale behind their model is that once a passive film covers the metal surface, there is very little current passing through, so that the current by dissolution could be treated as directly proportional to the metal surface that is not covered by the passive film. Adopting an Avrami growth kinetics for passive film formation, the current after scratch is given by:

$$I_{total} = I_{diss} + I_{film} = I_{bare}(1-\theta) + \theta A t^{-b}$$

where I_{diss} is the dissolution current at time t, I_{film} is the film formation current at time t, I_{bare} is the dissolution current when the whole area is exposed, θ is percentage coverage for the passive film, A and b are constants derived empirically. An assumption is made here that as long as a passive film forms at the surface, there is no further dissolution of the metal. The growth of passive film is modeled according to Avrami kinetics:

$$\theta = 1 - \exp(-kt^{n})$$

where k is the film formation rate constant and n is the Avrami exponent which takes a value of integer or half integer between 1/2 and 7/2.

To analyze our data on the effect of test environment on the repassivation behavior of stainless steels, scratch test data was treated in the same way as explained by Lillard et al. [119]. The current transient, 10 milliseconds after the scratch were used for modeling, in accordance with the model [119]. The highest current during the scratch was set as time 0. The current transient data was fitted according to the equation given above. A curve fit for 304L polarized at 0.1V vs. SCE in 0.6M NaCl solution is given in Figure 8-1.

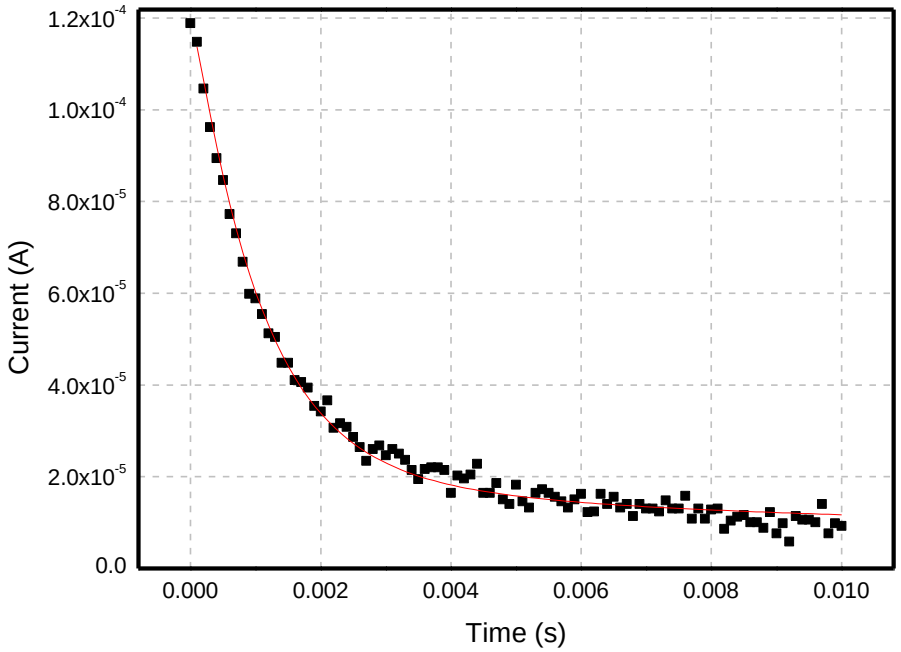

Figure 8-1. Curve fit for 304L polarized at 0.1V vs. SCE in 0.6M NaCl solution

As can be seen from Figure 8-1, a fairly good fit can be made assuming n=1 (attributed to be an island growth in two dimensions [119]). Dissolution current as well

as film formation current are shown in Figure 8-2.

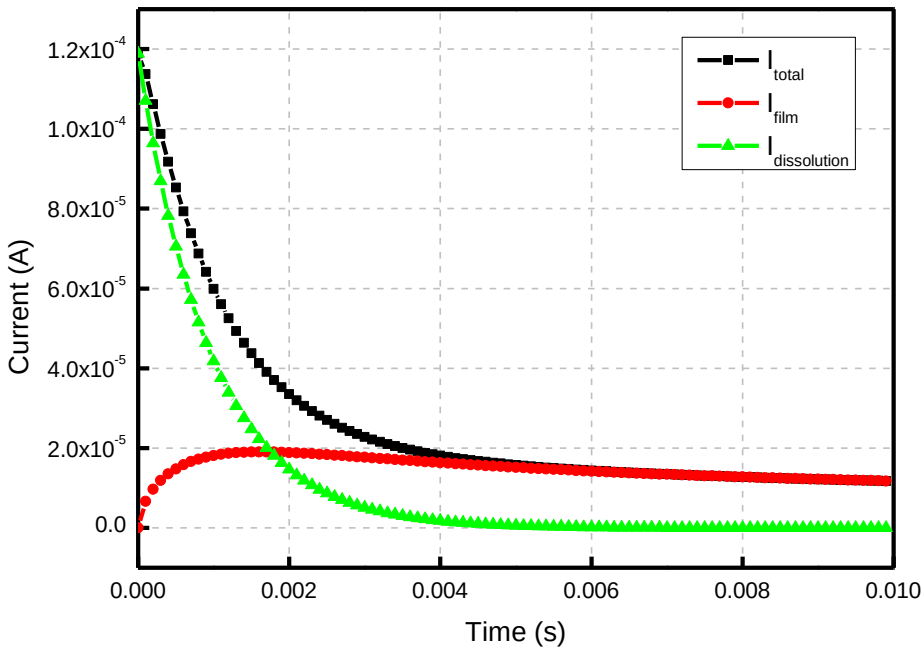

Figure 8-2. Total, dissolution, and film formation current for 304L polarized at 0.1V vs. SCE in 0.6M NaCl solution

The film formation current exceeds the dissolution current at around 2ms, and after approximately 7.5ms the surface is fully covered with the passive film. The fitted curve for 304L stainless steel polarized at 0.1V vs. SCE in 0.6M NaCl + 18mM $Na_2S_2O_3$ solution is given in Figure 8-3.

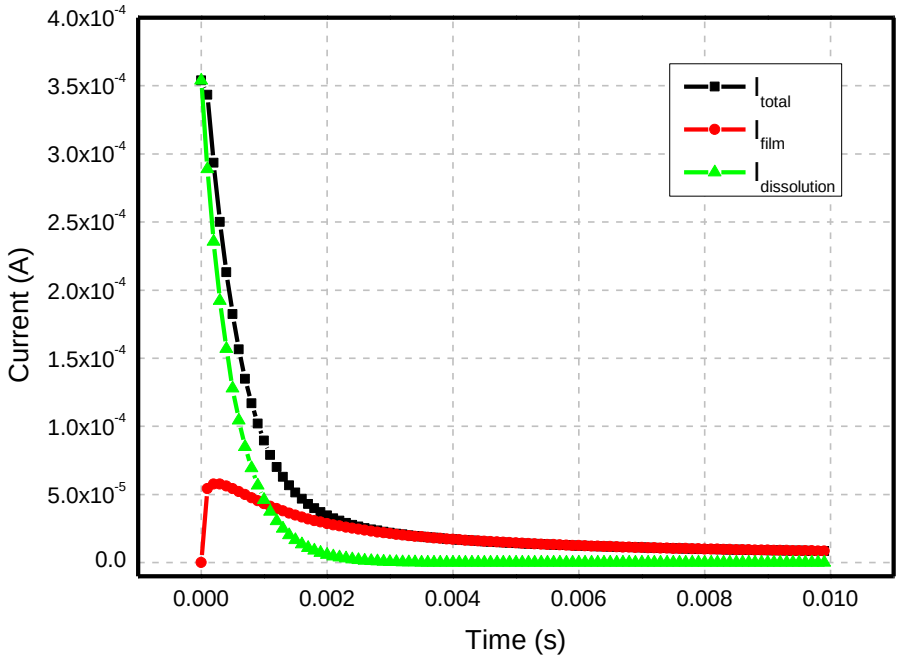

Figure 8-3. Total, dissolution, and film formation current for 304L polarized at 0.1V vs. SCE in 0.6M NaCl+ 18mM $Na_2S_2O_3$ solution

In this case, the film formation current exceeds the dissolution current at a much earlier time, at around 1.2ms. The film formation is complete at 4ms. It can be deduced from this model that the addition of thiosulfate accelerated the formation of full passive film on 304SS surface. However, observations of the tested sample under microscope indicates that this is not the case. The addition of 18mM $Na_2S_2O_3$ into 0.6M NaCl solution actually promoted pitting of 304L.

Derived film formation constants k from 2 experiments is shown in Figure 8-4. Individual analysis results for specimens polarized at 0.1V vs. SCE were shown or discussed here as the tested 304L samples started pitting corrosion on the general

surface even before the scratch, making repassivation analysis from scratch test invalid.

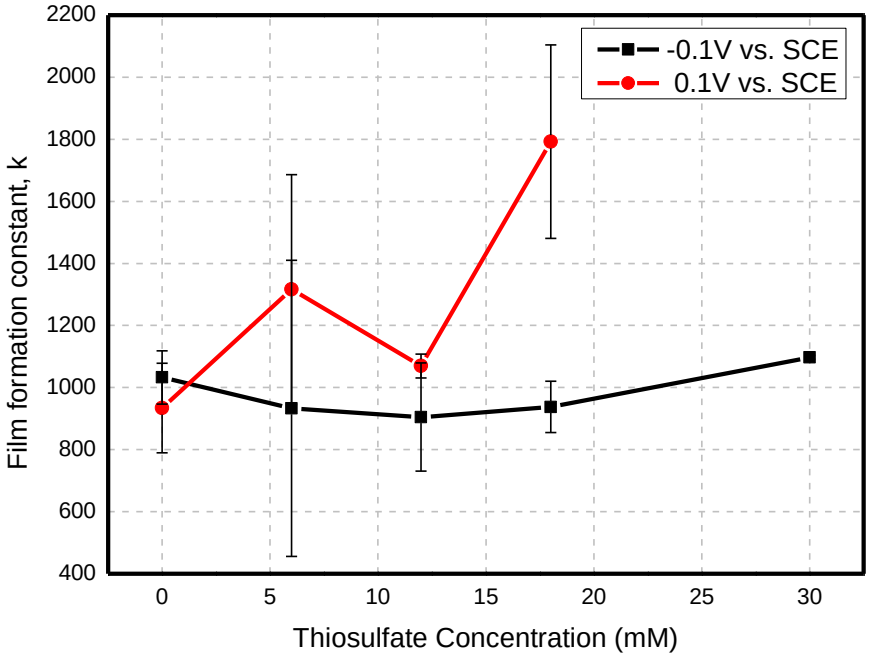

Figure 8-4. Derived film formation constants k from 2 experiments in solutions with various thiosulfate concentrations

As can be observed from Figure 8-4, for the specimens polarized at -0.1V vs. SCE, the addition of thiosulfate did not have a definitive influence in the film formation constant k. For specimens polarized at 0.1V vs. SCE, according to the model, the addition of thiosulfate resulted in an increase in the film formation rate, which is in fact not the case. The addition of 18mM $Na_2S_2O_3$ into 0.6M NaCl resulted in active pitting in the scratched area, after the scratch, for specimens polarized at 0.1V vs. SCE. It can thus be concluded that the dissolution and film coverage model does not work very well

in chloride and thiosulfate containing environments, especially where localized corrosion may start after the mechanical film disruption.

8.2. Passive film growth model

The film coverage model by Lillard et al. [119], as discussed in earlier section, mainly focuses on the first few milliseconds of a current transient in the repassivation process. However, Carranza et al. [123] demonstrated that for 304 in concentrated chloride containing environment such as 1M HCl solution and 1M NaCl solution, the current transient curve may not reflect SCC susceptibility of a material at all.

In the context of present study, another way to look at the repassivation problem is to probe how changes in thiosulfate concentration affect passive film growth. According to Burstein and Marshall [124], the current for repassivation is related to passive-film forming charge such that:

$$\log i(t) = \log A + \frac{BVzF\rho}{2.3Mq(t)},$$

where i(t) is the current density for film formation at time t, A and B are constants associated with energy barrier for ion movement in the film, V characterizes the electric voltage over the passive film, z is number of electrons per charge carrier in the film, F is Faraday's constant, ρ is density of film, M is molecular weight of the material forming the film, q(t) is the charge transferred during the formation of passive film till time t. Thus, if V is constant (especially under potentiostatic tests and where IR drop is negligible), log i(t) would be linearly proportional to 1/q(t). It was found that in the second stage of the repassivation process, log i(t) is indeed linearly proportional to

1/q(t), and the slope of the curve is an indicator of repassivation speed [125][126].

Kwon et al. [125], based on high-field ion conduction model [127], found that the slope of the linear region in the log i vs. 1/q graph, referred to as "cBV" value, is an effective indicator of repassivation speed and correlated it with SCC behavior in SS304. The higher the "cBV" value, the lower the repassivation rate. Cho et al. [126] followed up on the argument and divided the repassivation current transient into three stages. A film nucleation stage, a high field ion conduction stage, and a steady-state of repassivation. They found that when the film growth is by high-field ion conduction, log i is proportional to 1/q. They also studied the effect of alloy composition on the repassivation kinetics of stainless steels.

Take a current transient curve for 304L polarized at 0.1V vs. SCE in 0.6M NaCl + 12 mM $Na_2S_2O_3$ solution for example. The current transient curve was first converted into current density vs. time curve. The peak current was then chosen as time zero. After subtracting the passive current from the rest of the sample, the current transient curve is shown in Figure 8-5.

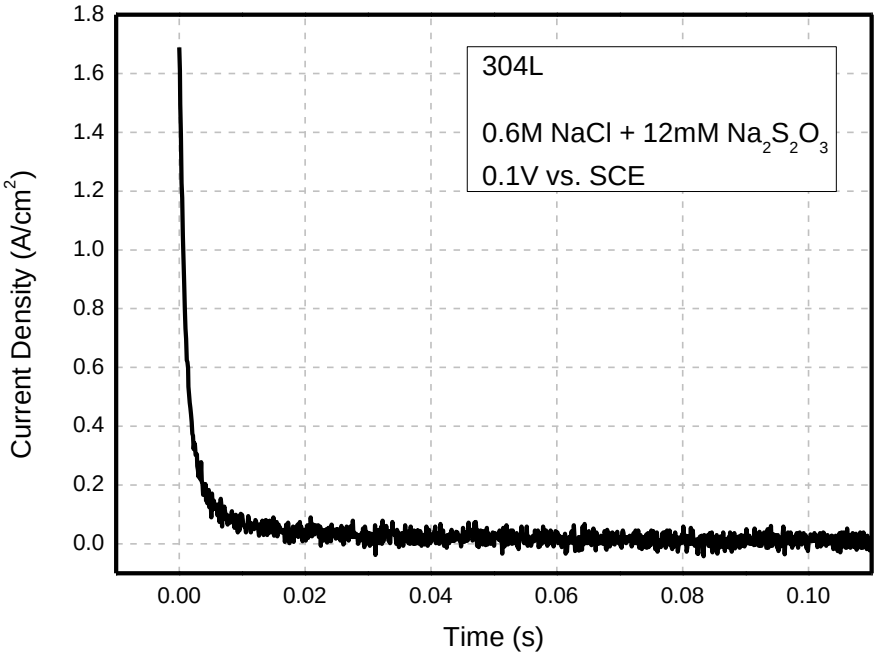

Figure 8-5. Current transient curve for 304L polarized at 0.1V vs. SCE in 0.6M NaCl + 12 mM $Na_2S_2O_3$ solution

The log i(t) vs. 1/q(t) curve for 304L specimen polarized at -0.1V in environments containing 6mM and 18mM thiosulfate is compared in Figure 8-6.

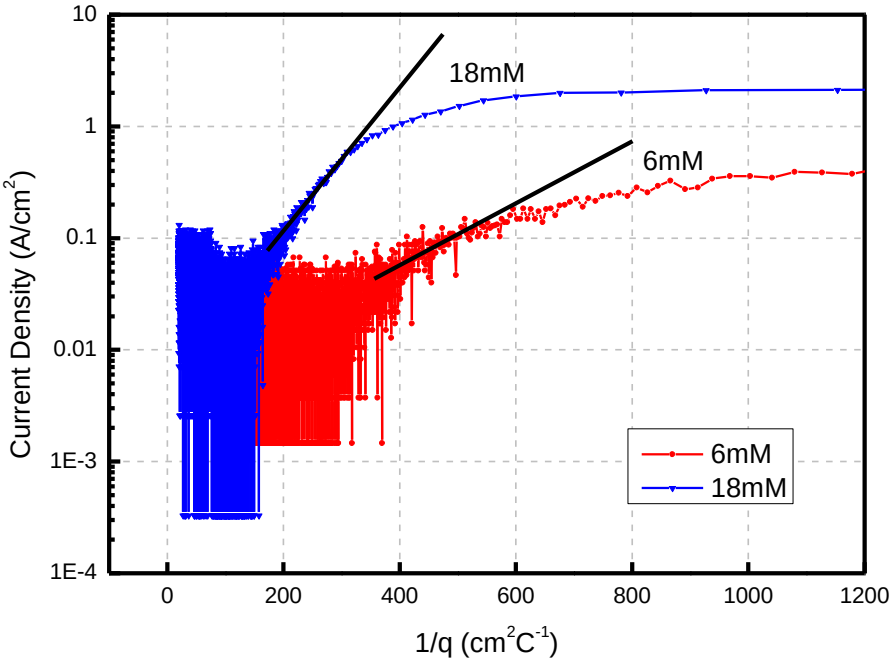

Figure 8-6. Log (i) vs. 1/q graph for 304L polarized at -0.1V vs. SCE in test solutions with 6mM and 18mM of thiosulfate added

As clearly shown in Figure 8-6, the slope of the linear region in the log(i) vs. 1/q graph for 18mM thiosulfate containing environment is higher than that of 6mM thiosulfate containing environment. The higher the slope (cBV), the higher the barrier for ion transport through the film, and thus the slower the repassivation rate is. It can be concluded that addition of 12mM thiosulfate in 0.6M NaCl + 6mM $Na_2S_2O_3$ solution caused a decrease repassivation rate for 304L stainless steel.

A compilation of curves for 304L specimen polarized at -0.1V and 0.1V vs. SCE are shown in Figure 8-7 and Figure 8-8, respectively. Each Figure contains data for tests conducted with different amounts of thiosulfate in 0.6M NaCl chloride solution. Lines

with slopes of the linear region were given on the graph for easy comparison.

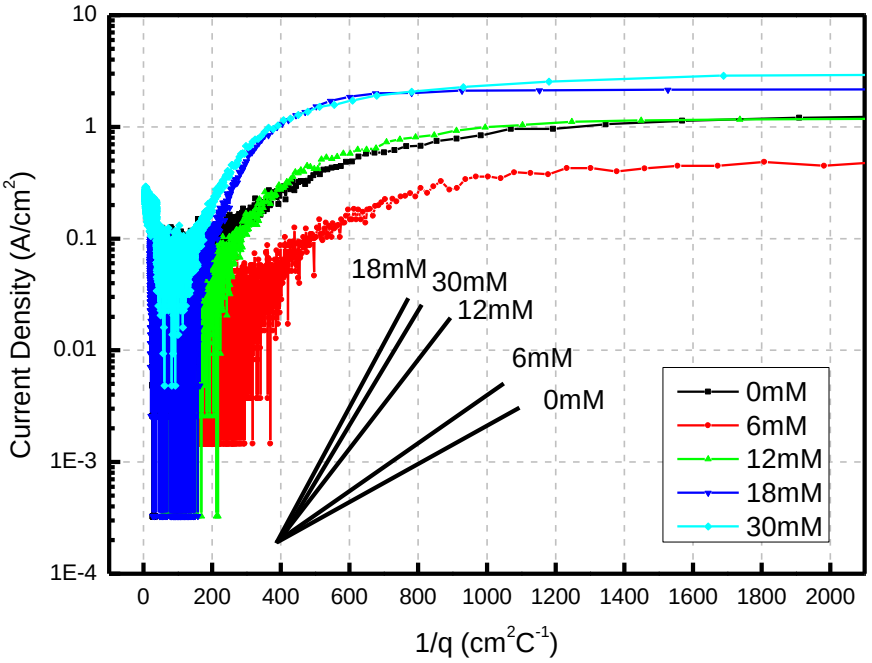

Figure 8-7. Log (i) vs. 1/q graph for 304L polarized at -0.1V vs. SCE in test solutions with different concentrations of thiosulfate added, as indicated by the legends, to 0.6M NaCl solution

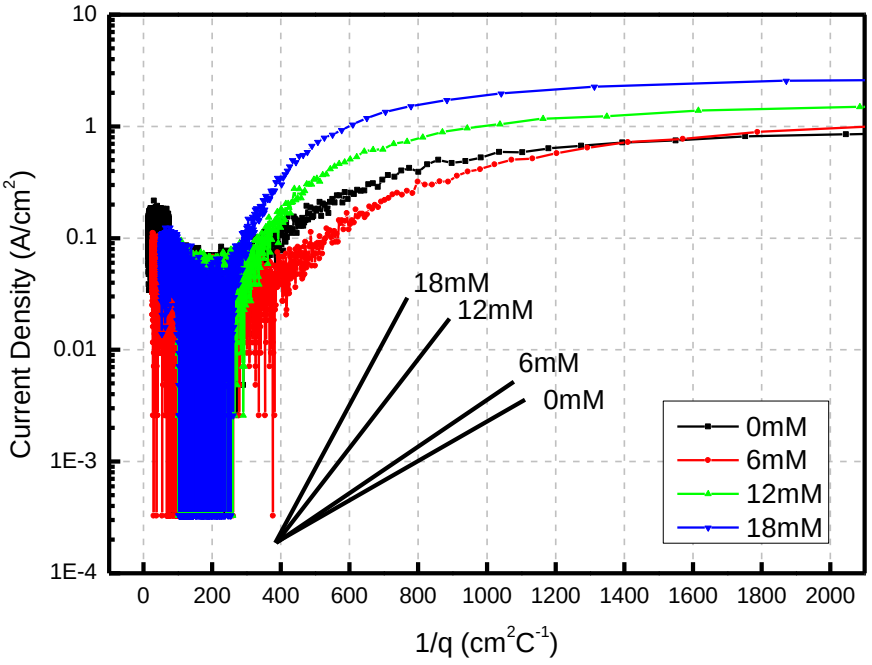

Figure 8-8. Log (i) vs. 1/q graph for 304L polarized at 0.1V vs. SCE in test solutions with different concentrations of thiosulfate added, as indicated by the legends, to 0.6M NaCl solution

As a general trend, the addition of thiosulfate resulted in an increase in the slope of the linear region in the curves. Since the slope of the curve, cBV, represents the barrier for ion conduction through the passive film, higher cBV value suggests slower movement of ions across the passive film, and thus lower repassivation rate. However, the differences in the slopes were considerably smaller than the ones reported in references [125] and [126]. This is probably because the addition of small amounts of thiosulfate only influence the repassivation of local areas but not repassivation of the whole surface, compared with drastic concentration changes in chloride for reference

[125].

In this section, repassivation curves of 304L was analyzed using the film growth model. Based on the results and according to the high-field ion conduction model, it is suggested that addition of up to 18mM thiosulfate in the 0.6M NaCl solution impedes the transport of ions across the passive film and slows down repassivation of 304L.

8.3. Conclusions

In this chapter, current transients from scratch tests in environments containing 0.6M NaCl and various concentrations of thiosulfate were evaluated with two existing repassivation models, the dissolution and film coverage model as well as the passive film growth model.

It was observed that addition of thiosulfate did not result in a change in the film formation constant k for samples polarized at -0.1V vs. SCE. Film formation constant k seemed to increase with thiosulfate concentration for samples polarized at 0.1V vs. SCE, which may be due to the aggressive pitting after scratches were made.

For film passive film growth model, the addition of thiosulfate generally resulted in an increase in the linear region for log(i) vs. 1/q curve, which suggests that addition of thiosulfate hinders the transportation of ions across the passive film. In Chapter 7, it was shown that reduced sulfur species formed on the scratched areas of 304L. It is possible that the presence of these reduced sulfur species is poisoning the film growth of 304L and slowing down the repassivation kinetics.

9. OVERALL SUMMARY AND RECOMMENDATIONS

The role of thiosulfate in pitting corrosion of austenitic and duplex stainless steels, based on the results discussed in previous chapters, is summarized in this chapter. The role of thiosulfate in pit initiation, pit growth and repassivation process of pitting corrosion is discussed. A mechanism of pitting corrosion of duplex stainless steel in chloride and thiosulfate containing environments is proposed.

9.1. Summary of Results

Phenomenological study of the effect of thiosulfate on pitting corrosion of stainless steels was motivated by papermachine white water environments (Chapter 4). Prior studies had shown the effect of thiosulfate in pitting corrosion for stainless steels in white water environment [72][73][78][81], but no study systematically reported the performance of duplex stainless steels, especially the lean duplex grades, in papermachine white water. It was found that although 2101 has higher chromium content than 304L, it is still susceptible to the activation of pitting with addition of thiosulfate in papermachine white water. In many cases, it is more susceptible to thiosulfate related pitting at lower potentials. Molybdenum containing duplex stainless steel 2205 was found to be completely immune to pitting in papermachine white water environments tested. The unique pit morphology on lean duplex stainless steels 2101 shown in Chapter 4 is a result of a preferential dissolution of ferritic phase compared to the hemispherical pits formed on 304L or 316L austenitic stainless steels.

Effect of thiosulfate on initiation of pitting, metastable pitting, and pit initiation was explored (Chapter 5). The effect of thiosulfate on pit initiation and metastable pitting of stainless steels had not been studied. In this study, it was found that an addition up to 18mM thiosulfate into 0.6M NaCl solution promotes pitting initiation and promotes the pit growth of metastable pits. This effect is more prominent for 304L grade rather than for 2101 DSS. Pits were found to initiate in the ferritic phase for DSS2101.

Effect of microstructure of DSS2101 on thiosulfate related pitting corrosion was demonstrated for the first time in this study (Chapter 6). The anisotropy of duplex stainless steel 2101 resulted in differences in the pitting susceptibility of its three surfaces due to microstructural differences in these orientation for the wrought product. It was found that 2101-X has much higher pitting potential, and lower pit growth time before repassivation for the metastable pits. This is because of the directionality of the ferritic phase on 2101-X surface compared to 2101-Y and 2101-Z. Pits tend to grow preferentially in the ferrite phase of lean duplex stainless steel 2101. In other words, the resistance to pitting is higher in the austenite phase for this grade. The thin layer of ferritic phase on 2101 surface does not allow the growth of pit whose pit chemistry is not aggressive enough to sustain pit growth in austenitic phases. This results in lateral growth of pits and early repassivation of metastable pits. On the other hand, pits on 2101-Y and 2101-Z surfaces may grow deep into the specimens due to the microstructure of the ferrite phase. The microstructure of 2101-Y and 2101-Z provides a small pit opening and longer diffusion path than 2101-X, which makes the transition of metastable pits into stable pit much easier. Furthermore, the difference in the

direction of the scratch may also result in a different pit growth rate for 2101 samples. This is because the pit growth is preferentially on the ferritic phase of 2101. Scratch made perpendicular to the ferritic stripes on 2101-Y and 2101-Z resulted in a pseudo-2D growth of pits, while scratches along the ferritic stripes resulted in a pseudo-1D growth of pits, which has lower pitting current than the pseudo-2D growth of pits.

The role of thiosulfate on growth stage of pitting and its effect as an inhibitor of repassivation of pits were systematically evaluated in the present study. Thiosulfate was shown to inhibit repassivation of pits [72]. The $([Cl^-]+[SO_4^{2-}])/[S_2O_3^{2-}]$ ratio is very important in thiosulfate-related pitting corrosion in the white water [77]. Thiosulfate is electro-reduced to reduced sulfur species inside a pit's isolated or stagnant environment, which promotes pitting corrosion and inhibits the repassivation of pits. Effect of thiosulfate is dependent on the applied potential, a low enough potential is required for the formation of reduced sulfur species to activate pitting corrosion [71]. Increase in temperature results in an increase in most aggressive chloride to thiosulfate ratio. Increase in the molybdenum content of an alloy results in a decrease in this ratio required for pitting to occur. Addition of thiosulfate decreases the critical pitting temperature (CPT) of stainless steel 904L from 50 ℃ to 30 ℃ [76]. In this study, interaction between thiosulfate and individual alloying element was revealed (Chapter 7). Thermodynamic analysis was combined with potentiodynamic polarization scans on pure element specimens to understand the corrosion reactions on the surface of stainless steels. XPS analysis was used to identify the chemical makeup of the reaction products at the surface to further reveal the role of thiosulfate in pitting and

repassivation. Polarization behavior of pure chromium did not change with the addition of thiosulfate in the test solution, in contrast to the change in the polarization curve on platinum foil, which suggests that the interaction between thiosulfate and the passive films formed on the surface of stainless steels (mostly chromium oxides) is limited. Polarization data on pure nickel showed that the passive region of nickel was destroyed by the presence of 58ppm thiosulfate, due to the formation of soluble $NiSO_4$. Addition of 58ppm thiosulfate enhanced corrosion of pure iron and resulted in a surface covered with black corrosion products, probably due to the formation of S^{2-} in the cathodic polarization region. In a pit environment, sulfur has the highest affinity for molybdenum, then nickel, and then hydrogen. Sulfur and sulfide were found in pits formed on the bare surface formed by mechanical scratch for the specimens polarized at -0.1V vs. SCE in 6000ppm Cl^- + 1160ppm $S_2O_3^{2-}$ solution. On the other hand, reduced sulfur species was found in the scratched area, formed in thiosulfate-only environment, although no pitting was seen in the scratched surface for these samples. This may explain why the pit initiation was promoted in the presence of thiosulfate and the pits are formed readily in the scratched area, when an aggressive pit environment was not available for the electro-reduction of thiosulfate.

Stress corrosion cracking of 304 and 2101 was shown to occur in chloride and thiosulfate containing environments [111][118], but the change in the repassivation kinetics of stainless steel due to the addition of thiosulfate had never been studied. In this study, an attempt to qualitatively analyze the change in the repassivation kinetics due to the addition of thiosulfate was made using two existing repassivation models

(Chapter 8). The passive film coverage model did not work very well in the chloride and thiosulfate containing environment, probably due to the fact that reduced sulfur species accompanies film growth, which may not fully inhibit dissolution current. On the other hand, the film growth model was shown to generally agree with the effect of thiosulfate on inhibition of repassivation.

9.2. The Role of Thiosulfate in Pitting Corrosion

Thiosulfate is not a thermodynamically stable species (Figure 7-8). However, when the localized film breakdown results in the exposure of bare metal surface, thiosulfate in contact with the bare metal surface of the stainless steel may partly electro-reduced to reduced sulfur species, which promotes pit initiation.

In the growth stage of pits, thiosulfate enters into the pit and is reduced into reduced-sulfur species, which promotes pitting corrosion. However, if too much thiosulfate is present in the pit, the reduction of thiosulfate will cause consumption of large amount of protons, which reduce the aggressiveness of the pit environment and stop the autocatalytic growth of pits. Sulfur has the highest affinity for molybdenum, forming MoS_2, which eliminates the possibility of formation of aggressive reduced sulfur species such as H_2S and the hydrolysis of molybdenum to further lower the pH of pits. Sulfur also forms NiS when nickel is available in the environment. Moreover, nickel was shown to be susceptible to the activation of pit growth by the addition of thiosulfate. Formation of H_2S and S has been known to the industry to promote corrosion of ferrous alloys, which is probably the main reason for the activation of pits

and inhibition of repassivation due to the presence of thiosulfate.

9.3. Mechanism of Pitting Corrosion of LDX 2101 in Chloride and Thiosulfate Containing Environments

In chloride-only environments, pits initiate preferentially on the ferritic phase of lean duplex stainless steel 2101. In the presence of thiosulfate, reduced sulfur species are formed when there is localized breakdown of passive film, which promotes pit initiation. It also promotes the growth of metastable pits.

Microstructure plays an important role in the metastable to stable pit transition phase in the growth of pits. Resistance to pitting corrosion is higher for austenite than for ferrite. Therefore, pit growth tend to extend along the phase boundary of 2101, instead of being hemispherical like pits formed in austenitic stainless steels. Therefore, the shape of the pits determines the susceptibility of pitting corrosion by influencing the stabilization of metastable pits. If the microstructure of 2101 does not allow the development of an aggressive pit environment and has a relatively short diffusion path so that metastable pits repassivate easily, the pitting resistance of the material would be high, as shown for 2101-X.

Due to the fact that pit growth occurs preferentially in the ferritic phase of 2101, the orientation of the mechanical scratch on the surface of 2101 may determine the pitting kinetics. Wherever the passive film is damaged on ferrite phase, it may act as an initiation point for a pit, which grows along the ferrite phase. Depending on the direction of the scratch, the pit growth may be 1-D or 2-D or something in between,

which determines the pitting kinetics.

9.4. Practical Implications

In industrial applications, sometimes the chemical process may be changed to minimize corrosion and degradation of equipment material. In other cases where the process stream cannot be altered, material selection becomes the key factor in mitigating corrosion. In this section, considerations and suggestions for both process optimization and material selection are given.

9.4.1. Process Stream Considerations

- Increase in temperature, decrease in pH, tend to increase the aggressiveness of the environment, so control of these process parameters may be used to mitigate localized corrosion in these process streams.
- Since there is a different optimum ($[Cl^-] + [SO_4^{2-}])/[S_2O_3^{2-}]$ ratio for the activation of pits in different grades of stainless steels, it is always safe to keep thiosulfate concentration away from these critical ratios. On the other hand, it is also important to note that thiosulfate is not a thermodynamically stable species and may degrade over time.
- Thiosulfate activation of pitting is very sensitive to the bare metal surface of stainless steels. Hard particles in process streams with high flow rate may result in scratches and dents on stainless steel surfaces, which may act as initiation sites for pitting.

9.4.2. Material Selection Considerations

- In neutral to acidic thiosulfate containing environment, molybdenum containing stainless steels tend to have higher pitting corrosion resistance.
- Higher chromium have a synergistic effect with the increase in molybdenum content in improving pitting corrosion resistance, it is especially effective in environments with higher chloride concentrations.
- When using an anisotropic duplex stainless steels in an environment containing thiosulfate, the effect of microstructure should be considered. Choosing the right material with a microstructure that minimizes the stabilization of pitting could further reduce the risk of pitting corrosion.

9.5. Suggestion for Future Research

A clearer picture of the role of thiosulfate in pitting corrosion is given in this research. Mechanism of pitting corrosion in thiosulfate containing environment of stainless steel 2101 is proposed. However, more research could be carried out to further the understanding of this issue:

(1) A more specific role of thiosulfate in the pitting corrosion could be revealed by in-situ high intensity high definition XPS.

(2) The transportation of sulfur species inside a growing pit, and the participation of thiosulfate in the repassivation stage of a scratched stainless steel surface could be studied using radioactive labelling.

(3) In environments where the austenitic phase of a duplex stainless steel is

preferentially attacked, it would be interesting to see how pit initiate and grow in the austenite phase and how addition of thiosulfate influence pitting corrosion of duplex stainless steels in these environments.

APPENDIX A

MATLAB PROGRAM FOR DETERMINING METASTABLE PIT GROWTH PARAMETERS

The following Matlab program is written together with Gaoxiang Wu:

```
function MP_3( file)
data = importdata (file);
[m,n]=size(data);
current=data(:,2)*10^9;
position=zeros(1,m);
noise=75;


i=1;
while i<m-5
    if (current(i)>current(i+1)) && (current(i+1)>current(i+2)) && (current(i)-
mean(current(i+3:i+6))>1.5*noise)
        position(i)=i;
    end
    i=i+1;
end
     position=position(position~=0);

i=length(position);
while i>1
     if position(i)-position(i-1)==1
          position(i)=0;
     end
     i=i-1;
end
     position=position(position~=0);
%so far, found peak positions
%--------------------------------------------------------------------------



i=1;
while i<=length(position)
     if i==1
```

```
        l=1;
    else
        l=position(i-1);
    end
    if i==length(position)
         r=length(current);
    else
         r=position(i+1);
    end
        l_to_r=sort(current(l:r));
        n=length(l_to_r);
        peak_current(i)=max(current(position(i)-5:position(i)))-l_to_r(fix(0.3*n));

   i=i+1;

end
position;
peak_current;
peak_time=0.02*position;
%found current_peak
%--------------------------------------------------------------------


t=1;
m=0;
while t==1
t=0;
i=1;
while i<length(position)
    l=position(i);
    r=position(i+1);
    last_droping=max(current(r-5:r))-peak_current(i+1);
    if min(current(l:r))-last_droping>(0.05+m)*current(r)
        t=1;
        m=m+0.01;
        if peak_current(i)>peak_current(i+1)
            peak_current(i+1)=[];
            position(i+1)=[];
        else
            peak_current(i)=[];
            position(i)=[];
        end
    else
        i=i+1;
```

```
    end
end
end
position;
peak_current;
peak_time=0.02*position;
% so far, we have revised all the peaks
%-------------------------------------------------------------------------


%now, we start to calculate the survival time.
i=1;
j=1; %smaller noise set, longer survival time
while i<=length(position)
    r=position(i);
    if i>1
      l=position(i-1);
    else
      l=1;
    end

    l_to_r=sort(current(l:r));
    n=length(l_to_r);
    while current(r-j)-l_to_r(fix(0.3*n))>noise*0.3
        j=j+1;
    end

    survival_time(i)=0.02*j;
    i=i+1;
    j=1;
end
peak_time=0.02*position;
peak_current;
survival_time;
%---------------------------------------------


final_file=[peak_time',peak_current',survival_time'];
final_file(1,4)=length(position);
final_file(3,4)=length(find(peak_time<=600));
final_file(4,4)=length(find((peak_time>600)&(peak_time<=1200)));
final_file(5,4)=length(find((peak_time>1200)&(peak_time<=1800)));
final_file(6,4)=length(find((peak_time>1800)&(peak_time<=2400)));
final_file(7,4)=length(find((peak_time>2400)&(peak_time<=3000)));
final_file(8,4)=length(find((peak_time>3000)&(peak_time<=3600)));
```

```
xlswrite([file,'_processed.xlsx'],final_file);

end
```

REFERENCES

[1] A. L. Schaeffler, Constitution diagram for stainless steel weld metal. Metal Progress, 56: 680-680B (1949)

[2] D. D. Macdonald, Passivity - the key to our metals-based civilization. Pure and Applied Chemistry, 71: 951-978 (1999).

[3] G. S. Frankel, Pitting corrosion of metals - A review of the critical factors. Journal of the Electrochemical Society, 145: 2186-2198 (1998).

[4] Y. Li, G. T. Burstein, I. M. Hutchings, Influence of Environmental Composition and Electrochemical Potential on the Slurry Erosion-Corrosion of Aluminum. Wear, 181: 70-79 (1995).

[5] H. Kwon, E. Cho, K. Yeom, Prediction of stress corrosion cracking susceptibility of stainless steels based on repassivation kinetics. Corrosion, 56: 32-40 (2000).

[6] D. Bonen, S. L. Sarkar, The superplasticizer adsorption capacity of cement pastes, pore solution composition, and parameters affecting flow loss. Cement and Concrete Research, 25: 1423-1434 (1995).

[7] S. Zhang, T. Shibata, T. Haruna, Initiation and propagation of IGSCC for sensitized Type 304 stainless steel in dilute sulfate solutions. Corrosion Science, 39: 1725-1739 (1997).

[8] G. S. Eklund, Initiation of pitting at sulfide inclusions in stainless steel. Journal of the Electrochemical Society, 121: 467-473 (1974).

[9] T. Taira, K. Tsukada, Y. Kobayashi, H. Inagaki, T. Watanabe, Sulfide corrosion

cracking of linepipe for sour gas service. Corrosion, 37: 5-16 (1981).

[10] A. El-Yazgi, D. Hardie, Stress corrosion cracking of duplex and super duplex stainless steels in sour environments. Corrosion science, 40: 909-930 (1998).

[11] A. Garner, 2010 Frank Newman Speller Award Lecture: Identifying the Critical Damage Mechanism. Corrosion, 67: 65006-65006 (2011).

[12] H. H. Uhlig, Passivity in metals and alloys. Corrosion science, 19: 777-791 (1979).

[13] I. Olefjord, B.-O. Elfstrom, The composition of the surface during passivation of stainless steels. Corrosion, 38: 46-52 (1982).

[14] C. McBee, J. Kruger, Nature of passive films on iron-chromium alloys. Electrochimica Acta, 17: 1337-1341 (1972).

[15] D. Zuili, V. Maurice, P. Marcus, In situ scanning tunneling microscopy study of the structure of the hydroxylated anodic oxide film formed on Cr (110) single-crystal surfaces. The Journal of Physical Chemistry B 103, 7896-7905 (1999).

[16] V. Maurice, W. Yang, P. Marcus, XPS and STM Study of Passive Films Formed on Fe‐22Cr (110) Single‐Crystal Surfaces. Journal of The Electrochemical Society 143, 1182-1200 (1996).

[17] V. Maurice, W. Yang, P. Marcus, X‐Ray Photoelectron Spectroscopy and Scanning Tunneling Microscopy Study of Passive Films Formed on (100) Fe‐18Cr‐13Ni Single‐Crystal Surfaces. Journal of the Electrochemical Society 145, 909-920 (1998).

[18] T. P. Hoar, D. C. Mears, G. P. Rothwell, The relationships between anodic passivity, brightening and pitting. Corrosion Science, 5: 279-289 (1965).

[19] H. H. Uhlig, Adsorbed and Reaction‐Product Films on Metals. Journal of the Electrochemical Society, 97: 215C-220C (1950).

[20] N. Sato, A theory for breakdown of anodic oxide films on metals. Electrochimica Acta, 16, 1683-1692 (1971).

[21] D. D. Macdonald, The point defect model for the passive state. Journal of the Electrochemical Society, 139: 3434-3449 (1992).

[22] C. Wagner, Theoretical analysis of the diffusion processes determining the oxidation rate of alloys. Journal of the Electrochemical Society 99, 369-380 (1952).

[23] J. Galvele, Transport processes in passivity breakdown—II. Full hydrolysis of the metal ions. Corrosion Science 21, 551-579 (1981).

[24] P. Ernst, N. J. Laycock, M. H. Moayd, and R. C. Newman, The Mechanism of Lacy Cover Formation in Pitting, Corrosion Science, 39: 1133-1136 (1997)

[25] G. S. Frankel, L. Stockert, F. Hunkerler, H. Boehni, Metastable Pitting of Stainless Steesl. Corrosion, 43: 429-436 (1987).

[26] M. H. Moayed, R. C. Newman, Evolution of Current Transients and Morphology of Metastable and Stable Pitting on Stainless Steel Near the Critical Pitting Temperature. Corrosion Science, 48: 1004-1018 (2006).

[27] J. Scully, N. Budiansky, Y. Tiwary, A. Mikhailov, J. Hudson, An alternate explanation for the abrupt current increase at the pitting potential. Corrosion

Science, 50: 316-324 (2008).

[28] Y. Zuo, H. Wang, J. Zhao, J. Xiong, The effects of some anions on metastable pitting of 316L stainless steel. Corrosion Science, 44: 13-24 (2002).

[29] P. Pistorius, G. Burstein, Metastable pitting corrosion of stainless steel and the transition to stability. Philosophical Transactions of the Royal Society of London. Series A: Physical and Engineering Sciences 341: 531-559 (1992).

[30] Anon., "Iron(II) Chloride", http://en.wikipedia.org/wiki/Iron%28II%29_chloride (Accessed April 16, 2015)

[31] Anon., "Iron(II) Sulfate", http://en.wikipedia.org/wiki/Iron%28II%29_sulfate (Accessed April 20, 2015)

[32] J. W. Oldfield, Test techniques for pitting and crevice corrosion resistance of stainless steels and nickel-base alloys in chloride-containing environments. International materials reviews 32, 153-172 (1987).

[33] E. Lizlovs, Polarization Cell for Potentiostatic Crevice Corrosion Testing. Journal of The Electrochemical Society 117, 1335-1337 (1970).

[34] R. Qvarfort, New electrochemical cell for pitting corrosion testing. Corrosion Science 28, 135-140 (1988).

[35] W. Rudd, J. Scully, The function of the repassivation process in the inhibition of pitting corrosion on aluminium. Corrosion Science 20, 611-631 (1980).

[36] R. J. Brigham, E. W. Tozer, Temperature as a Pitting Criterion. Corrosion 29, 33-36 (1973); published online Epub1973/01/01 (10.5006/0010-9312-29.1.33).

[37] R. Qvarfort, Critical pitting temperature measurements of stainless steels with an improved electrochemical method. Corrosion Science 29, 987-993 (1989).

[38] P. Ernst, R. C. Newman, Explanation of the effect of high chloride concentration on the critical pitting temperature of stainless steel. Corrosion Science 49, 3705-3715 (2007).

[39] M. H. Moayed, R. Newman, Deterioration in critical pitting temperature of 904L stainless steel by addition of sulfate ions. Corrosion Science 48, 3513-3530 (2006).

[40] B. Deng, Y. Jiang, J. Liao, Y. Hao, C. Zhong, J. Li, Dependence of critical pitting temperature on the concentration of sulphate ion in chloride-containing solutions. Applied Surface Science 253, 7369-7375 (2007).

[41] B. Deng, Z. Wang, Y. Jiang, H. Wang, J. Gao, J. Li, Evaluation of localized corrosion in duplex stainless steel aged at 850℃ with critical pitting temperature measurement. Electrochimica Acta 54, 2790-2794 (2009).

[42] M. H. Moayed, N. J. Laycock, R. C. Newman, Dependence of the Critical Pitting Temperature on surface roughness. Corrosion Science 45, 1203-1216 (2003).

[43] J. Horvath, H. Uhlig, Critical Potentials for Pitting Corrosion of Ni, Cr‐Ni, Cr‐Fe, and Related Stainless Steels. Journal of the Electrochemical Society 115, 791-795 (1968).

[44] C. O. A. Olsson, D. Landolt, Passive films on stainless steels - chemistry, structure and growth. Electrochimica Acta 48, 1093-1104 (2003); published

online EpubApr (10.1016/s0013-4686(02)00841-1).

[45] R. Roberge, Effect of the nickel content in the pitting of stainless steels in low chloride and thiosulfate solutions. Corrosion 44, 274-280 (1988).

[46] J. Galvele, J. Lumsden, R. Staehle, Effect of molybdenum on the pitting potential of high purity 18% cr ferritic stainless steels. Journal of the Electrochemical Society 125, 1204-1208 (1978).

[47] H. Ogawa, H. Omata, I. Itoh, H. OKADA, Auger electron spectroscopic and electrochemical analysis of the effect of alloying elements on the passivation behavior of stainless steels. Corrosion 34, 52-60 (1978).

[48] K. Sugimoto, Y. Sawada, The role of molybdenum additions to austenitic stainless steels in the inhibition of pitting in acid chloride solutions. Corrosion Science 17, 425-445 (1977).

[49] K. Asami, K. Hashimoto, An X-ray photo-electron spectroscopic study of surface treatments of stainless steels. Corrosion Science 19, 1007-1017 (1979).

[50] N. Boucherit, A. Hugot-Le Goff, S. Joiret, Influence of Ni, Mo, and Cr on Pitting Corrosionof Steels Studied by Raman Spectroscopy. Corrosion 48, 569-579 (1992).

[51] G. O. Ilevbare, G. T. Burstein, The role of alloyed molybdenum in the inhibition of pitting corrosion in stainless steels. Corrosion Science 43, 485-513 (2001)

[52] J. E. Truman, M. J. Coleman, K. R. Pirt, Note on the Influence of Nitrogen Content on the Resistance to Pitting Corrosion of Stainless Steels. British

Corrosion Journal 12, 236-238 (1977).

[53] R. F. A. Jargelius-Pettersson, Application of the Pitting Resistance Equivalent Concept to Some Highly Alloyed Austenitic Stainless Steels. Corrosion 54, 162-168 (1998).

[54] J. O. Nilsson, Super duplex stainless steels. Materials Science and Technology 8, 685-700 (1992).

[55] K. Adhe, V. Kain, K. Madangopal, H. Gadiyar, Influence of sigma-phase formation on the localized corrosion behavior of a duplex stainless steel. Journal of materials engineering and performance 5, 500-506 (1996).

[56] T. Suter, H. Bohni, A new microelectrochemical method to study pit initiation on stainless steels. Electrochimica Acta 42, 3275-3280 (1997)10.1016/s0013-4686(70)01783-8).

[57] S. J. Pawel, E. E. Stansbury, C. D. Lundin, Role of Nitrogen in the Pitting Resistance of Cast Duplex CF-Type Stainless Steels. Corrosion 45, 125-133 (1989); published online Epub1989/02/01 (10.5006/1.3577829).

[58] P. Marshall, T. Gooch, Effect of composition on corrosion resistance of high-alloy austenitic stainless steel weld metals. Corrosion 49, 514-526 (1993).

[59] Z. Cvijović, G. Radenković, Microstructure and pitting corrosion resistance of annealed duplex stainless steel. Corrosion science 48, 3887-3906 (2006).

[60] N. Sridhar, J. Kolts, Effects of nitrogen on the selective dissolution of a duplex stainless steel. Corrosion 43, 646-651 (1987).

[61] T. Hong, M. Nagumo, Effect of surface roughness on early stages of pitting

corrosion of type 301 stainless steel. Corrosion science 39, 1665-1672 (1997).

[62] G. Burstein, P. Pistorius, Surface roughness and the metastable pitting of stainless steel in chloride solutions. Corrosion 51, 380-385 (1995).

[63] J. H. Wang, C. C. Su, Z. Szklarska-Smialowska, Effects of Cl− Concentration and Temperature on Pitting of AISI 304 Stainless Steel. Corrosion 44, 732-737 (1988).

[64] H. H. Uhlig, J. R. Gilman, Pitting of 18-8 Stainless Steel in Ferric Chloride Inhibited by Nitrates. Corrosion 20, 289t-292t (1964).

[65] H. Leckie, H. Uhlig, Environmental factors affecting the critical potential for pitting in 18–8 stainless steel. Journal of the Electrochemical Society 113, 1262-1267 (1966).

[66] P. Pistorius, G. Burstein, Growth of corrosion pits on stainless steel in chloride solution containing dilute sulphate. Corrosion Science 33, 1885-1897 (1992).

[67] M. A. Ameer, A. M. Fekry, F. E.-T. Heakal, Electrochemical behaviour of passive films on molybdenum-containing austenitic stainless steels in aqueous solutions. Electrochimica Acta 50, 43-49 (2004).

[68] P. Ernst, R. Newman, Pit growth studies in stainless steel foils. II. Effect of temperature, chloride concentration and sulphate addition. Corrosion Science 44, 943-954 (2002).

[69] J. Park, T. Suter, H. Bohni, Role of manganese sulfide inclusions on pit initiation of super austenitic stainless steels, Corrosion, 59 (2003) 59-67.

[70] P. Marcus, Corrosion mechanisms in theory and practice, CRC Press, 2011.

[71] R. Newman, Pitting of stainless alloys in sulfate solutions containing thiosulfate ions, Corrosion, 41 (1985) 450-453.

[72] A. Garner, Thiosulfate Corrosion in Paper-Machine White Water. Corrosion 41, 587-591 (1985).

[73] A. Garner, Sources of thiosulphate in papermachine white water, part II: thiosulfate formation during sodium hydrosulphite brightening. J. Pulp Paper Sci 10, J51-57 (1984).

[74] T. Hakkarainen, Microbiologically influenced corrosion of stainless steels–What is required for pitting? Materials and Corrosion 54, 503-509 (2003).

[75] E. Abd El Meguid, N. Mahmoud, S. Abd El Rehim, The effect of some sulphur compounds on the pitting corrosion of type 304 stainless steel. Materials chemistry and physics, 63: 67-74 (2000).

[76] N. Laycock, Effects of temperature and thiosulfate on chloride pitting of austenitic stainless steels, Corrosion, 55 (1999) 590-595.

[77] R. C. Newman, W. P. Wong, H. Ezuber, A. Garner, Pitting of Stainless-Steels by Thiosulfate Ions. Corrosion 45, 282-287 (1989).

[78] T. Laitinen, Localized corrosion of stainless steel in chloride, sulfate and thiosulfate containing environments, Corrosion science, 42 (2000) 421-441.

[79] A. Thomas, Y.E. Sung, M. Gamboa‐Aldéco, K. Franaszczuk, A. Wieckowski, Investigation of thiosulfate adsorption on 316 stainless steel in neutral solutions by radioactive labeling, electrochemistry, and Auger electron spectroscopy, Journal of The Electrochemical Society, 142 (1995) 476-484.

[80] A. Elbiache, P. Marcus, The role of molybdenum in the dissolution and the passivation of stainless steels with adsorbed sulphur, Corrosion science, 33 (1992) 261-269.

[81] T. Laitinen, Comparison of stainless steels in simulated paper machine environments, Corrosion, 55: 858-869 (1999).

[82] D. Tromans, L. Frederick, Effect of Thiosulfate on Crevice Corrosion of Stainless Steels. Corrosion, 40: 633-639 (1984).

[83] W. T. Tsai, T. F. Wu, Pitting Corrosion of Alloy 690 in Thiosulfate-containing Chloride Solutions. Journal of Nuclear Materials, 277: 169-174 (2000)

[84] J. T. Ho, G. P. Yu, Pitting Corrosion of Inconel 600 in Chloride and Thiosulfate Anion Solutions at Low Temperature. Corrosion, 48: 147-158 (1992)

[85] D. Jones, Localized surface plasticity during stress corrosion cracking, Corrosion, 52 (1996) 356-362.

[86] R. Parkins, Mechanistic aspects of intergranular stress corrosion cracking of ferritic steels, Corrosion, 52 (1996) 363-374.

[87] J. Galvele, A stress corrosion cracking mechanism based on surface mobility, Corrosion Science, 27 (1987) 1-33.

[88] S. Lynch, Environmentally assisted cracking: overview of evidence for an adsorption-induced localised-slip process, Acta Metallurgica, 36 (1988) 2639-2661.

[89] J. Perdomo, P. M. Singh, J. Oteng, J. Mahmood, Stress Corrosion Cracking (SCC) and Corrosion Fatigue (CFC) of a Duplex Stainless Steel in White Water

Environments, CORROSION 2003, (2003).

[90] P. M. Singh, J. Perdomo, J. Oteng, J. Mahmood, Stress corrosion cracking and corrosion fatigue cracking of a duplex stainless steel in white water environments, Corrosion, 60 (2004) 852-861.

[91] J. Truman, The influence of chloride content, pH and temperature of test solution on the occurrence of stress corrosion cracking with austenitic stainless steel, Corrosion Science, 17 (1977) 737-746.

[92] G. Cragnolino, L. Lin, Z. Szklarska-Smialowska, Stress Corrosion Cracking of Sensitized Type 304 Stainless Steel in Sulfate and Chloride Solutions at 250 C and 100 C, Corrosion, 37 (1981) 312-320.

[93] R. Newman, K. Sieradzki, H. Isaacs, Stress-corrosion cracking of sensitized type 304 stainless steel in thiosulfate solutions, Metallurgical Transactions A, 13 (1982) 2015-2026.

[94] D.B. Wells, J. Stewart, R. Davidson, P.M. Scott, D.E. Williams, The Mechanism of Intergranular Stress-Corrosion Cracking of Sensitized Austenitic Stainless-Steel in Dilute Thiosulfate Solution, Corrosion Science, 33 (1992) 39-71.

[95] H. Isaacs, Initiation of stress corrosion cracking of sensitized type 304 stainless steel in dilute thiosulfate solution, Journal of the Electrochemical Society, 135: 2180-2183 (1988).

[96] M. Gomez-Duran, D.D. Macdonald, Stress corrosion cracking of sensitized Type 304 stainless steel in thiosulphate solution. II. Dynamics of fracture,

Corrosion science, 48: 1608-1622 (2006).

[97] R. W. Staehle, The Theory of Stress Corrosion Cracking in Alloys, p. 223. NATO, Brussels (1971).

[98] D. A. Vermilyea, A theory for the propagation of stress corrosion cracks in metals, Journal of Electrochemical Society, 119: 405 (1972).

[99] W. R. Wearmouth, G. P. Dean, and R. N. Parkins, Role of stress in the stress corrosion cracking of a Mg-Al alloy. Corrosion, 29: 251-260 (1973).

[100] G. J. Bignold, Electrochemical Aspects of Stress Corrosion of Steels in Alkaline Solutions. Corrosion, 28: 307-312 (1972).

[101] T. R. Beck, Stress Corrosion Cracking of Titanium Alloys II. An Electrochemical Mechanism, Journal of Electrochemical Society, 115: 890 (1968).

[102] J. C. Scully, The interaction of strain-rate and repassivation rate in stress corrosion crack propagation. Corrosion Science 20: 997-1016 (1980).

[103] G. Ruijini, S. C. Srivastava, and M. B. Ives, Pitting Corrosion Behavior of UNS N08904 Stainless Steel in a Chloride/Sulfate Solution. Corrosion, 45: 874-882 (1989).

[104] Y. Wang, P.M. Singh, “Corrosion and Repassivation Behavior of Stainless Steels in Chloride and Thiosulfate Containing Environments,” 19th International Corrosion Congress (Seoul, Korea: ICC, 2014).

[105] R. Moser, P. M. Singh, L. F. Kahn, K. E. Kurtis, Chloride-induced Corrosion Resistance of High-strength Stainless Steels in Simulated Alkaline

and Carbonated Concrete Pore Solutions. Corrosion Science, 241-253 (2012).

[106] R. F. Garfias-Mesias, J. M. Sykes, and C. D. S. Tuck, The Effect of Phase Composition on the Pitting Corrosion of 25 Cr Duplex Stainless Steel in Chloride Solutions, Corrosion Science, 1995. 38(8): p. 1319-1330

[107] R. C. Newman, Stress Corrosion Cracking Mechanisms in P. Marcus, J. Oudar, Corrosion Mechanisms in Theory and Practice, 311-372, New York, NY, Marcel Dekker, Inc. (1995).

[108] A. Bhattacharya, P. M. Singh, Stress Corrosion Cracking of Welded 2205 Duplex Stainless Steel in Sulfide-containing Caustic Solution, Journal of Failure Analysis and Prevention, 7: 371-377 (2007).

[109] K. R. Chasse, S. Raji, and P. M. Singh, Effect of Chloride Ions on Corrosion and Stress Corrosion Cracking of Duplex Stainless Steels in Hot Alkaline-Sulfide Solutions, Corrosion, 68: 932-949 (2012).

[110] A. Bhattacharya, P. M. Singh, Effect of Heat Treatment on Corrosion and Stress Corrosion Cracking of S32205 Duplex Stainless Steel in Caustic Solution, Metallurgical and Materials Transactions A, 40: 1388-1399 (2009).

[111] F. Zanotto, V. Grassi, A. Balbo, C. Monticelli, and F. Zucchi, Stress Corrosion Cracking of LDX 2101 Duplex Stainless Steel in Chloride Solutions in the Presence of Thiosulphate, Corrosion Science, 80: 205-212 (2014).

[112] I. Calliari, E. Ramous, and P. Bassani, Phase Transformation in Duplex Stainless Steels After Isothermal Treatments, Continuous Cooling and Cold Working, Materials Science Forum, 638-642: 2986-2991 (2010).

[113] T. Suzuki, M. Yamabe, and Y. Kitamura, Composition of Anolyte Within Pit Anode of Austenitic Stainless Steels in Chloride Solution. Corrosion, 29: 18-22 (1973).

[114] Anon., " Chromium(III) sulfate ", https://en.wikipedia.org/wiki/Chromium%28III%29_sulfate (Accessed April 16, 2015)

[115] Anon., " Nickel(II) sulfate", https://en.wikipedia.org/wiki/Nickel%28II%29_sulfate (Accessed April 16, 2015)

[116] Y. Wang, P. M. Singh, Corrosion Behavior of Duplex Stainless Steels in Paper Machine White Water. CORROSION 2014 (2014).

[117] A. V. Naumkin, A. Kraut-Vass, S. W. Gaarenstroom, and C. J. Powell, NIST X-ray Photoelectron Spectroscopy Database, NIST Standard Reference Database 20, Version 4.1 (2012).

[118] T. Haruna, T. Shibata, and R. Toyota, Initiation and propagation of stress corrosion cracks for type 304L stainless steel in chloride solutions containing thiosulfate, Corrosion Science, 39: 1935-1947 (1997).

[119] R. S. Lillard, G. Vasquez Jr., and D. F. Bahr, The Kinetics of Anodic Dissolution and Repassivation on Stainless Steel 304L in Solutions Containing Nitrate, Journal of Electrochemical Society, 158: 194-201 (2011)

[120] T. R. Beck, Electrochemistry of freshly-generated titanium surfaces—I. Scraped-rotating-disk experiments. Electrochimica Acta, 18: 807-814 (1973).

[121] M. Fleischmann and H. R. Thirsk, Advances in Electrochemistry and Electrochemical Engineering, p. 123, John Wiley & Sons, New York (1963).

[122] M. Avrami, Kinetics of phase change. I General theory, The Journal of Chemical Physics, 7: 1103-1112 (1939).

[123] R. M. Carranza and J. R. Galvele, Repassivation Kinetics in Stress Corrosion Cracking — I. Type AISI 304 Stainless Steel in Chloride Solutions, Corrosion Science, 28: 233-249 (1988).

[124] G. Burstein, P. Marshall, The coupled kinetics of film growth and dissolution of stainless steel repassivating in acid solutions, Corrosion Science, 24: 449-462 (1984).

[125] H. Kwon, E. Cho, K. Yeom, Prediction of stress corrosion cracking susceptibility of stainless steels based on repassivation kinetics, Corrosion, 56: 32-40 (2000).

[126] E. Cho, C.-K. Kim, J.-S. Kim, H.-S. Kwon, Quantitative analysis of repassivation kinetics of ferritic stainless steels based on the high field ion conduction model, Electrochimica Acta, 45: 1933-1942 (2000).

[127] N. Cabrera, N. Mott, Theory of the oxidation of metals, Reports on Progress in Physics, 12: 163 (2002).